Experimental Investigation of Thermodynamic and Kinetic Properties of Semi-volatile Organic Aerosols

by

Rawad Saleh

Department of Civil and Environmental Engineering
Duke University

Date:_____

Approved:

_____
Andrey Khlystov, Supervisor

_____
Ana Barros

_____
Prakash Bhave

_____
Claudia Gunsch

_____
Alan Shihadeh

Dissertation submitted in partial fulfillment of
the requirements for the degree of Doctor of Philosophy in the Department of
Civil and Environmental Engineering in the Graduate School
of Duke University

2010

ABSTRACT

Experimental Determination of Thermodynamic and Kinetic Properties of Semi-volatile Organic Aerosols
by

Rawad Saleh

Department of Civil and Environmental Engineering
Duke University

Date:_____
Approved:

_____
Andrey Khlystov, Supervisor

_____
Ana Barros

_____
Prakash Bhave

_____
Claudia Gunsch

_____
Alan Shihadeh

An abstract of a dissertation submitted in partial
fulfillment of the requirements for the degree
of Doctor of Philosophy in the Department of
Civil and Environmental Engineering in the Graduate School
of Duke University

2010

Copyright by
Rawad Saleh
2010

Abstract

We have developed and applied novel experimental techniques for determination of thermodynamic and kinetic properties of semi-volatile organic aerosols. The thermodynamic properties investigated were the saturation pressure (P_{sat}), enthalpy of vaporization (ΔH) and activity coefficient (γ), and the kinetic property was the evaporation coefficient (α).

The thermodynamic properties were determined using the integrated volume method (IVM), which relies on measurements of aerosol particle concentrations at different thermodynamic equilibrium states. The measured decrease in particle concentration upon heating in a flow tube, a thermodenuder, can be correlated with P_{sat} and ΔH via the IVM equation, which was derived from fundamental principles, namely the Clausius-Clapeyron relation, mass conservation, and ideal gas law. The main advantage of the IVM over other methods reported in the literature is that the other methods use kinetic-based techniques to measure thermodynamic properties which require assumptions on the usually unknown evaporation coefficient; the IVM, on the other hand, is equilibrium-based and thus requires no assumption on the evaporation coefficient. We have applied the IVM to C-4, -6, -7, and -9 dicarboxylic acid aerosols, which are pertinent to atmospheric secondary organic aerosols. P_{sat} and ΔH values

obtained for these compounds were respectively 3.7×10^{-4} Pa and 88 kJ/mol, 3.4×10^{-5} Pa and 135 kJ/mol, 7.2×10^{-5} Pa and 149 kJ/mol, and 1.4×10^{-5} Pa and 145 kJ/mol.

The IVM was also used to determine activity coefficients of individual compounds in binary mixtures as a function of their mole fractions. We demonstrated this method using the following four model systems. System 1: adipic acid – pimelic acid, which illustrated polar organic – polar organic interactions. Non-ideal behavior was observed with activity coefficients of approximately three at infinite dilution. System 2: adipic acid – dioctyl sebacate, which illustrated polar organic – non-polar organic interactions. The compounds in this experiment did not form a solution. System 3: adipic acid – ammonium sulfate, which illustrates polar organic – inorganic interactions. The compounds in this experiment did not form a solution. System 4: adipic acid – ambient extracts, which illustrated the potential use of the method to study partitioning behavior of individual components in a complex matrix approximating that of real ambient aerosol. The measured activity coefficient of adipic acid was less than unity for the tested range of mixing ratios, indicating suppression of volatility of this compound in ambient organic matrix.

We have investigated three controversial issues associated with the IVM as well as other methods which utilize thermodenuders and/or aerosol generation by spray atomization and drying: 1) equilibration time scales in thermodenuders, 2) the need for an activated carbon (AC) denuder in the cooling section, and 3) the effect of residual

solvent on measured thermodynamic properties of aerosols generated by spray atomization and drying. Both numerical simulations and experiments showed that the aerosols approached equilibrium within reasonable residence times (15 s – 30 s) for aerosol size distributions typical for laboratory measurements. We have also performed dimensional analysis on the problem of equilibration in TDs, and derived a dimensionless equilibration parameter which can be used to determine the residence time needed for an aerosol of given sized distribution and kinetic properties to approach equilibrium. Using both model simulations and experiments, we have shown that with aerosol size distributions relevant to both ambient and laboratory measurements re-condensation in the cooling section, with and without an AC denuder, was negligible. Thus, there is no significant benefit in using an AC denuder in the cooling section. To investigate the effect of residual solvent on measured thermodynamic properties, we compared measurements of P_{sat} and ΔH of C-6 (adipic) and C-9 (azelaic) dicarboxylic acid aerosols generated by atomization of aqueous solutions to those generated by homogeneous condensation using a modified Sinclair - La Mer generator. We found no statistically significant difference between the tested aerosol generation methods, indicating that residual solvent carried by the particles had no impact on the measurements.

To determine the evaporation coefficient, we developed the integrated volume – tandem differential mobility analysis (IV-TDMA) method. This thermodenuder-based

method allows separate determination of the three parameters governing aerosol evaporation, namely, P_{sat}, surface free energy (σ), and α. P_{sat} was determined using the IVM, while α and σ were determined by fitting particle evaporation rates measured under non-equilibrium conditions to a numerical model of the evaporation process. α was determined in a size range where surface free energy effects were negligible, allowing for single parameter optimization. We obtained α and σ values of 0.07 and 0.15 J/m^2, 0.08 and 0.17 J/m^2 and 0.24 and 0.23 J/m^2 for C-4, -6, and -7 dicarboxylic acids, respectively.

Contents

List of Tables

List of Figures

Acknowledgements

It has been an honor to work with Prof Khlystov, whose scientific talent and skills are unmatched. I learned something new in every single meeting we have had. To say the least, I have been more than lucky to have Prof Khlystov as my PhD advisor.

I am grateful to my PhD committee members, Prof Barros, Dr Bhave, Prof Gunsch, and Prof Shihadeh. I thank Dr Bhave for the valuable feedback and for introducing me to the world of Air Quality Modeling. Prof Shihadeh's contribution to this dissertation was substantial, and being hosted in his aerosol lab every summer had always been a fruitful and fun experience.

Many thanks to the people of Hudson basement and Annex for such an enjoyable ride, especially to Andreas – we had a lot of good ones. The help of Ezzat, Sarah, and Hassan made my "express missions" in the AUB aerosol lab doable; the stress induced by time constraints was hugely overcome by the fun of working with you guys.

Mom, dad, Roham, Ruba, and Saleh, your support during my PhD was a continuation of your life-long support. Thanks for bearing with me through my grad school years, while I could have made things much easier by going to work in Dubai instead, like everybody does. Lynn, the dynamics you maintain brings about ultimate happiness and comfort, which have materialized in all aspects of my life, including graduate studentship.

1. Introduction

1.1 Motivation and significance

The importance of understanding ambient/atmospheric aerosols arises from the extensive evidence of their effect on mankind in terms of health hazards and impact on climate. Ambient aerosols have been associated with respiratory diseases (Koren and O'Neill, 1998), cardiopulmonary diseases, cancer, and adverse reproductive effects (Lewtas, 2007). Atmospheric aerosols can cause warming or cooling of the atmosphere by absorbing or scattering light (Chung and Seinfeld, 2002; Maria et al., 2004). One of the largest uncertainties on the Earth's radiation budget is associated with the ability of atmospheric aerosols to uptake water to form clouds (IPCC 4th assessment report, 2007).

Ambient aerosols are complex mixtures of organics, inorganics, and water (Saxena and Hildemann, 1996; Ohta et al, 1990; Bardouki et al, 2002; Hueglen et al, 2004), with organic compounds comprising up to 50% of the total mass concentration (Chow et al., 1994; Murphy et al., 1998). Despite the substantial progress in the past few decades, predictions of organic aerosol (OA) concentrations by local, regional and global air quality models are still unable to fully reproduce ambient observations (Heald et al., 2005; Vutkuru et al., 2006). One of the main uncertainties is associated with semi-volatile OA, which constitutes a major fraction of both primary and secondary OA (Donahue et al., 2006). Semi-volatile compounds constantly re-partition between the particle and the

gas phases as the temperature, relative humidity and concentrations of semi-volatile species change with time (Turpin et al., 1991; Chow et al., 1994). Thus, understanding the volatility of these organic species is of paramount importance for our ability to predict OA concentrations (Fuzzi et al., 2006; Robinson et al., 2007). Volatility of semi-volatile OA, or the extent to which they partition to the particulate phase, is a function of their thermodynamic properties, namely, saturation pressure (P_{sat}), enthalpy of vaporization (ΔH), and the activity coefficient (γ) with respect to the particulate phase matrix.

OA is comprised of hundreds or sometimes thousands of compounds (Seinfeld and Pandis, 1998), the thermodynamic properties of which are mostly unknown, which makes individual representation of compounds in air quality models impossible. Researchers have resorted to "lumping" compounds into groups with effective P_{sat} and ΔH obtained from fits to yields of smog chamber experiments – controlled experiments in which parent hydrocarbons are oxidized in the presence of ozone and UV light to produce secondary organic aerosols (SOA) which simulate the reaction pathways that occur in the atmosphere. One of the widely used models is the *N.2P* model of Odum et al. (1997), where the compounds produced by each parent hydrocarbon are lumped into two products, one with a low P_{sat} and one with a high P_{sat}, with ΔH assumed to be equal for both. A newer approach is the volatility basis set (VBS) of Donahue et al. (2006). In

the VBS, semi-volatile organic compounds are lumped into fixed "volatility bins" with decadal-spaced P_{sat} values and decreasing ΔH with increasing P_{sat}. The concentration in each bin, or the "volatility distribution", is obtained, again, from fits to smog chamber yields. Pankow and Barsanti (2009) argued that the main limitation of the *N.2P* and VBS is that the lumping of compounds is not based on fundamental molecular characteristics, which puts the validity of extrapolation from smog chamber experimental conditions to ambient conditions into question, especially due to the arbitrary assigned ΔH values. Also, the lumping approaches do not allow the treatment of interaction between groups, and thus the activity coefficients (γ) are assumed to be unity. Pankow and Barsanti (2009) suggested a more fundamental approach to lump semi-volatile organic compounds based on the number of carbon atoms and molecular polarity.

While the approach of Pankow and Barsanti (2009) is promising, the paucity of data on thermodynamic properties of individual (or surrogate) semi-volatile organic compounds hinders the progress in this direction. The reason is that standard bulk measurement techniques used for volatile compounds cannot be applied to semi-volatile compounds, and the new techniques developed for semi-volatiles over the past few decades suffer from a variety of limitations, which has lead to results varying over 2-3 orders of magnitude (Clegg et al., 2008). Thus, there is a need for experimental investigation of saturation pressures (P_{sat}) and enthalpy of vaporizations (ΔH) of semi-

volatile organic compounds pertinent to atmospheric OA, as well as activity coefficients (γ) in the presence of other compounds.

It should be noted that the time scales of interest in air quality models are long enough that phase change kinetics of semi-volatile OA – the time needed to achieve equilibrium (re-partition between the particulate phase and the gas phase) in response to a perturbation – is not relevant; the aerosol is assumed to be at equilibrium at each time step. However, the time scales in laboratory and ambient measurements of thermodynamic properties are comparable to those of phase change kinetics. The knowledge of kinetic properties, namely the evaporation coefficient (α) is thus essential for measurement interpretations.

1.2 The state of the art and the scientific gaps

1.2.1 Techniques used to determine P_{sat} and ΔH of semi-volatile organic aerosols

There has been extensive work on estimating thermodynamic properties – mainly saturation pressure (P_{sat}) and enthalpy of vaporization (ΔH) – of organic compounds that pertain to semi-volatile OA. The most widely used method is the Tandem Differential Mobility Analyzer (TDMA) (Rader and McMurry, 1986). In TDMA, quasi-monodisperse aerosol is heated in a thermodenuder, a temperature controlled flow tube, and the size change due to evaporation is measured. The observed particle

evaporation is compared to theoretical evaporation kinetics, from which P_{sat} can be estimated. Repeating the procedure at several different thermodenuder temperatures, $P_{sat}(T)$ is obtained, and ΔH can be estimated using Clausius-Clapeyron relation. Another technique is the temperature programmed thermal desorption (TPTD) (Chattopadhyay and Ziemann, 2005; Cappa et al., 2007). In TPTD, aerosol is deposited in a temperature controlled vacuum chamber. The evaporation rate is monitored using a mass spectrometer, and P_{sat} is estimated from comparison with the theoretical evaporation rate given by the kinetic theory of gases. A recently developed technique is the Knudsen Effusion Mass Spectrometer (KEMS) (Booth et al., 2009), where similar to TPTD, Psat is obtained from comparing observed evaporation rates in a vacuum chamber to the evaporation rate predicted by the kinetic theory of gases.

The major limitation of the methods briefly described above is that P_{sat}, an equilibrium property, is measured using non-equilibrium (kinetics-based) techniques. This requires the assumption of ideal evaporation, which is mathematically represented by an evaporation coefficient (α) equal to 1; this is not necessarily the case as outlined in section 2.5. Thus, there is a need for developing an experimental technique that decouples the effect of kinetics from measurements of P_{sat} and ΔH; put in other words, this technique needs to rely on equilibrium-based measurements.

1.2.2 Techniques used to determine activity coefficients (γ)

In a multi-component solution, the vapor pressure of each component is suppressed relative to P_{sat} by the presence of other compounds according to $P_{v,i} = x_i \gamma_i P_{sat,i}$, where x_i is the mole fraction of component i in the solution and γ_i is the activity coefficient. Most of the work reported in the literature has been on activity coefficients of water in solution with organic compounds. There are two widely used techniques, namely the Electrodynamic Balance (EDB) (Peng et al., 2001; Choi and Chen, 2002) and the Hygroscopic Tandem Differential Mobility Analyzer (HTDMA) (Moore and Raymond, 2008). In EDB, a single 5 μm – 40 μm droplet of aqueous solution is charged then trapped and levitated in a temperature and humidity controlled chamber by applying AC and DC fields. Relative change in mass at various controlled RH settings is determined from the required DC voltage to balance the gravitational forces. Knowing the concentration of the organic compound in the solution, γ can be obtained from Kohler theory ($RH = \gamma x_w$), where x_w is the mole fraction of water in the solution. Peng et al. (2001) employed the EDB technique to obtain water activity in the presence of water soluble organic compounds. The HTDMA is one of the variations of the tandem differential mobility analyzer (TDMA) developed by Rader and McMurry (1986). Dry quasi-monodisperse aerosol is sent to a reactor after mixing with a humidified air stream to achieve a final RH; different RH values can be achieved by changing the mixing ratios. Aerosol droplets grow due to water uptake to a final equilibrium size according

to Kohler theory, from which γ can be obtained. Moore and Raymond (2008) used the HTDMA technique to estimate water activity present in solution with dicarboxylic acids. The main limitation of the EDB and HTDMA methods is that the solute should be much less volatile than the solvent, because it is assumed that only the solvent – water in this case – undergoes partitioning with the gas phase. Thus, they can't be used to determine γ values of components with comparable P_{sat} in organic mixtures.

The only experimental investigation of γ's in organic-organic mixtures relevant to atmospheric aerosol was reported by Cappa et al. (2008) using TPTD. γ values were found to be less than unity for lower molecular mass dicarboxylic acids and larger than unity for heavier dicarboxylic acids in an equi-molar mixture of C3-C10 and C12 di-carboxylic acids. As mentioned in section 2.1, the TPTD suffers from the required assumption of unity evaporation coefficient.

The paucity of data on γ's of semi-volatile organic compounds hinders their incorporation in air quality models, which may account for part of the uncertainty (Pankow and Barsanti, 2009). This illustrates the importance of developing experimental techniques that estimate γ's of atmospheric-relevant semi-volatile organic compounds.

1.2.3 Aerosol generation and the effect of residual solvent

In all the aforementioned studies, organic aerosols were generated by atomization of solutions – in water or alcohol – with subsequent stripping of the solvent

from the aerosol by diffusion (e.g. in a diffusion dryer or activated carbon denuder). There has been evidence that part of the solvent can be retained in the aerosol (Cappa et al. 2007 & 2008) when atomizing mono- and di- carboxylic acid solutions in water, methanol, and 1-propanol. Cappa et al. (2007 & 2008) recommended preheating the generated aerosol to evaporate the retained solvent. They reported an overestimation of saturation pressure by up to a factor of 25, and underestimation of enthalpy of vaporization by around 20% when the aerosol was not preheated. This was attributed to 1) contribution of retained solvent (which has greater P_{sat} and lower ΔH than the investigated compounds) to the evaporation flux in the Temperature Programmed Desorption (TPD) experiments, and 2) the residual solvent molecules causing disruption of the molecular structure at the surface of the organic aerosol, which enhanced evaporation over the case of pure crystal structure. Since the vast majority of the P_{sat} and ΔH values reported in the literature were obtained without pre-heating the aerosol, the effect of remaining solvent on the volatility properties of organic substances needs to be investigated.

1.2.4 Thermodenuders

Thermodenuders have been widely used in aerosol volatility studies, both in the lab (e.g. An et al., 2007; Saleh et al., 2008; Fuallhaber et al., 2009) and in the field (e.g. Wehner et al., 2004; Huffman et al., 2008; Dzepina et al., 2009). A thermodenuder is

simply a temperature controlled flow tube. When a volatile/semi-volatile aerosol is heated as it flows through a thermodenuder, the aerosol particles respond by evaporating. The extent to which the particles evaporate – the difference between initial and final particle size distributions – gives information about their volatility.

There have been differences in configurations in the use of thermodenuders as well as in interpretations of measurements, which has sometimes led to contradictory conclusions. For example, Riipinen et al. (2010) concluded that equilibration time scales in thermodenuders increase with increasing aerosol volatility, while Cappa (2010) reached the very opposite conclusion. There is thus a need for theoretical and experimental investigation of the technicalities of thermodenuders in order to provide a solid foundation for proper use and data interpretation.

1.2.5 The evaporation coefficient

The evaporation coefficient is generally defined as the ratio of the molecular flux desorbed from a particle to the maximum theoretical flux predicted by kinetic theory, which is given by $J = \frac{\bar{c}}{4} P_{sat}(T) \frac{M}{RT}$ where $\bar{c}$ is the mean molecular speed corresponding to a Maxwell-Boltzmann velocity distribution and is given by $\bar{c} = \sqrt{\frac{8kT}{\pi M}}$ in which k is Boltzmann's constant. A variety of surface and bulk interior effects may limit the rate at which molecules are made available for desorption at the particle

interface (Somorjai and Lester, 1967), thus the vapor pressure at the particle interface during evaporation may be considerably depressed relative to P_{sat}. In addition, the velocity distribution of molecules leaving the particle interface may not be Maxwellian (Li and Davis, 1996). These phenomena render the actual flux less than the theoretical flux predicted by kinetic theory; the evaporation coefficient ($0 < \alpha < 1$) is used to account for the evaporation rate depression.

Although the concept of the evaporation coefficient was introduced in the mid nineteenth century by Maxwell (1859, 1860a, b), there is no reliable theoretical basis to date to estimate its magnitude. There is paucity of data on α of organic compounds relevant to organic ambient aerosols, and when available, they are often contradictory. Li and Davis (1996) found α close to unity for dibutyl phthalate droplets evaporating using EDB. Riipinen et al. (2006) also reported α close to unity for succinic acid in aqueous solution. Their findings were based on a comparison between Tandem Differential Mobility Analysis (TDMA) experiments and simulations performed with an evaporation / condensation model (BCOND). On the other hand, Stanier et al. (2007) estimated that α values of less than 0.1 are required to match their evaporation simulations using a basis-set approximation with TDMA measurements for SOA generated in a smog chamber by α-pinene ozonolysis. Another smog chamber study by

Bowman et al. (1997) estimated α between 0.1 and 1 for aerosol resulting from m-xylene/NOx experiments.

Given the scarcity and controversy associated with data on α's of semi-volatile organic species, and their potential impact on aerosol volatility studies (if α's have values different from unity), experimental investigation of this parameter is of paramount importance.

1.3 Objectives

In an attempt to fill the scientific gaps identified in the previous section and subsequently improve the understanding of semi-volatile organic aerosols, the research described in this dissertation aimed to fulfill the following objectives:

- Develop an equilibrium-based experimental technique to measure thermodynamic properties of lab generated semi-volatile organic compounds pertinent to atmospheric OA. This technique was used to determine P_{sat} and ΔH values of di-carboxylic acid aerosols, as well as γ values of binary mixtures of di-carboxylic acids, and binary mixtures of di-carboxylic acids with other organic and inorganic compounds.
- Develop an experimental technique to measure kinetic properties of lab generated semi-volatile organic compounds pertinent to atmospheric OA, and demonstrate

the use of this technique to determine α values by applying it to di-carboxylic acid aerosols.

- Provide a metric for equilibration time scales in thermodenuders base on theoretical and experimental investigation, as well as guidelines for proper use and data interpretation.

1.4 Research hypotheses and chapter flow

The main hypothesis of this research is that thermodynamic properties of semi-volatile organic aerosols can be inferred from change in particle volume concentrations measured at different thermodynamic equilibrium states. The change in partitioning between the particulate phase and the gas phase as the aerosol is brought from a reference state to a heated state gives information about the saturation pressure and enthalpy of vaporization, as well as the activity coefficients of individual compounds in a mixture. Central to the main hypothesis is that the measurements at different states, more specifically different temperatures, can be performed at thermodynamic equilibrium. In this dissertation, the hypothesis described was materialized via development of the integrated volume method (IVM), a novel experimental technique which utilizes a thermodenuder (see section 1.2.4 for description of a thermodenuder) to equilibrate aerosols at different temperatures. The use of IVM to determine saturation pressures and enthalpies of vaporization is presented in Chapter 2, and the

determination of activity coefficients of compounds in binary mixtures is presented in Chapter 3. In Chapter 4, we present an investigation of the effect of residual solvent on measured thermodynamic properties of aerosols generated by spray atomization and drying, a method used in most studies on thermodynamic properties of organic aerosols. Chapter 5 is dedicated to the analysis of transport phenomena in thermodenuders, which dictate the equilibration time scales.

The second part of this research is based on the hypothesis that the kinetic property dubbed "the evaporation coefficient" can be estimated from interpreting aerosol particle size change at non-equilibrium conditions using evaporation kinetics theory. The size change measurements were performed using the tandem differential mobility analyzer technique (TDMA). The details of the experimental measurements and the data analysis performed to estimate evaporation coefficients are given in Chapter 6.

2. Determination of saturation pressure and enthalpy of vaporization of semi-volatile aerosols

In this chapter, the integrated volume method (IVM) is described. The main advantage of the IVM is that the aerosol is investigated at equilibrium states, which excludes kinetics from the analysis and thus eliminates the need for the knowledge of the evaporation coefficient (α). We present the theoretical background and the derivation of the IVM equation used to estimate saturation pressure (P_{sat}) and enthalpy of vaporization (ΔH) values. We also present detailed description of the experimental setup used for IVM measurements. The IVM was applied to determine P_{sat} and ΔH for several dicarboxylic acids, namely succinic, adipic, pimelic, and azelaic acid. The results are compared with previous data reported in the literature.

2.1 The integrated volume method (IVM)

Consider the process of the aerosol flow in the thermodenuder, in which aerosol deposition losses are negligible. The aerosol is initially in equilibrium at ambient temperature T_0 and with a total particle mass concentration C_0; the vapor concentration in the gas phase is $C_{sat,0}$ and the corresponding vapor pressure is $P_{sat,0}$ (state "0"). The aerosol is heated to T_1 in the thermodenuder and the particles respond by evaporating towards equilibrium, that is to bring the gas phase to saturation, $C_{sat,1}$ ($P_{sat,1}$) provided that the particles have enough mass (i.e. $C_0 > C_{sat,1}$) , or else they will evaporate

completely before saturating the gas phase. Reaching equilibrium at T_1, the particles attain a new mass concentration C_1 (state "1"). The aerosol is then cooled back to T_0 as it exits the thermodenuder. Assuming that excess vapor condenses on the tube walls without significant re-condensation to the particles, the particle mass concentration remains equal to C_1, while the vapor mass concentration goes back to $C_{sat,0}$ (state "2").

If we take a control volume over a bolus of aerosol, the increase of mass of species in the vapor phase from state "0" to state "1" can be written as:

$$\Delta m_v = c_{sat,1}V_1 - c_{sat,0}V_0 \tag{2.1}$$

in which V_0 and V_1 are the control volumes in state 0 and 1, respectively. Using the ideal gas law ($P = \frac{cRT}{M}$) and Charles' law at constant pressure ($\frac{V_1}{V_0} = \frac{T_1}{T_0}$), we can re-write equation (1) as:

$$\Delta m_v = \frac{P_{sat,1}M}{RT_1}\frac{V_0T_1}{T_0} - \frac{P_{sat,0}M}{RT_0}V_0 = \frac{V_0M}{RT_0}\left(P_{sat,1} - P_{sat,0}\right) \tag{2.2}$$

Noting that $\Delta m_v = \Delta m_p$, and that $\Delta m_v = \Delta CV_0$ (ρ_p being the particle density and v_p being the aerosol volume concentration), the change in volume concentration of particles is given by:

$$\Delta v_p = \frac{M}{\rho_p RT_0}\left(P_{sat,1} - P_{sat,0}\right) \tag{2.3}$$

P_{sat} and ΔH can be linked by the Clausius-Clapeyron equation, with the assumption that ΔH is constant over the temperature range:

$$\ln\left(P_{sat,1}\right)-\ln\left(P_{sat,0}\right)=-\frac{\Delta H}{R}\left(\frac{1}{T_1}-\frac{1}{T_0}\right) \tag{2.4}$$

Exponentiating and subtracting $P_{sat,0}$ from both sides yields:

$$P_{sat,1}-P_{sat,0}=P_{sat,0}\left[\exp\left(-\frac{\Delta H}{R}\left(\frac{1}{T_1}-\frac{1}{T_0}\right)\right)-1\right] \tag{2.5}$$

Combining equations (2.3) and (2.5), we can write:

$$\Delta v_p=\frac{P_{sat,0}M}{\rho_p R T_0}\left[\exp\left(-\frac{\Delta H}{R}\left(\frac{1}{T_1}-\frac{1}{T_0}\right)\right)-1\right] \tag{2.6}$$

Δv_p is measured at different temperatures (T_1), and equation (2.6) is used to fit the data set (Δv_p vs $1/T_1$) to obtain estimates on $P_{sat,0}$ and ΔH.

2.2 Experimental section

The experimental setup, shown in Figure 2.1, consists of three main subsystems: aerosol generator, thermodenuder (laminar flow reactor), and sizing system.

2.2.1 Aerosol generator

To generate aqueous aerosol, we use an atomizer (TSI model 3076) operated in recirculation mode at 3 SLPM air flow with 0.1% acid solution in de-ionized 18 MΩ water. The wet aerosol is sent to a 20 liter chamber to mix with dry particle free air at 40

SLPM for dilution and drying. 2 SLPM are drawn through a diffusion dryer (TSI model 3062) to ensure that the aerosol is dry, while the excess is sent to the exhaust. The 2 SLPM dry aerosol is split into two 1 SLPM lines; one is sampled for reference measurements and the other is sent through the thermodenuder.

2.2.2 The thermodenuder

As shown in Figure 2.1, 1 SLPM of the aerosol is drawn through the thermodenuder (TD). For some of the experiments, the flowrate in the TD was increased to 2 SLPM to verify that the aerosol has achieved equilibrium. The flow section is a stainless steel tube with a length of 100 cm and inner diameter of 2.5 cm. The wall temperature of the TD is controlled with a miniature microprocessor (OMEGA model CN900A) and T-type thermocouple (OMEGA) set to a cycle time of 0.3s. The thermocouple is located at the axial midpoint of the heated tube. The controller set point was calibrated by comparing to measurements of air temperature along the radial center of the tube. The TD is wrapped with Kaowool for insulation and housed in an aluminum tube of 100 cm length and 10.2 cm inner diameter. Temperature is recorded minutely using a micrologger (Campbel Scientific model CR23x). The average residence time in the heating section is 24.3 s at room temperature; this value decreases with increasing temperature in the TD.

2.2.3 The sizing system

To measure the aerosol size distribution, we use two Differential Mobility Analyzer (TSI model 3071) – Condensation Particle Counter (TSI model 3010) combinations. The DMAs are operated at 4 SLPM sheath air with a HEPA-filtered recirculation flow provided by an AMETEK Minispiral blower. The flow rate is monitored using a mass flowmeter (TSI model 4140). The aerosol sampling flow rate is 1 SLPM, as dictated by the critical orifices in the CPCs. The voltage is supplied to the DMAs by a high voltage power supply (Beta model 605C). The two systems are operated in the SMPS mode (Wang and Flagan 1990) with a voltage range of 10 V – 10000 V, which, given a sheath air flow rate of 4 SLPM, results in a size range of 10 nm – 600 nm. The scanning time is 120 s.

As depicted in Figure 2.1, one SMPS samples the aerosol upstream of the thermodenuder (reference aerosol) and the other samples the aerosol downstream of the denuder (heated aerosol). To eliminate the variability between the two instruments, we calibrate the two SMPS systems against each other by sampling through the upstream and downstream SMPS without heating the thermodenuder. Since the aerosol is in equilibrium at room temperature, the particles do not evaporate or grow in the thermodenuder. Discrepancy between the two instruments is assessed by switching the position of the SMPS systems and is indicated by a difference between upstream and

downstream size distributions. The ratio of volume concentrations at each size is used as a size-dependent correction factor applied to the downstream SMPS to match the upstream SMPS. Applying the correction to the upstream SMPS instead of the downstream SMPS has a small effect on the resulting $P_{sat,0}$ (less than 3%). The discrepancy in total volumes measured by the uncorrected instruments is usually less than 15%.

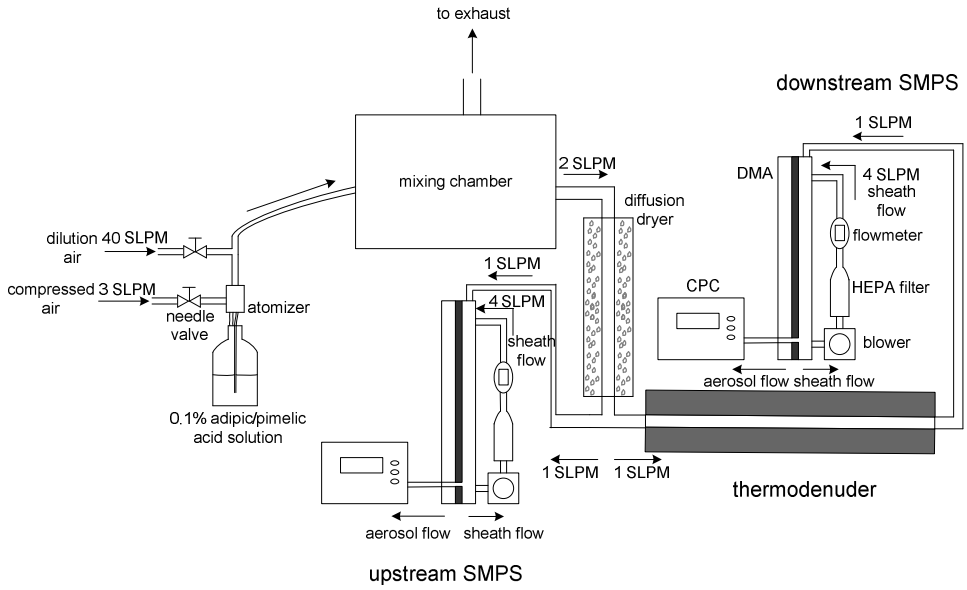

Figure 2.1: IVM experimental setup

2.2.4 Experimental procedure

The TD is heated to the desired maximum temperature using the temperature controller, then allowed to cool down gradually to ambient temperature. Upstream and downstream aerosol size distributions are measured continuously from the onset of the

cooling by the upstream and downstream SMPS and data is acquired via the continuous mode of TSI Aerosol Instrument Manager Software version 5.2.0. The thermodenuder and ambient temperatures are recorded to a micrologger (Campbell Scientific model CR23x) as 60 s averages. The micrologger and SMPS software times are synchronized such that each data point consists of the reference ambient temperature, the thermodenuder set-temperature, the reference size distribution and the heated size distribution.

Another configuration could be employed to eliminate uncertainty associated with instrument inter-comparability by having one SMPS system downstream of the TD and with a bypass from upstream of the thermodenuder to the reference SMPS. In this configuration, the continuous cooling technique is inappropriate due to insufficient temporal resolution, especially at high temperatures where the cooling curve is steep (Figure 2.2). The cooling/heating needs to be performed in a stepwise manner, which is more time consuming.

2.3 Results and discussion

2.3.1 P_{sat} and ΔH

Plots of total aerosol volume change versus inverse of TD temperature obtained from IVM experiments are shown in Figure 2.2. Estimates of $P_{sat,0}$ and ΔH determined from the 2-parameter fit (equation(2.6)) are given in Table 2.1. Also given are data

reported by Tao and McMurry (1989) and Bilde et al. (2003) using the TDMA method, and Cappa et al. (2008) using TPTD.

As shown in Table 2.1, our $P_{sat,298K}$ values are generally in good agreement (same order of magnitude) with the values reported by Tao and McMurry (1989) and Bilde et al. (2003), with our findings being larger, except for pimelic acid. The maximum difference is a factor of 6 for succinic acid. The values reported by Cappa et al. (2007) are lower by 1-2 orders of magnitude. One possible reason for IVM measurements being consistently larger than other methods is that it relies on SMPS measurements assume the aerosol particles to be spherical, while they are not, which can lead to an overestimation in P_{sat}. This overestimation, however, is less than 30% as will be discussed in details in Chapter 4. Another possible, and more prominent, reason is that the IVM operates at equilibrium, which eliminates the need for knowledge of evaporation kinetics; the other techniques are based on evaporation rates, which usually involve the assumption that the evaporation coefficient (α) is equal to unity. This leads to substantial underestimation of P_{sat}. As will be presented in Chapter 6, we have estimated α values to be on the order of 10^{-1} for several di-carboxylic acids. Thus, assuming α of unity would result in an order of magnitude underestimation of P_{sat}.

On the other hand, there is general agreement in ΔH values across the different techniques. This is because ΔH is a measure of how steep the change of P_{sat} with

temperature is, as the Clausius-Calpeyron equation implies, and is not affected by the absolute values of $P_{sat,298K}$.

If the integrated volume method is to be applied to an aerosol with unknown density and molecular weight, equation (2.6) implies that this lack of information has no effect on the value of ΔH. However, the uncertainty associated with P_{sat} is proportional to the uncertainty in the assumptions on the density and molecular weight.

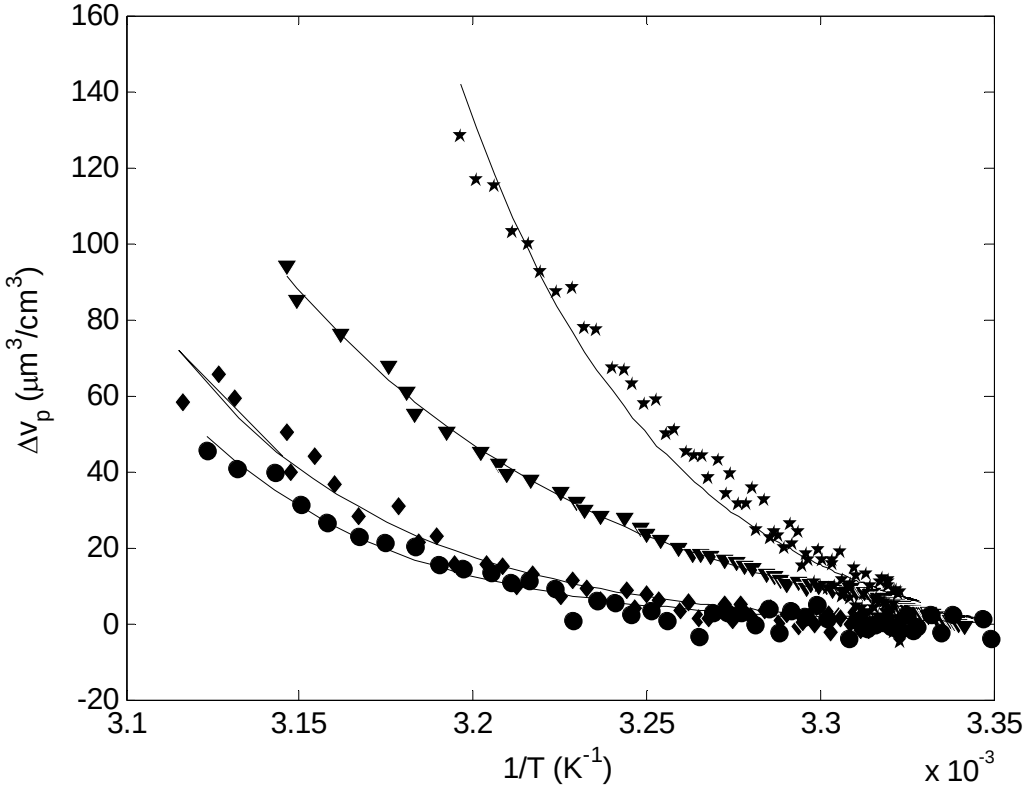

Figure 2.2: IVM measurements. Triangles: succinic acid; diamonds: adipic acid; stars: pimelic acid; circles: azelaic acid. Solid lines are 2-parameter fits based on equation 2.6

Table 2.1: Enthalpies of vaporization and saturation pressures at 298 K of the dicarboxylic acids

Thermodynamic property	Acid	Current study	Tao and McMurry (1989)	Bilde et al. (2003)	Cappa et al. (2008)
ΔH (kJ/mol)	Succinic	88 (± 3)	-	138 (± 11)	128 (± 2)
	Adipic	135 (± 13)	140 (± 21)	154 (± 6)	145 (± 5)
	Pimelic	149 (± 10)	-	147 (± 11)	153 (± 4)
	Azelaic	145 (± 15)	-	153 (± 24)	178 (± 5)
$P_{sat,0}$ (10^{-5} Pa)	Succinic	37 (± 11)	-	5.7 (± 2.2)	3.2 (± 0.6)
	Adipic	3.4 (± 1.2)	1.8 (± 0.3)	1.5 (± 0.7)	0.26 (± 0.1)
	Pimelic	7.2 (± 1.7)	-	7.6 (± 3)	0.39 (± 0.06)
	Azelaic	1.4 (± 0.5)	-	0.6 (± 0.24)	10^{-3} (± 0.6×10^{-3})

2.3.2 Issues of special consideration regarding the IVM

Aerosol concentration at the reference temperature should be greater than the vapor saturation concentration (C_{sat}) at the maximum temperature in the experiment; otherwise there will be not enough aerosol mass to saturate the gas phase at high temperatures. The maximum temperature should in turn be significantly greater than the reference temperature in order to obtain a sufficiently wide temperature range for a robust fit to the data. Failure to meet these conditions can be due to 1) a low aerosol concentration, or 2) high aerosol volatility. A remedy for this problem is to increase the aerosol concentration or perform the experiments at low reference temperatures in a temperature controlled environment.

Establishing equilibrium in the thermodenuder is an essential condition for the applicability of the integrated volume method. Chapter 5 of this manuscript is dedicated for this crucial issue.

In this study we use a stainless steel thermodenuder, which is inert with respect to the investigated compounds. This has been verified by confirming that the aerosol reaches equilibrium in the thermodenuder. If the vapor reacted with the thermodenuder, the thermodenuder wall would act as a sink and equilibrium would never be achieved. When working with aerosol species that can react with a metal thermodenuder, we recommend replacing the stainless steel with an inert material. The choice of the material will depend on the substance being studied and the desired temperature range. Potential substitution materials are Teflon, glass or quartz.

3. Determination of activity coefficients of binary mixtures

This chapter presents an experimental technique to estimate activity coefficients of semi-volatile organic compounds of atmospheric relevance in binary solutions. This technique also provides information on whether certain compounds form solutions or not. This technique can also be used to estimate the activity coefficients of organic compounds when present in a complex matrix of ambient extracts. The experimental method employed is an extension to the integrated volume method (IVM) described in the previous chapter. To illustrate, experimental results are shown for the following mixtures: adipic acid – pimelic acid, adipic acid – dioctyl sebacate, and adipic acid – ambient extracts.

3.1 Experimental section

3.1.1 Experimental setup and procedure

The IVM experimental setup is described in detail in the previous chapter. A brief description of the extension in experimental procedure for activity coefficient measurements is given here.

Aerosol is produced by spraying aqueous (in de-ionized 18 MΩ water) or ethanol solutions (for dioctyl-sebacate mixtures) of pure compounds or binary mixtures using a TSI Constant Output Atomizer. The aerosol is sent to a 20 liter chamber to mix with dry

particle free air at 40 SLPM for dilution and drying. 2 SLPM are drawn through a diffusion-dryer to ensure that the aerosol is dry, while the excess is sent to exhaust. When the solvent used is ethanol, the diffusion dryer is replaced with an activated carbon denuder. The 2 SLPM dry aerosol are split into two 1 SLPM lines; one is sampled for reference measurements via the upstream SMPS, and the other is sent through a 2.5 cm ID × 1 m long stainless steel heated tube (thermodenuder) maintained at 35 ^{0}C, and is then sized via the downstream SMPS. The cooling section downstream the thermodenuder is a 7 mm ID × 50 cm long copper tube. We do not use an activated carbon denuder in the cooling section, because its use can produce larger errors than errors due to re-condensation of organic vapor on the particles in the cooling section. This issue will be discussed in detail in Chapter 5. The set temperature of 35 ^{0}C was chosen because it is high enough to obtain volume changes significantly greater than the noise in the measurements, and is at the same time close to ambient / atmospheric conditions.

3.1.2 Sample preparation

The two compounds are dissolved in water or ethanol (for dioctyl-sebacate mixtures). The solution is then atomized and dried, to end up with a binary-mixture aerosol. The experiments are repeated at several mole fractions, which are achieved by changing the relative concentrations of the compounds in the solution.

For experiments with adipic – "ambient" mixtures, adipic acid was mixed with an aqueous extract of ambient aerosol. Ambient air samples were collected on (20.3 cm × 25.4 cm) glass-fiber filters for 3-4 days using a High-Volume air sampler installed on the roof of one of the buildings on Duke University campus. The filters were then extracted in water to form a solution of the soluble fraction of the ambient aerosol. The individual extracts were combined and divided into 6 fractions. One fraction was left unmodified (to test the volatility properties of the ambient extract) and the remaining 5 were "doped" with different amounts of adipic acid to obtain different mole fractions of this acid in the resulting solution. The obtained solutions were then atomized as described above.

3.2 Theory and data analysis

3.2.1 Extension of the IVM to multi-component aerosols

The theoretical background for IVM was presented in details in Chapter 2. Here, a brief review is given.

Consider a control volume of volatile (or semi-volatile) aerosol initially in equilibrium with its surrounding at temperature T_0 sent through a thermodenuder at temperature $T_1 > T_0$; the particles will evaporate to bring the system back to equilibrium at the new temperature T_1. The total change of aerosol volume can be expressed as:

$$\Delta v_p = \frac{M}{\rho_p R T_0}\left(P_{sat,1} - P_{sat,0}\right) \tag{3.1}$$

P_{sat} and ΔH can be linked by the Clausius-Clapeyron equation, with the assumption that ΔH is constant over the temperature range:

$$\ln\left(P_{sat,1}\right) - \ln\left(P_{sat,0}\right) = -\frac{\Delta H}{R}\left(\frac{1}{T_1} - \frac{1}{T_0}\right) \tag{3.2}$$

Combining equations (3.1) and (3.2), the IVM equation reads:

$$\Delta v_p = \frac{P_{sat,0} M}{\rho_p R T_0}\left[\exp\left(-\frac{\Delta H}{R}\left(\frac{1}{T_1} - \frac{1}{T_0}\right)\right) - 1\right] \tag{3.3}$$

For a multi-component aerosol, in a solution, the saturation pressure of component i is given by:

$$P^*_{sat,i} = x_i \gamma_i P_{sat,i} \tag{3.4}$$

where x_i is the mole fraction of the component, γ_i is the activity coefficient, and $P_{sat,i}$ is the saturation pressure of the pure component.

The change in volume of component i can be obtained by substituting equation (3.4) in equation (3.1):

$$\Delta v^*_{p,i} = \frac{M_i}{\rho_{p,i} R T_0}\left(x_{i,1}\gamma_{i,1} P_{sat,i,1} - x_{i,0}\gamma_{i,0} P_{sat,i,0}\right) \tag{3.5}$$

The change in total volume of the multi-component aerosol is written as:

$$\Delta v_{p,tot} = \sum \Delta v^*_{p,i} \tag{3.6}$$

3.2.2 Algorithm to calculate activity coefficients

The following iterative algorithm is used to calculate activity coefficients of the individual components in the mixture. The main steps of the algorithm involve estimating mole fraction of the components (section 3.2.2.1), then estimating the activity coefficients (3.2.2.2), after which the procedure is repeated until convergence. Since the molecular mass of organics in ambient extracts is not known, calculations for the adipic acid – "ambient" mixtures involve estimation of the activity-weighed average molecular weight of the ambient extracts (section 3.2.2.3). Individual stages of the algorithm are described below.

3.2.2.1 Mole fraction calculation

The mole fractions of the components in the mixture change upon evaporation because the more volatile species evaporates more than the less volatile. The final equilibrium mole fractions can be estimated as follows.

Assume that we have an aerosol composed of a binary mixture of species *A* and species *B* initially at equilibrium at T_0 (state "0"); the aerosol is then brought to equilibrium at a higher temperature T_1 (state "1"). Conservation of mass requires that the total mass of the species in the particle and gas phase at state"0" is equal to that at state "1":

$$C_{A,0} + \gamma_A x_{A,0} C_{sat,A,0} = C_{A,1} + \gamma_A x_{A,1} C_{sat,A,1} \tag{3.7}$$

$$C_{B,0} + \gamma_B (1 - x_{A,0}) C_{sat,B,0} = C_{B,1} + \gamma_B (1 - x_{A,1}) C_{sat,B,1} \tag{3.8}$$

where C is the molar concentration in the particle phase, and C_{sat} is the saturation molar concentration. For this stage of calculations, γ is assumed to be constant over the range of mole fractions.

Knowing that $C_B = \frac{1 - x_A}{x_A} C_A$ (since $x_A = \frac{C_A}{C_A + C_B}$ and $x_B = \frac{C_B}{C_A + C_B}$), equation (3.7) and equation (3.8) can be combined to obtain the following quadratic equation in the final mole fractions:

$$\begin{aligned} &\left[\gamma_B C_{sat,B,1} - \gamma_A C_{sat,A,1}\right] x_{A,1}^2 \\ &+ \left[C_{A,0} + C_{B,0} + \gamma_A x_{A,0} C_{sat,A,0} + \gamma_B (1 - x_{B,0}) C_{sat,B,0} + \gamma_A C_{sat,A,1} - \gamma_B C_{sat,B,1}\right] x_{A,1} \\ &+ \left[-C_{A,0} - \gamma_A x_{A,0} C_{sat,A,0}\right] = 0 \end{aligned} \tag{3.9}$$

3.2.2.2 Activity coefficients

To estimate activity coefficients in binary mixtures, we use the empirical Van Laar equation (Smith and Van Ness, 1987):

$$\ln \gamma_1 = \frac{A}{\left[1 + \frac{A x_1}{B x_2}\right]^2} \quad \text{and} \quad \ln \gamma_2 = \frac{B}{\left[1 + \frac{B x_2}{A x_1}\right]^2} \tag{3.10}$$

where A and B are experimentally obtained fit parameters.

Equation (3.10) is substituted in equation (3.6), which is used as a model fit for the experimental data - $\Delta v_{p,tot}$ vs x – to obtain the parameters A and B; activity

coefficients are then calculated using equation (3.10). Finally, equation (3.9) is used to update the values of the mole fractions.

This procedure constitutes one iteration, and is repeated until convergence.

3.2.2.3 Estimation of molecular weight of organic components in ambient extracts

A recent field study on the chemical composition of $PM_{2.5}$ in the Research Triangle Park area performed by EPA (Lewandowski et al, 2007) reported 41% organic matter, 2% elemental carbon, 12% ammonium, 37% sulfate, and 1% nitrate and oxalate. 50% of the organics were found to be water-soluble (WSOC); other field studies have also reported WSOC concentrations of 30% - 70% of the total organics (Sempere and Kawamura, 1994; Mader et al., 2004).

For the purpose of this research, we assume that 50% of the ambient extracts are inorganic salts and 25% are WSOC, with densities of 1.8 g/cm^3 and 1.3 g/cm^3 respectively. Thus, WSOC constitutes 40% of the total aerosol volume in the aqueous extract. Adipic acid is assumed to interact only with the organic fraction of the ambient extracts to form solution. We base this assumption on our experimental findings which show that adipic acid does not form solution with ammonium sulfate in a binary mixture; discussion on the validity of this assumption is given in section 3.3.2. The organic fraction is lumped together, and is assigned a molar mass of M_{amb}, which is estimated in the following fashion.

Assuming volume additivity, the mole fraction of adipic acid in the mixture can be expressed as:

$$x_a = \frac{n_a}{n_a + n_{amb}} = \frac{\rho_a V_a / M_a}{\rho_a V_a / M_a + \rho_{amb} V_{amb} / M_{amb}} \tag{3.11}$$

Where, V_a and V_{amb} are the volumes of adipic acid and organic ambient extract in the aerosol, M_a and M_{amb} are the molar masses, and ρ_a and ρ_{amb} are the densities. The molar mass of the organic ambient extract can be isolated from equation (3.11):

$$M_{amb} = \frac{\rho_{amb}}{\rho_a} \frac{V_{amb}}{V_a} M_a \left(\frac{1}{x_a} - 1 \right)^{-1} \tag{3.12}$$

Equation (3.12) is incorporated in the iteration scheme to estimate M_{amb}.

3.2.2.4 Uncertainty analysis

The parameter measured in our experiments is the total change in aerosol volume, $\Delta v_{p,tot}$. The error in the measurements is random, and is assumed to be normally distributed with a standard deviation of $\sigma_{\Delta v}$. To estimate the effect of error propagation in our model, we perform 100 model runs, each with a perturbed $\Delta v_{p,tot}$ defined as:

$$\Delta v_{p,tot}^{perturbed} = \Delta v_{p,tot} + \phi \sigma_{\Delta v} \tag{3.13}$$

Where ϕ is a vector of random variables with elements $-1 < \phi_i < +1$.

Results from the 100 model runs are used to calculate means and standard deviations of the activity coefficients.

3.3 Results and discussion

3.3.1 Adipic acid – pimelic acid

Figure 3.1-a shows the total change in aerosol volume of adipic acid – pimelic acid mixtures versus adipic acid mole fraction; also shown is the theoretical fit based on the model described in section 3.2.2.1, and the envelopes obtained by the uncertainty analysis as outlined in section 3.2.2.4.

The points where adipic acid mole fraction is equal to 1 and 0 represent the change in saturation vapor pressure (as expressed in terms of aerosol volume change) of pure adipic acid and pimelic acid, respectively. Although it might be expected that pimelic acid (a C-7 diacid) should be less volatile than the smaller (C-6) adipic acid, the odd-number acids tend to have higher vapor pressures (Bilde et al., 2003). It should be noted that saturation vapor pressures of pimelic acid and adipic acid measured with the IVM agree very well with other studies (Saleh et al., 2008). For example, the saturation vapor pressure of pimelic acid measured with the IVM is 0.76×10^{-4} Pa at 25°C and 5.1×10^{-4} Pa at 35°C, as compared to 0.72×10^{-4} Pa at 25°C and 5.2×10^{-4} Pa at 35°C based on Bilde et al. (2003) data.

Observing the change in aerosol volume at different adipic acid mole fractions makes it clear that the adipic acid and pimelic acid interact with each other in the mixture, i.e. form a "solution", because the volume change (Δv) of the mixtures lies below the sum of the volume changes of the pure components. If the substances were not interacting, the resulting change in aerosol volume would have been the sum of those of pure compounds (around 110 $\mu g/m^3$) for all mole fractions, since there would be no decrease in equilibrium vapor pressure.

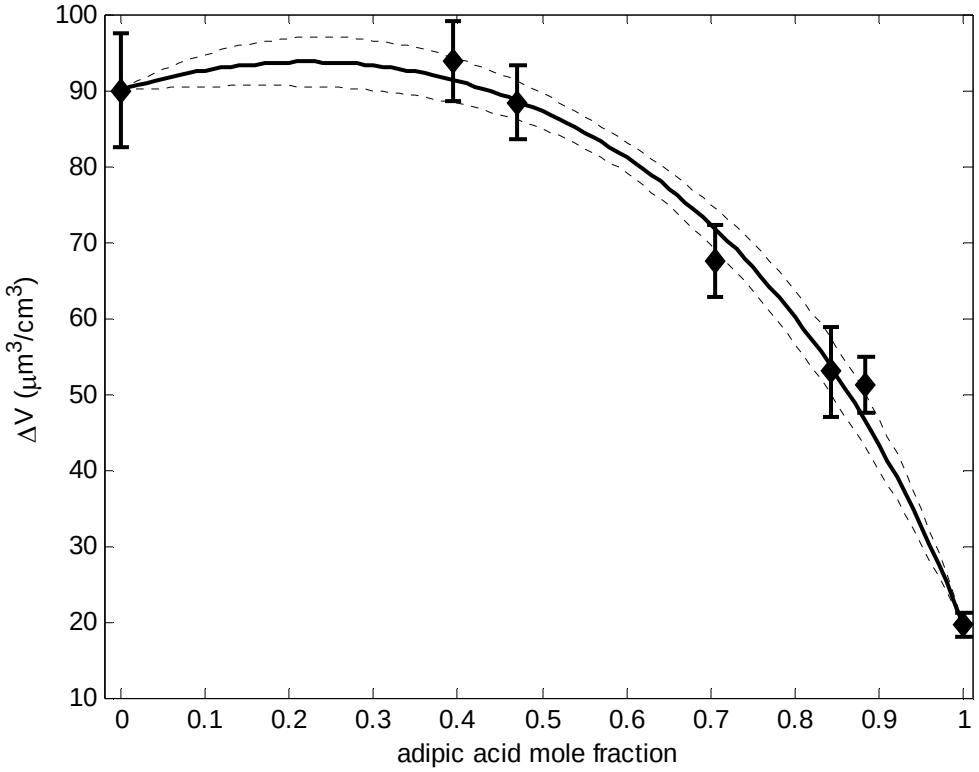

Figure 3.1-a: Change in total aerosol volume for adpic acid – pimelic acid mixtures between 25 ^{0}C and 35 ^{0}C. The solid line is the fit based on the model described in section 3.2.2.1. The dotted lines are uncertainty envelopes, based on the analysis in section 3.2.2.4

The evaporation of this binary mixture aerosol cannot be described by Raoult's law. If the mixture were ideal, the resulting change in volume would have been the molar fraction – weighed Δv of the pure compounds (as implied by equations 5 and 6), and the data points would lie on a straight line connecting the points representing pure substances. To account for the non-ideal behavior, activity coefficients for both compounds need to be incorporated in the analysis using the model given in section

3.2.2. Values of the activity coefficients as a function of adipic acid mole fraction are shown in Figure 3.2-b, along with the envelopes defined by the uncertainty analysis. For both acids, the maximum uncertainties occur at infinite dilution, with numerical values of 22% and 17% for pimelic acid and adipic acid respectively.

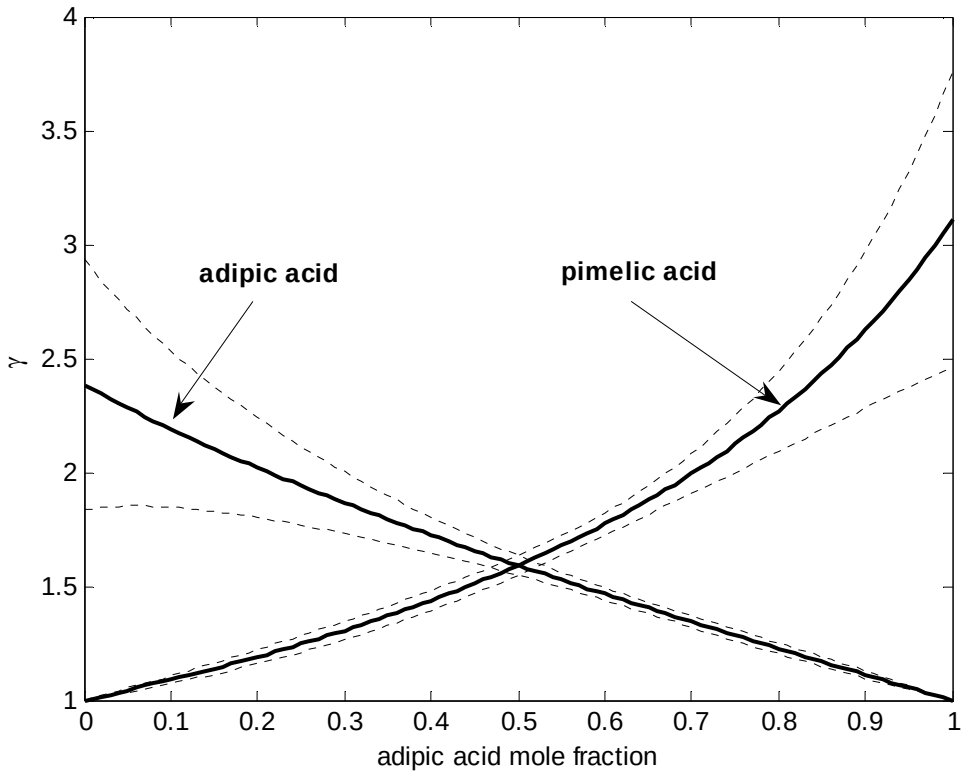

Figure 3.1-b: Activity coefficients for adipic acid and pimelic acid when present in a binary solution, based on the model described in section 3.2.2. The dotted lines are uncertainty envelopes, based on the analysis in section 3.2.2.4

It should be noted that in this study we had no means to determine whether the compounds are in a solid or a subcooled liquid solution. Therefore, we can not attribute

the observed values of the activity coefficients to one or the other state. However, the mixtures were most probably in a solid state, because the melting point depression for any of the two compounds is expected to be not more than about 10 ^{o}C for the range of molar fractions tested in our experiments. Because the melting points of adipic acid and pimelic acid are, respectively, 152 ^{o}C and 104 ^{o}C (Linstrom and Mallard, 2009), the mixture should remain solid at the temperature of our experiments (35 ^{o}C).

The condition of the particles (solid or liquid) can affect the calculation of the activity coefficients. If the particles are solid, diffusion limitations may cause a radial gradient of chemical composition within the particles. The solid-state diffusion coefficients of the acids are of the order of 10^{-14} m^2/s (Lide, 2007). The corresponding mixing time scale for 100 nm particles, the VMD of our aerosol distribution, can be estimated using $\tau \approx r^2/D$ (in which τ is the characteristic time, r is the particle radius and D is the diffusion coefficient) to be of the order of 1 s. Therefore, it is reasonable to assume that the average residence time in our thermodenuder (30 s) is long enough to have a fairly uniform composition within the particles and, thus, to assume that the diffusion limitation within particles have a negligible effect on the calculated values of activity coefficients.

The non-uniform distribution of points along the x-axis in Fig 2-a is explained by the difficulty of producing aerosol with a high mole fraction of pimelic acid. The reason

is that for the temperature change in this experiment (25 ^{o}C to 35 ^{o}C), pimelic acid undergoes a larger relative increase of P_{sat} than adipic acid (in terms of aerosol volume change: Δv is 90 $\mu m^3/cm^3$ for pure pimelic acid versus 20 $\mu m^3/cm^3$ for pure adipic acid). Therefore, more pimelic acid is evaporated from the particles relative to the less volatile adipic acid, decreasing its mole fraction in the particle phase. At high aerosol concentrations (relative to the change in vapor pressure concentrations) the change in aerosol composition after the re-equilibration is small. However, to keep the concentrations such that the CPCs in the SMPS systems are not overloaded, we had to work at concentration levels which cause an appreciable change in aerosol composition, especially at the high mixing ratios of the more volatile compound. This makes it difficult to obtain data points for low adipic acid mole fractions, which is the reason for the non-uniform distribution of experimental data points. This problem can be alleviated by installing a dilution system in front of the SMPS to avoid overloading at high concentration.

We have compared the measured activity coefficients with the UNIFAC group contribution method (Fredenslund et al., 1975) predictions. The activity coefficients predicted by the UNIFAC were 1.02 or lower, significantly below the values observed in this study. Although it would be expected that mixtures of dicarboxylic acids should exhibit activity coefficients close to unity given the similarity in structure, activity

coefficients much different than one were also observed in multi-component dicarboxylic acid mixtures (Cappa et al., 2008).

3.3.2 Adipic acid – dioctyl sebacate and adipic acid – ammonium sulfate

Pure dioctyl sebacate did not exhibit measurable volume change when heated from 25 ^{0}C to 35 ^{0}C, and it can thus be assumed to be non-volatile in this temperature range; consequently dioctyl sebacate is not expected to partition to the gas phase. Adipic acid on the other hand is expected to partition, but, as depicted in Figure 3.2, partitioning of adipic acid (change in total aerosol volume) is not affected by the presence of dioctyl sebacate. This leads to the conclusion that the two species do not form a solution, which is expected since adipic acid is polar while dioctyl sebacate is non-polar. This was confirmed by attempting to dissolve adipic acid crystals in pure dioctyl sebacate oil: the crystals did not dissolve even at ratios higher than used in this study. It should be noted, that the sebacate / adipic acid aerosol was produced by nebulizing and drying an ethanol solution of these compounds as described in section 3.1. Both compounds formed a uniform mixture with ethanol (i.e. no suspension or physical separation of phases was observed). Therefore, the aerosol produced by atomizing this solution is internally mixed, i.e. both compounds are present in each particle. The fact that no interaction between the compounds was observed means that the oil and the acid were in separate phases in each particle.

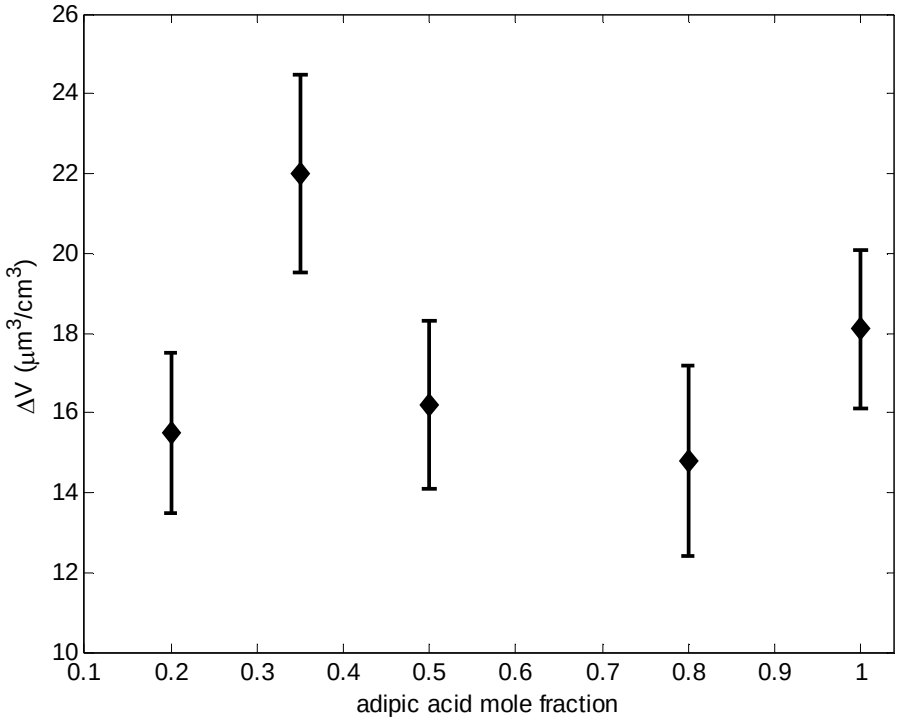

Figure 3.2: Change in total aerosol volume for adipic acid – dioctyl sebacate mixtures between 25 ^{0}C and 35 ^{0}C.

Ammonium sulfate is also non volatile in the temperature range of our experiments. Similar to dioctyl sebacate, our data suggest that ammonium sulfate did not form a solution with adipic acid. As shown in Figure 3.3, there is no suppression or enhancement of the evaporation of adipic acid. It is interesting to note that Cappa et al. (2008) observed mutual dissolution of sodium nitrate and several dicarboxylic acids. One reason for this discrepancy can be that in our binary aerosol ammonium sulfate and adipic acid were present in the same particles, but, apparently, in separate crystalline

phases, while in the Cappa et al. (2008) study the multi-component mixture was in subcooled liquid state, which may have promoted dissolution and interaction of sodium nitrate in the mixture. Another possible reason for discrepancy is that different inorganic salts behave differently; consequently, interaction between organic and inorganic fractions in ambient aerosols could be particle size dependent: ammonium sulfate is a dominant inorganic component in fine aerosol, while sodium nitrate is found mostly in coarse particles.

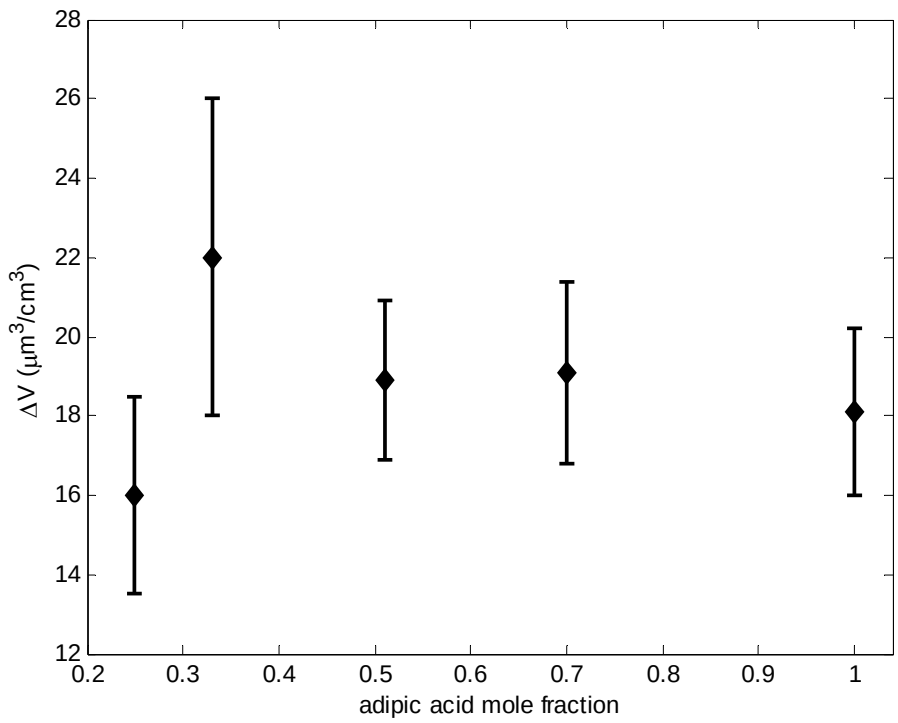

Figure 3.3: Change in total aerosol volume for adipic acid – ammonium sulfate mixtures between 25 ^{0}C and 35 ^{0}C.

These experiments indicate that compounds present in ambient or smog chamber aerosols might not form solution. The implication is that when estimating partitioning of individual compounds, or classes of compounds, activities need to be calculated with respect to the solutions they are part of, and not the whole mass of the aerosol. However, these findings are not conclusive because compounds that do not dissolve each other in a binary mixture might still form solution in a more complex matrix.

3.3.3 Adipic acid – ambient extracts

Figure 3.4-a shows the total change in aerosol volume of adipic acid – ambient matrix mixtures versus adipic acid mole fraction. The volume change of the pure ambient extract (0.7 $\mu m^3/cm^3$) is not shown on the Figure in order to emphasize the region where most of the measurements were performed (adipic acid mole fractions higher than 0.7). The reason why there are no data points for adipic acid mole fraction of less than 0.7 is that the concentration of ambient extract was too low to produce more points. Our experimental setup requires about 150 ml of solution per experiment. The solution should be concentrated enough to produce an aerosol concentration that would be sufficient to saturate the gas stream at the temperature of our experiments. Because the ambient extract concentration was rather low, we could not dilute the extract to produce enough aerosol volume for experiments at lower adipic acid fractions. This is a limitation of the method, which can be solved by collecting a larger ambient aerosol

sample (i.e. by sampling higher ambient aerosol concentrations and / or for longer period of time).

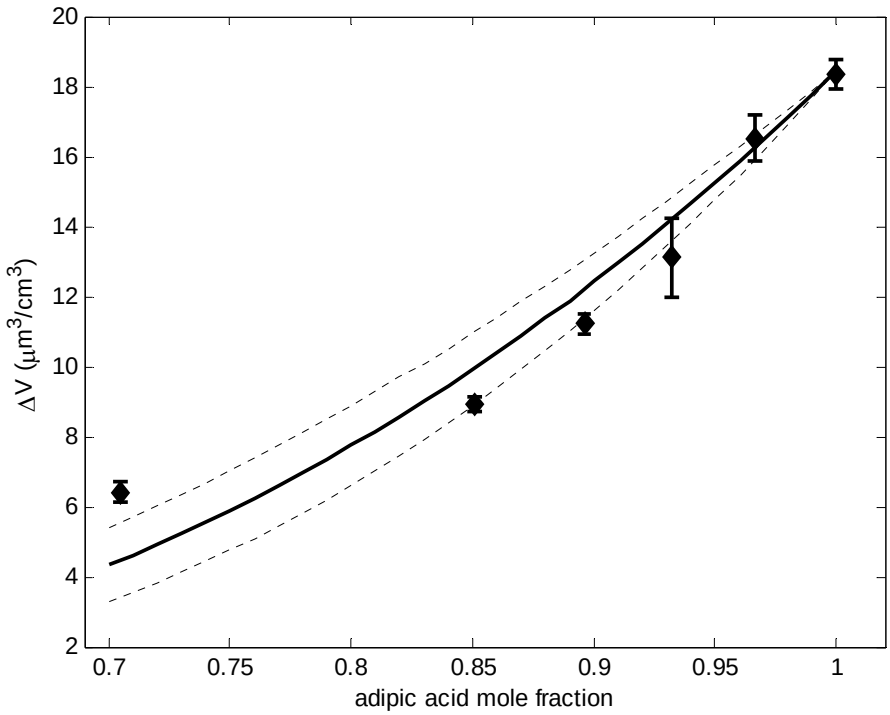

Figure 3.4-a: Change in total aerosol volume for adipic acid – ambient extracts mixtures between 25 ^{0}C and 35 ^{0}C. The solid line is the fit based on the model described in section 3.2.2. The dotted lines are uncertainty envelopes, based on the analysis in section 3.2.2.4. The volume change of the pure ambient extract (0.7 μm^3/cm^3) is not shown, but was taken into account when calculating the fit and the uncertainty envelopes.

Figure 3.4-a also shows the theoretical fit based on the model described in section 3.2.2, and the envelopes defined by the uncertainty analysis as outlined in section 3.2.2.4. Though the point of pure ambient extract is not included in Figure 3.4-a, it was used in

calculating the fit and the uncertainty bounds. It is clear that the behavior of adipic acid in the ambient aerosol matrix is highly non-ideal, with activity coefficients significantly lower than 1 (Figure 3.4-b).

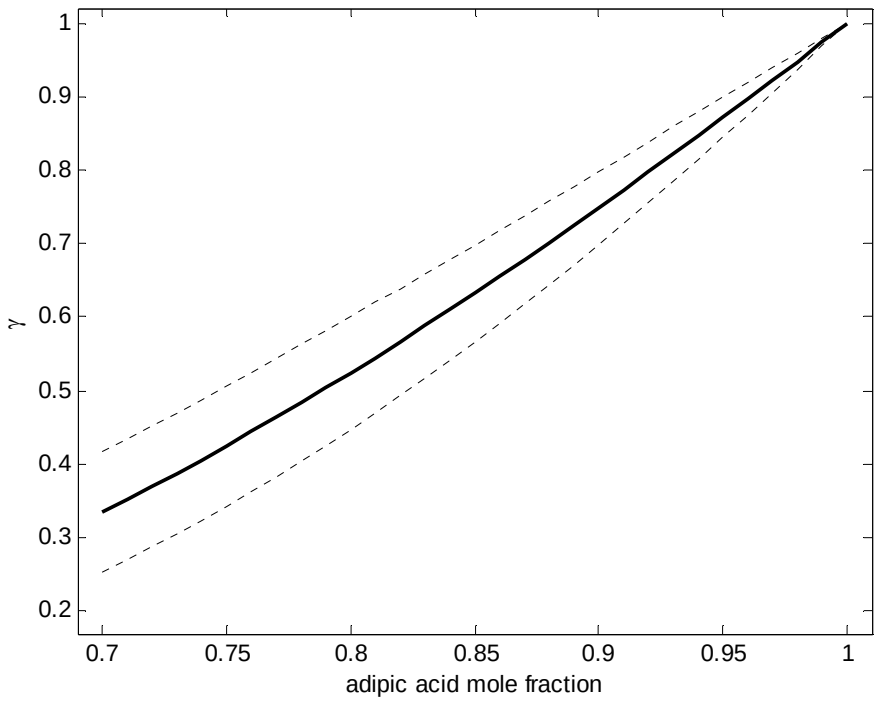

Figure 3.4-b: Activity coefficients for adipic acid when present in a solution with ambient extracts, based on the model described in section 3.2.2. The dotted lines are uncertainty envelopes, based on the analysis in section 3.2.2.4

Using the analysis described in section 3.2.2.3, we obtained an effective ambient WSOC molar mass of 176 ± 26 g/mol. This value depends on the assumption that the volume fraction of WSOC in the aerosol is 40%. Assuming WSOC volume fractions of 30% and 50% gives molar masses of 149 ± 10 g/mol and 212 ± 40 g/mol respectively.

These values are not meant to be quantitative estimates; however, they might suggest that the compounds constituting WSOC in our samples are mostly high molar mass multifunctional compounds. The estimated molecular weight is within the range reported for water soluble organic aerosol. Ambient samples from K-pustza and Jungfraujoch were reported to have average molecular weights in the range 200-300 g/mol (Kiss et al., 2003, Krivácsy et al., 2001).

Saxena and Hildemann (1996) reported that the major constituents of WSOC in atmospheric aerosols are C2 to C7 multifunctional compounds. The compounds suggested by Saxena and Hildemann have saturation pressures at 25 ^{0}C comparable to those of adipic and pimelic acid or (up to several orders of magnitude) higher. Their selection of compounds seems to contradict our observations: the aerosol generated from the ambient aqueous extract has very low volatility compared to pure adipic acid and pimelic acid. The total volume change of the ambient matrix at thermodenuder set-temperature of 35 ^{0}C is 0.7 $\mu m^3/cm^3$ versus 18 $\mu m^3/cm^3$ for adipic acid and 90 $\mu m^3/cm^3$ for pimelic acid. Since the change in volume observed in our experiments is the average volatility of all the components in the mixture, the measurements show that the WSOC portion of the ambient aerosol is less volatile than the components proposed by Saxena and Hildemann. Our results (both the volatility and molecular weight) are more consistent with longer chain dicarboxilic acids (such as azelaic acid) or C8-C10 polyols.

On the other hand, the compounds selected by Saxena and Hildemann have been observed in ambient aerosols (Grosjean et al., 1978; Kawamura and Kaplan, 1987; Sempere and Kawamura, 1994; Rogge et al, 1993). The behavior of adipic acid when in mixture with the WSOC ambient matrix observed in this study shows activity coefficients significantly lower than one (Figure 6), which agrees with the findings of Cappa et al. (2008) for lab generated multicomponent dicarboxylic acid mixtures. This suggests that evaporation of adipic acid is strongly reduced in the ambient matrix, which would shift its partitioning to the aerosol phase. Whether such behavior is observed for other dicraboxylic acids and other ambient aerosol matrices was beyond the scope of this study and needs to be investigated.

3.4 Conclusions

This chapter demonstrates the application of the integrated volume method to estimate activity coefficients of binary organic mixtures pertinent to ambient/atmospheric aerosols. The method is applied to adipic acid – pimelic acid as an example for polar – polar organic mixtures, adipic acid – dioctyl-sebacate as an example for polar – non-polar mixtures, adpic acid – ammonium sulfate as an example of polar organic – inorganic mixtures, and adipic acid – ambient extracts to illustrate application to realistic ambient systems. Adipic acid – pimelic acid mixture exhibited highly non-ideal behavior with activity coefficients of about 3 at infinite dilution, which stresses the

importance of activity coefficients in portioning of semi-volatile organics in ambient aerosols. On the other hand, adipic acid – dioctyl-sebacate and adipic acid – ammonium sulfate mixtures did not form a solution; adipic acid partitioned to the gas phase in the same manner as in the pure case. Care needs to be taken when calculating mole fractions of compounds in ambient or smog chamber aerosols to estimate their activities, since an aerosol particle might be comprised of multiple phases/solutions depending on the affinities of the species. When mixed with ambient extracts, adipic acid exhibited activity coefficients significantly less than unity, which suggests that the volatility of this compound could be strongly suppressed in ambient aerosol, favoring its partitioning to the aerosol phase. The tested water extract of ambient aerosol exhibited behavior consistent with average molecular weight of about 180 g/mol and average volatility of C8 – C10 dicarboxylic acids.

4. Effect of aerosol generation method on measured thermodynamic properties

In this chapter, we investigate the effect of residual solvent on saturation pressure and enthalpy of vaporization obtained for C-6 (adipic) and C-9 (azelaic) dicarboxylic acid aerosols generated by two methods: 1) atomization and drying of aqueous solutions, and 2) homogenous condensation of organic vapor. Because the second method involves no solvent, it provides a control condition in which any potential solvent effect has been eliminated. A comparison of the thermodynamic properties measured with the two generation methods provides a measure of the effect of retained water, if any is present in the particles. The P_{sat} and ΔH were determined using the Integrated Volume Method (IVM) (Saleh et al., 2008). We also obtained SEM images of the aerosol particles produced by the two methods to compare their morphology.

4.1 Methods

The experimental setup is shown in Figure 4.1. It consists of an aerosol generation system, two Scanning Mobility Particle Sizer (SMPS) systems, and a thermodenuder. The individual parts of the set-up are described in separate sections below.

4.1.1 Aerosol generation

The aerosol was generated by two different techniques: 1) the conventional aqueous solution atomization and 2) homogeneous condensation. For the former, 0.1 wt % aqueous (in de-ionized 18 MΩ water) solutions of the dicarboxylic acids were atomized using a 6-jet atomizer (TSI, model 9306). Two out of the 6 jets were operated and the aerosol flowrate was 3 SLPM, while the dilution flowrate was set to 15 SLPM (the dilution system is integral to the atomizer). The purpose of dilution flow (particle-free and < 10% RH) was to decrease the particle number concentration to within the detection limit of our SMPS systems, as well as to dry the aerosol. A flow of 2 SLPM was drawn from the diluted stream through a diffusion-dryer for additional drying, while the excess was sent to exhaust. Typically, the Volume Median Diameter (VMD) of the aerosol particles was approximately 180 nm, the total volume concentration was approximately 200 $\mu m^3/cm^3$, and the geometric standard deviation (σ_g) was approximately 1.8.

For the homogeneous condensation generation method, a Condensation Monodisperse Aerosol Generator (CMAG, TSI, model 3475) was utilized. Although the conventional use of the CMAG is to generate monodisperse aerosols by condensation on seed particles, it can also be operated without seed particles to produce a polydisperse aerosol by homogeneous nucleation. For a material that is solid at room temperature, the

CMAG operating procedure normally entails heating the material to above its melting point and bubbling a controlled flow of nitrogen through the liquid in a saturator. The vapor-laden nitrogen then passes through a condenser where it cools to room temperature, causing super-saturation and subsequent nucleation of aerosol particles. For the purposes of this study, we used a sublimation technique in which the nitrogen flowed over a bed of solid acid crystals instead of bubbling through melted acids. This modification had two benefits. First, it allowed acid vapor generation at relatively low temperatures, thus avoiding thermal degradation (preliminary experiments at temperatures slightly above melting point with adipic acid caused discoloration of the acid upon re-solidification). Second, with sublimation we were able to obtain aerosol concentrations within the detection limit of our sizing system without the need for dilution.

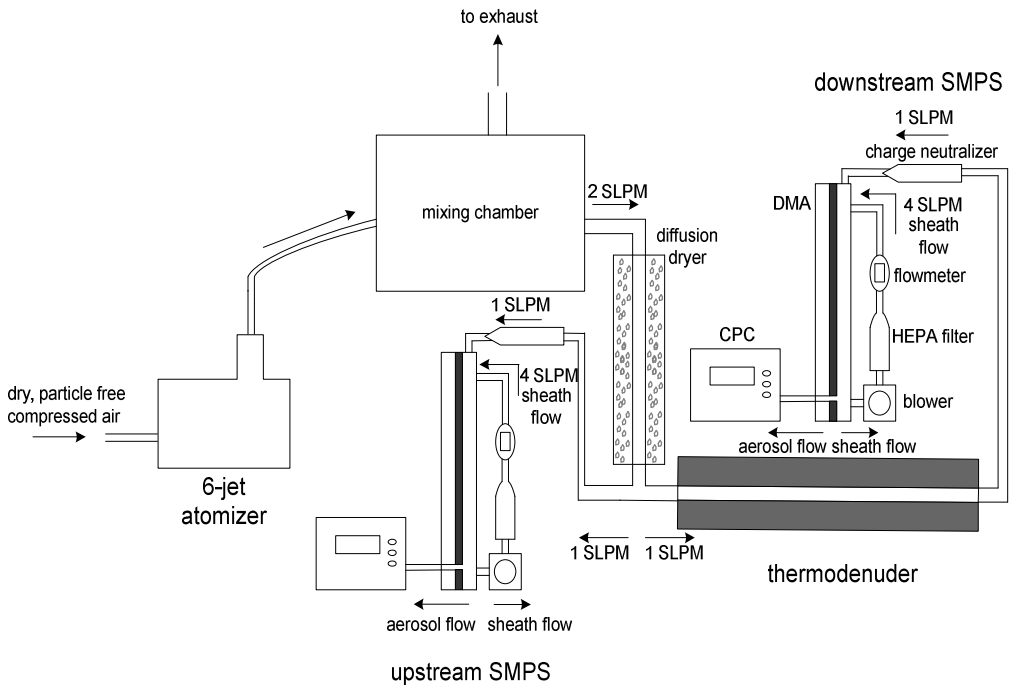

Figure 4.1: Schematic of IVM experimental setup. For homogeneous condensation, the 6-jet atomizer is replaced with a CMAG, and the diffusion dryer is removed

The CMAG was operated with total and bypass nitrogen flows of 3.6 SLPM and 0.25 SLPM respectively. The optimum saturator temperature that produced a large enough aerosol concentration with a size distribution within the detection limit of our sizing system was found by trial and error to be approximately 140 ^{0}C for adipic acid and 100 ^{0}C for azelaic acid. A flow of 2 SLPM was drawn for sampling, while the excess was sent to exhaust. VMD of the aerosol ranged between 150 nm and 200 nm, the total volume concentration between 150 $\mu m^3/cm^3$ and 250 $\mu m^3/cm^3$, and σ_g between 1.7 and 1.8.

4.1.2 Aerosol sizing and conditioning

The 2 SLPM aerosol flow was split into two 1 SLPM lines. One was sampled for reference measurements by the upstream SMPS, and the other was sent through a thermodenuder of 1 m length and 3.5 cm inner diameter. The final size distribution was measured by the downstream SMPS. The thermodenuder was heated to a desired maximum temperature and then allowed to cool down gradually to room temperature; the upstream and the downstream aerosol size distributions as well as the thermodenuder temperature were continuously measured and recorded from the onset of cooling. The average residence time in the thermodenuder was 58 s. As described in Saleh et al. (2008), IVM requires that the time required for the aerosol to reach equilibrium should be less than the residence time in the thermodenuder. To confirm that equilibrium was achieved at the reference state, the total particle volume was measured at reference temperature by the upstream SMPS and the downstream SMPS (after the aerosol has spent an extra 58 s in the thermodenuder) and found to be equal to within instrument uncertainty (~20%). To verify the equilibration assumption in the thermodenuder we used the evaporation kinetics model described in Saleh et al. (2008) to estimate equilibration times of our test aerosols over the range of experimental temperatures. The particle size distributions used in the simulations are given in section 4.1.1 for both atomization and homogeneous nucleation techniques. The value of

evaporation coefficient used for adipic acid was 0.08 (Saleh et al., 2009). While the evaporation coefficient of azelaic acid has not been previously reported, our recent measurements of evaporation coefficient for adipic, pimelic, and succinic acids, suggest that the evaporation coefficients of dicarboxylic acids in air are of the order 10^{-1}. For the purpose of the simulations, we assumed a value for the evaporation coefficient of azelaic acid to be equal to that of adipic acid. The simulations predicted equilibration times of less than 30 s for all cases, which is considerably less than the 58 s residence time of the thermodenuder. Detailed analysis on equilibration in thermodenuders is presented in the next chapter.

4.1.3 The integrated volume method

The thermodynamic properties of the test compounds were determined using the Integrated Volume Method (IVM), which is described in detail in Chapter 2. Briefly, the IVM uses temperature dependent aerosol volume changes to derive the saturation vapor pressure, P_{sat}, and enthalpy of vaporization, ΔH, of the test compound. The integrated aerosol volume changes, Δv_p, are measured at several temperatures and the results are fit into the following equation to obtain P_{sat}, and ΔH:

$$\Delta v_p(T) = \frac{P_{sat} M}{\rho_p R T_0}\left[\exp\left(-\frac{\Delta H}{R}\left(\frac{1}{T}-\frac{1}{T_0}\right)\right)-1\right] \tag{4.1}$$

in which T is the thermodenuder temperature, and T_0 is the reference temperature, M is the molecular weight of the compound, ρ_p is the particle density (1360 kg/m^3 and 1225 kg/m^3 for adipic and azelaic acid respectively) , R is the universal gas constant.

The IVM is advantageous in that the aerosol is investigated at equilibrium. Therefore, knowledge of other properties associated with the evaporation kinetics, namely the diffusion coefficient, surface free energy, and evaporation coefficient, is not required to estimate P_{sat} and ΔH. In contrast, methods that employ evaporation kinetics such as the Tandem Differential Mobility Analyzer (TDMA) method (Tao and McMurry, 1989; Bilde et al., 2003) and Temperature Programmed Desorption (TPD) method (Cappa et al., 2007 & 2008), normally require the assumption that the evaporation coefficient is unity when estimating P_{sat}.

4.1.4 SEM imaging

Samples for SEM imaging were collected on 47 mm Nuclepore Polycarbonate filters which were inserted downstream of the aerosol generators (downstream of the diffusion dryer in the case of aqueous solution atomization). Sampling times were 1 - 3 hours at 1 SLPM.

Square 1 cm × 1 cm sections were cut out of the filters and mounted on the SEM stubs. Prior to imaging, the samples were coated with gold to enhance conductivity and suppress potential volatilization at the low operating pressure of the SEM.

4.2 Results and discussion

4.2.1 Saturation pressures and enthalpies of vaporization

Plots of the integrated aerosol volume change versus the inverse of thermodenuder temperature obtained from the IVM experiments are depicted in Figure 4.2 for aerosol generated by aqueous solution atomization and by homogeneous condensation. Also shown are the theoretical fits based on equation (4.1), where $P_{sat,0}$ and ΔH are fitting parameters. For adipic acid, we obtained $P_{sat,0}$ of 3.3×10^{-5} ($\pm0.9\times10^{-5}$) Pa and ΔH of 132 (±8) kJ/mol with atomization, and $P_{sat,0}$ of 4.2×10^{-5} ($\pm2.2\times10^{-5}$) Pa and ΔH of 126 (±21) kJ/mol with homogeneous condensation. For azelaic acid, we obtained $P_{sat,0}$ of 1.4×10^{-5} ($\pm0.5\times10^{-5}$) Pa and ΔH of 145 (±15) kJ/mol with atomization, and $P_{sat,0}$ of 0.9×10^{-5} ($\pm0.3\times10^{-5}$) Pa and ΔH of 158 (±17) kJ/mol with homogeneous condensation.

It should be noted that the IVM experiments in this study were performed with a different SMPS / thermodenuder system than in Saleh et al. (2008) (Chapter 2). The excellent agreement in $P_{sat,0}$ and ΔH (Table 4.1) obtained with the 2 different experimental setups is thus assuring.

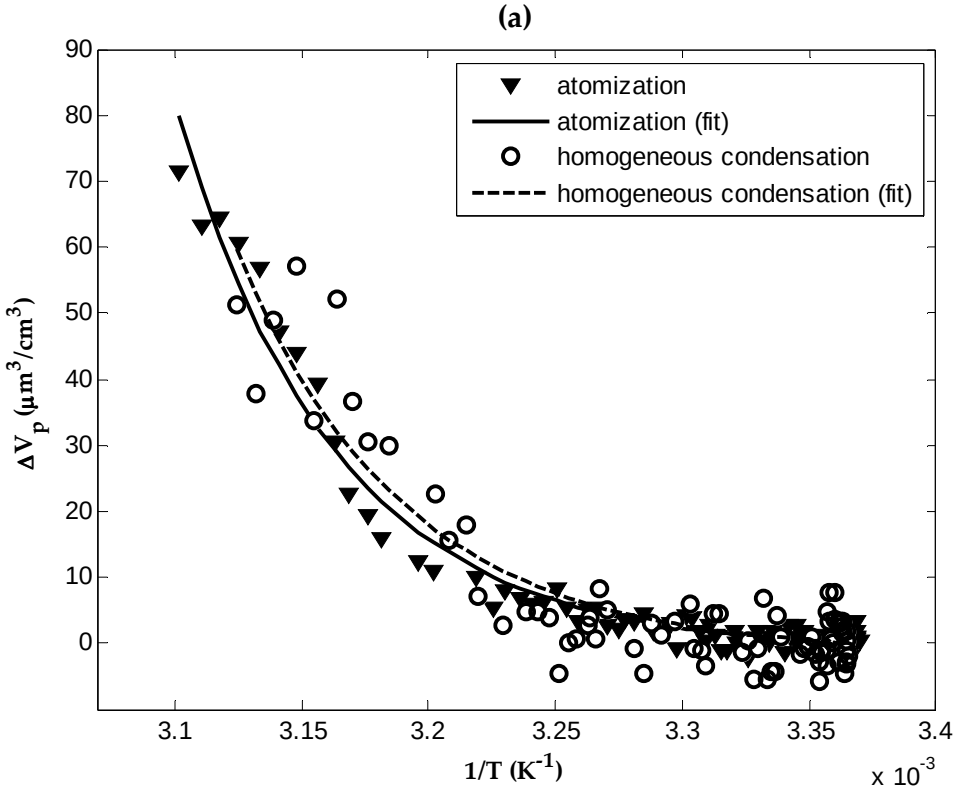
(a)
atomization
atomization (fit)
homogeneous condensation
homogeneous condensation (fit)
ΔV_p (μm³/cm³)
1/T (K⁻¹)
x 10⁻³
90
80
70
60
50
40
30
20
10
0
3.1
3.15
3.2
3.25
3.3
3.35
3.4

Figure 4.2

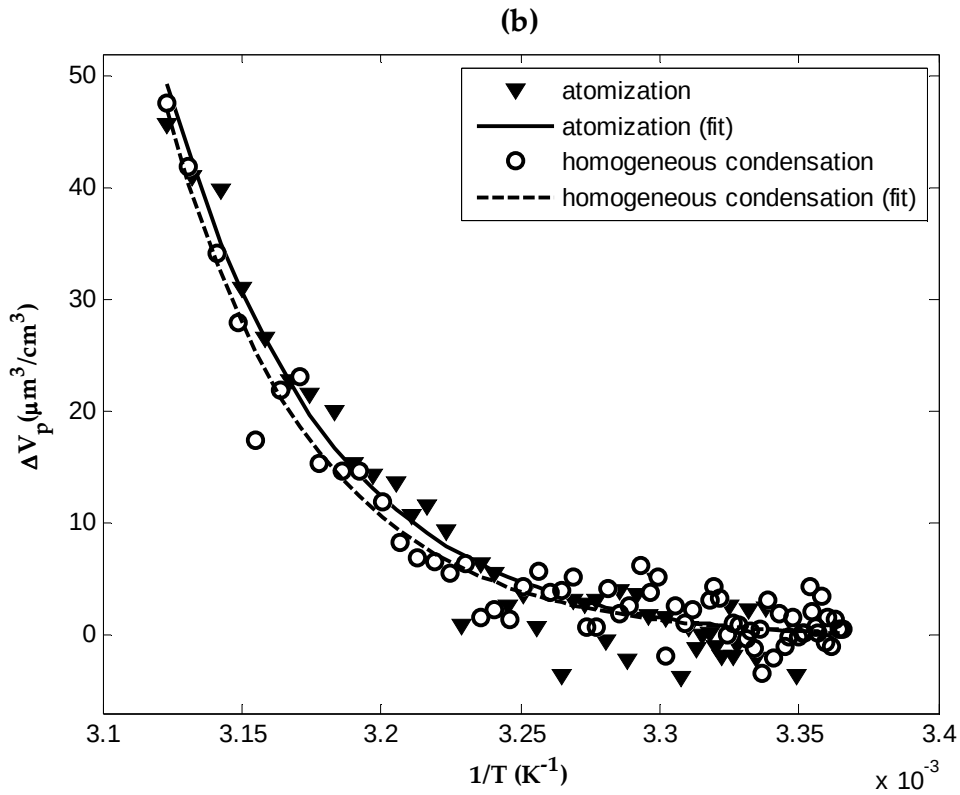

Figure 4.2 (continued): Measured change in total volume concentration of adipic acid (a) and azelaic acid (b) aerosol particles versus inverse of set-temperature

As shown in Figure 4.2-a and Figure 4.2-b, both adipic acid and azelaic acid exhibit similar total particle volume change as a function of temperature when using either of the two aerosol generation methods. Consequently, the values obtained for $P_{sat,0}$ and ΔH (Table 4.1) are within the experimental uncertainty. This indicates that the quantity of residual water in the aerosol when generated by conventional atomization and drying, if any, is insufficient to significantly impact the thermodynamic properties of the investigated dicarboxylic acids. This seems to contradict the observation of Cappa

et al. (2007) that when they pre-heated the atomized aerosol, the measured $P_{sat,0}$ decreased by an order of magnitude, which was attributed to retained solvent. At the simplest level, this contradiction can be due to inadequate drying in the aerosol generation setup employed in Cappa et al. (2007), leaving the particles with an amount of residual solvent substantial enough to cause bias in measured $P_{sat,0}$. Another potential reason for this discrepancy is that the observed pre-heating effect in Cappa et al. (2007) was not due to the presence of solvent, but that pre-heating-induced evaporation changed the size, and possibly the shape, of the particles, which were deposited to form a cone-shaped mound from which evaporation rate was measured. The surface area of the mound was estimated based on a smooth cone assumption; the results are thus sensitive to the actual packing of the particles. The small pre-heated particles could be more densely packed than larger particles, decreasing the total surface area of the mound, thus decreasing the evaporation rate, which would result in a lower measured $P_{sat,0}$.:

Table 4.1: Enthalpies of vaporization and saturation pressures at 298 K of the dicarboxylic acids.

Acid	Study	$P_{sat,0}$ (10^{-5} Pa)	ΔH (kJ/mol)
Adipic	Saleh et al. (2008)	3.4 (± 1.2)	135 (± 13)
	This study (atomization)	3.3 (± 0.9)	132 (± 8)
	This study (homogeneous condensation)	4.2 (± 2.2)	126 (± 21)
Azelaic	This study (atomization)	1.4 (± 0.5)	145 (± 15)
	This study (homogeneous condensation)	0.9 (± 0.3)	158 (± 17)

4.2.2 SEM images

SEM images taken for adipic acid and azelaic acid aerosol particles produced by homogeneous condensation and atomization of aqueous solutions are shown in Figure 4.3. For both acids, there is no obvious difference in surface morphology as a function of generation method, which supports the similarity in thermodynamic properties. However, the outcome of these SEM images should only be treated as an indication since the level of detail provided is not sufficient to be conclusive. Details on the molecular structure can be obtained using Transmission Electron Microscopy (TEM), which would provide better information on disruption of molecular structure by presence of solvent, if any. However, given that the IVM results provided similar thermodynamic properties for the two generation methods, the surface irregularities due to the generation method (if any) apparently have a negligible effect for the studied compounds.

Figure 4.3 shows that the dicarboxylic acid particles are not spherical; this may cause bias in our total measurements which assume spherical particles. In an SMPS, particle size is inferred from electrical mobility in a differential mobility analyzer (DMA). Electrical mobility is given by $Z = \frac{neC}{3\pi\mu d_{ev}\chi}$, where n is the number of charges,

e is the elementary charge, C is Cunningham correction factor, μ is air viscosity, d_{ev} is the equivalent volume diameter, and χ is the dynamic shape factor for non-spherical particles which usually has a value greater than one. Assuming spherical particles leads to overestimation of d_{ev} by a factor of χ, and the particle volume by a factor of χ^3. The total volume is thus overestimated by a factor of χ^3, and so is $P_{sat,0}$. For Cylinders (L/D = 2) and cubes, χ is 1.09 and 1.08 respectively (Hinds, 1999); based on the SEM images, a crude estimate of χ for our particles is around these values. χ of 1.05 – 1.1 yields overestimation of $P_{sat,0}$ by 15% - 30%. A potential remedy for bias caused by non-sphericity is to replace the SMPS systems by an integrated mass measurement instrument, such as a piezo-balance.

(a)

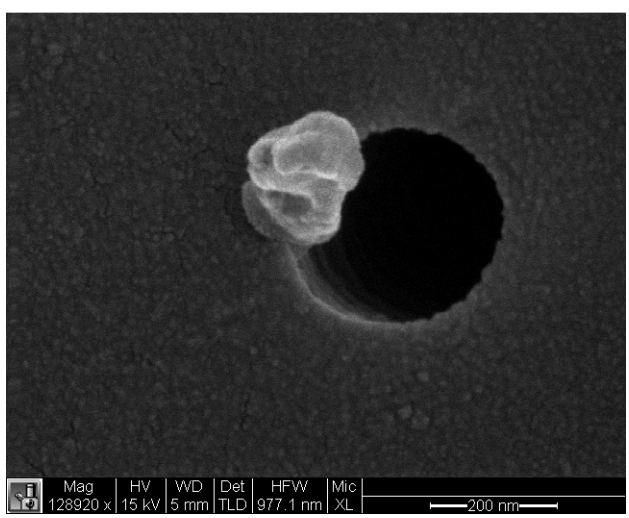

Figure 4.3

(b)

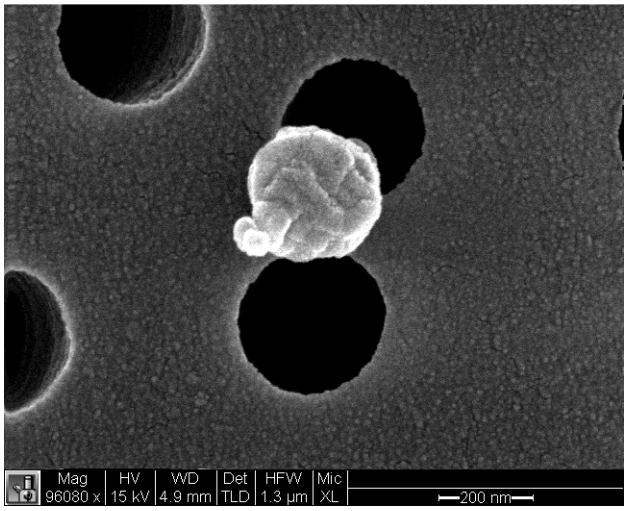

Figure 4.3 (continued)

(c)

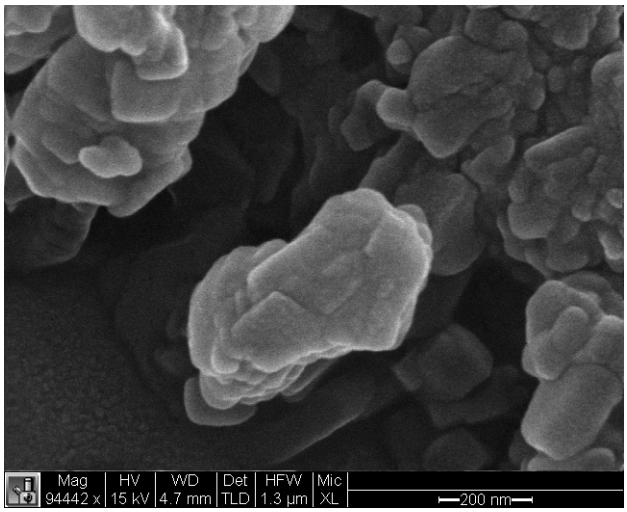

Figure 4.3 (continued)

(d)

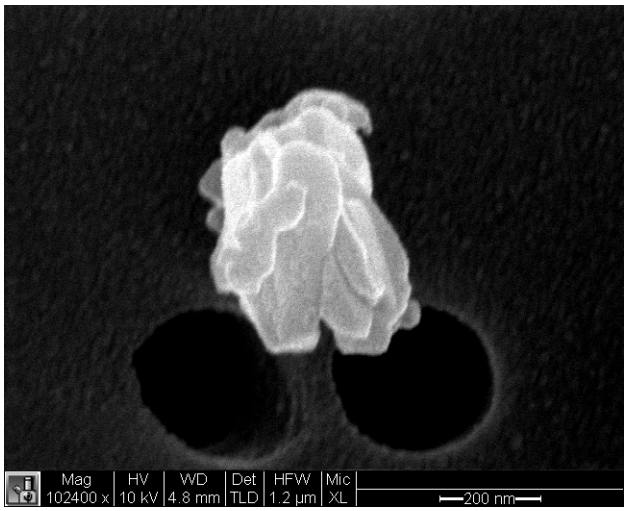

Figure 4.3 (continued): SEM images for (a) adipic acid generated by homogeneous condensation, (b) adipic acid generated by atomization, (c) azelaic acid generated by homogeneous condensation, and (d) azelaic acid generated by atomization

4.3 Conclusions

We have investigated the effect of aerosol generation method on thermodynamic properties of adipic acid and azelaic acid aerosols. Saturation pressures at 298 K and enthalpies of vaporization were determined for the dicarboxylic acids generated by 1) atomization of aqueous solutions and 2) homogeneous condensation of organic vapor. We found no significant difference between the thermodynamic properties as a function of generation method. This implies that retained water in the test aerosol generated using conventional atomization/drying techniques, if any, does not affect the measured thermodynamic properties. Also, SEM images showed no apparent difference in surface morphology between aerosol particles generated by the two methods.

5. On transport phenomena and equilibration time scales in thermodenuders

5.1 Introduction

Thermodenuders have been widely used in aerosol volatility studies, both in the lab (e.g. An et al., 2007; Saleh et al., 2008; Fuallhaber et al., 2009) and in the field (e.g. Wehner et al., 2004; Huffman et al., 2008; Dzepina et al., 2009). A thermodenuder (TD) is simply a temperature controlled flow tube. When a volatile/semi-volatile aerosol is introduced into a heated TD, the particles respond by evaporating. The extent to which the particles evaporate – the difference between initial and final size distributions – provides information about their volatility. Although the operation of the TD is relatively simple, it has been the subject of some confusion. There are two main, sometimes controversial, issues associated with TDs: 1) equilibration and 2) the need for an activated carbon denuder in the cooling section connecting the TD to the sizing instrument. The intent of including a denuder is to minimize re-condensation of the evaporated vapor back to the particles from which it originated, and thereby avoid particle size changes from the outlet of the TD to the sizing instrument.

Researchers have recently recognized the importance of kinetic limitations to volatility studies in TDs. For reliable volatility measurements, the aerosol should approach equilibrium within the residence time available in the TD, otherwise volatility would be underestimated (An et al., 2007; Saleh et al., 2008; Riipinen et al., 2010). Saleh

et al. (2008, 2009, 2010) and Saleh and Khlystov (2009) found by numerical simulation and empirical measurements that the residence time in a typical TD is sufficient for equilibration at the experimental conditions of their study (aerosol concentrations higher than 200 μg/m^3 and a residence time of 30 s). On the other hand, Riipinen et al. (2010) and Cappa (2010) argued, based on their evaporation kinetics models, that equilibration is not likely to be achieved for most ambient/laboratory aerosol systems within reasonable residence times. They concluded that kinetic models are necessary to interpret TD volatility measurements. It should be noted that these two studies arrived at opposite conclusions with regard to the effect of the aerosol volatility on the equilibration time scales: Riiponen et al. (2010) found that the lower volatility compounds could be equilibrated on time scales of milliseconds, if the aerosol concentration is sufficiently high, while Cappa (2010) argued that low volatility compounds cannot be equilibrated at any reasonable time scales. However, as will be shown in this chapter, equilibration time is not affected by volatility.

The second controversy relates to the cooling section of thermodenuders, where the aerosol is returned to room temperature. In the cooling section, the concentration gradient is reversed, causing condensation on the aerosol particles and the walls of the cooling section. It has been feared that this re-condensation will lead to bias in the measurements, and therefore most researchers have used activated carbon (AC)

denuders for cooling sections to strip the organic vapor and minimize re-condensation on the particles (e.g. An et al., 2007; Faullhaber et al., 2009; Huffman et al., 2009). It should be noted that the inclusion of an AC denuder in these studies was not justified theoretically or experimentally. Some studies, (e.g. Sakurai et al., 2003 and Saleh et al., 2008, 2009, 2010) found that the effect of re-condensation is negligible in their systems, and thus operated without an AC denuder. Using an aerosol evaporation kinetics model, Cappa (2010) found that bias due to re-condensation is small at low aerosol loadings, but might become substantial at high loadings.

Most of the TD studies have used aerosol particles mass fraction remaining (MFR) as an indication of aerosol volatility. MFR is defined as the ratio of aerosol particle mass concentration exiting the TD to the initial (reference) mass concentration. MFR has been used in 2 ways to infer aerosol volatility: 1) at a constant TD temperature, volatilities of different aerosol species are compared based on their MFR – the lower the MFR, the more volatile is the aerosol (e.g. An et al., 2007); 2) the TD temperature is varied until a certain MFR is reached (say 50%), and the required TD temperatures are compared – the lower the temperature the more volatile is the aerosol (Faullhaber et al., 2009). The use of MFR to estimate volatility is theoretically unjustifiable however and leads to spurious results. The reason is that volatility (C_{sat}) does not depend on particle mass concentration, but on equilibrium between the particle phase and the gas phase. To

illustrate, consider an aerosol with $C_{sat}(T)$ of 50 μg/m^3, and 2 initial particle concentrations 100 μg/m^3 and 500 μg/m^3. If both achieve equilibrium in a TD, ΔC will be 50 μg/m^3 in both cases (assuming that initial C_{sat} is much smaller than $C_{sat}(T)$), while MFR will be 0.5 and 0.9 respectively. Using MFR, the same aerosol would be mistakenly thought to have different volatility. The change in aerosol concentration, ΔC, on the other hand is an appropriate metric for volatility studies (Saleh et. al 2008; Saleh and Khlystov, 2009).

In this chapter, we present a theoretical and experimental exploration of heat and mass transport, and evaporation kinetics in thermodenuders. A plug flow computational model (Saleh and Shihadeh, 2007) is used to investigate equilibration time scales in TDs as well as potential re-condensation in the cooling section. Dimensional analysis is performed to identify the governing parameters in the equilibration problem. Theoretical findings are compared to experiments performed with pure and mixed semi-volatile dicarboxylic acid aerosols.

5.2 Theory

Consider a volatile or semi-volatile aerosol initially at equilibrium with its surrounding gas phase. The total particle mass concentration is C_0 and the vapor concentration in the gas phase is $C_{sat,0}$, the saturation concentration at the equilibrium temperature T_0. When the aerosol flows through the heating section of a TD maintained

at $T_1 > T_0$, a concentration gradient is created between the surface of the particles and the gas phase, and the particles respond by evaporating to bring the system to equilibrium at T_1, which corresponds to vapor concentration of $C_{sat,1}$ in the gas phase. If the residence time in the TD is longer than equilibration time, and provided that $C_0 > C_{sat,1}$, the aerosol approaches equilibrium; in other words, the gas phase approaches a saturation ratio $SR = C_g / C_{sat,1} = 1$, where C_g is the vapor concentration in the gas phase. If the residence time in the TD is shorter than the equilibration time, the aerosol exits the TD with $SR < 1$. In the cooling section, the aerosol temperature is brought back to T_0, causing the gas phase to supersaturate with the vapor, and thereby reversing the concentration gradient. Vapor starts to condense on the particles as well as the walls of the cooling section.

The heat and mass transport phenomena in the heating and cooling sections of the TD are similar, and can be modeled using the same set of equations but with different boundary conditions. In section 5.2.1, we describe a plug flow model where the fluid dynamics is simplified by assuming a well-mixed flow. Dimensional analysis on the plug flow model is presented in section 5.2.2 and is utilized to identify key parameters that govern equilibration in TDs. In section 5.2.3, the relative importance of condensation on aerosol particles and the walls in the cooling section is investigated in terms of the coupling number previously derived by Saleh and Shihadeh (2007).

5.2.1 Plug flow formulation

In a bounded flow such as in a TD, the plug flow assumption means that there are no velocity/temperature/concentration gradients in the radial direction. This reduces the heat and mass transport problem to a set of ODEs that can be solved as a function of axial distance or time (Saleh and Shihadeh, 2007). Furthermore, for semi-volatile organics, thermal inertia of the aerosol particles and latent heat effects can be neglected (Saleh et al., 2008). Under these assumptions, the equations governing the evolution of the particulate and gas phase are as follows:

Gas phase temperature

$$\rho_a c_{pa} \frac{dT}{dt} = \frac{4}{d_t} h(T_w - T) \tag{5.1}$$

where ρ_a is air density, c_{pa} is air specific heat, d_t is the TD diameter, T_w is the TD temperature, and h is the average heat transfer coefficient. For laminar flow, h is given by the Nusselt number correlation (Incropera and DeWitt, 2002) $Nu = \frac{hd_t}{k} = 3.66$, where k is the thermal conductivity.

Gas phase vapor concentration

$$\frac{dC_g}{dt} = -\frac{4}{d_t} h_m (C_w - C_g) - \sum_{i=1}^{n} \frac{dm_{p,i}}{dt} N_i \tag{5.2}$$

The first term on the right hand side is the mass transfer rate to the wall of the TD. C_w is the vapor concentration at the TD wall and h_m is the average mass transfer coefficient. By analogy to heat transfer, h_m can be calculated as $h_m = \frac{h}{\rho_a c_{pa} Le^{2/3}}$ (Incropera and DeWitt, 2002), where $Le = \frac{D_{th}}{D}$ is Lewis number, the ratio of thermal diffusivity to mass diffusivity. The second term on the right hand side is the net mass transfer rate to/from the ensemble of aerosol particles, which are distributed into n discrete size bins, each characterized by a single diameter d_{pi} and number concentration N_i. While the number concentration is held constant (i.e. no coagulation or deposition), the diameter is allowed to vary in accordance with mass transfer. The mass transfer from a single particle is given by the Maxwell equation corrected for non-continuum effects (see below).

Particle mass

$$\frac{dm_{p,i}}{dt} = -2\pi d_{p,i} DF\left(KC_{sat} - C_g\right) \tag{5.3}$$

where D is the diffusion coefficient; C_{sat} is the saturation concentration;

$K = \exp\left(\frac{4\sigma M}{\rho_p T d_p}\right)$ is Kelvin correction where ρ_p is the particle density, M is the molar mass, and σ is the surface free energy; $F = \frac{1+Kn}{1+0.3773Kn+1.33Kn(1+Kn)/\alpha}$ is the

Fuchs-Sutugin correction for non-continuum effects (Fuchs and Sutugin, 1971) where α is the evaporation coefficient.

Equations (5.1) – (5.3) are solved using MATALB ODE23 solver, and the profiles of temperature, vapor concentration, and particle size distribution are obtained as a function of residence time in the TD. This model is used to simulate transport phenomena in both the heating section and cooling section (with and without an AC denuder) of the TD. In the heating section, a no-flux boundary condition is imposed for mass transfer at the TD wall, that is the first term in equation (2) is zero when $C_g < C_{sat}(T_w)$. If the gas phase is supersaturated due to Kelvin effect, i.e. $C_g > C_{sat}(T_w)$, the appropriate boundary condition is $C_w = C_{sat}(T_w)$. For the cooling section with no AC denuder, the boundary condition is set to $C_w = C_{sat}(T_w)$, and for the cooling section with an AC denuder, the wall is assumed to be a perfect sink with $C_w = 0$.

The validity of using a plug flow model was tested by comparison with a full laminar flow model (Khlystov et al., 2009), and the difference in temperature and vapor concentration profiles for different representative cases was found to be negligible.

5.2.2 The equilibration parameter (t_r / τ)

To elucidate the parameters governing equilibration in the heating section of the TD we non-dimensionalized the above mass conservation and rate equations. For a monodisperse aerosol with no mass transfer to the walls, equation (5.2) simplifies to:

$$\frac{dC_g}{dt} = -\frac{dm_p}{dt} N_{tot} \tag{5.4}$$

Equations (5.3) and (5.4) can be non-dimensionalized using $t^* = t/t_r$ where t_r is the residence time in the TD, $d_p^* = d_p/d_{p,in}$ where $d_{p,in}$ is the initial particle diameter, and $C^*_g = C_g/C_{sat}$, where C_{sat} is the saturation concentration at the TD temperature. In this analysis, the time required for the thermal boundary layer to grow to fully developed conditions is assumed to be much shorter than the total residence time in the TD. This assumption is reasonable for conventional TD designs. Substituting equation (5.3) in equation (5.4) and inserting the dimensionless parameters yields:

$$\frac{dC_g^*}{dt^*} = 2\pi N_{tot} d_{p,in} DF t_r (K - C_g^*) d_p^* = \frac{t_r}{\tau}(K - C_g^*) d_p^* \tag{5.5}$$

where $\tau = \dfrac{1}{2\pi N_{tot} d_{p,in} DF}$. It can be readily shown that τ physically represents the characteristic evaporation time required for an aerosol of fixed diameter and kinetic properties to produce a change in concentration in the gas phase equal to 1/e of the initial difference in vapor concentration between the layer immediately surrounding the droplet phase and the gas phase, ($KC_{sat} - C_g$). We should note that the expression of τ is similar to the equilibration time scale previously derived by Wexler and Seinfeld (1990). t_r/τ thus represents the ratio of time available in the TD to the characteristic time of evaporation in a bounded aerosol.

Equation (5.5) shows that the evolution of the dimensionless gas concentration (C^*_g) in a heated TD is characterized by a single dimensionless parameter, t_r/τ, which has no dependence on the thermodynamic properties of the aerosol, contrary to the conclusions of Riipinnen et al. (2010) and Cappa (2010). It only depends on the aerosol size distribution (the total aerosol length $N_{tot}.d_{p,in}$) and kinetic properties of the aerosol, D and α (through F; see equation (3)). When coupled with experimental data, τ can be used as a semi-empirical tool to predict the required residence time required for a certain aerosol to achieve equilibrium, as described in section 5.4.4.

This analysis can be readily extended to polydisperse aerosol, where the effect of the size distribution is accounted for by using the condensation sink diameter (Lehtinen et al., 2003)., The condensation sink diameter is the particle diameter of a monodisperse aerosol that exhibits the same net evaporation or condensation rate as a polydisperse aerosol, both with a given number concentration. The condensation sink diameter can be calculated for a certain particle size distribution from the moment average

$$d_{p,cs} = \left(\frac{\sum_{i=1}^{n} N_i d_{p,i}^{a}}{\sum_{i=1}^{n} N_i} \right)^{1/a}$$

, where the exponent a varies between unity for the continuum regime and 2 for the free molecular regime. For the transition regime, it is obtained by

differentiating the natural logarithm of the condensation sink $CS = 2\pi DC_m d_{p,cs} \sum_{i=1}^{n} N_i$

with respect to the natural logarithm of $d_{p,cs}$ (Lehtinen et al., 2003):

$$a = \frac{d\ln(CS)}{d\ln(d_{cs})} = \frac{1}{CS} \times \frac{Kn + \left(0.754 + \frac{8}{3\alpha}\right)Kn^2 + \left(0.377 + \frac{16}{3\alpha}\right)Kn^3 + \frac{8}{3\alpha}Kn^4}{\left[Kn + \left(0.377 + \frac{4}{3\alpha}\right)Kn^2 + \frac{4}{3\alpha}Kn^3\right]^2} \quad (5.6)$$

5.2.3 Re-condensation in the cooling section

In the cooling section, vapor in the gas phase condenses on both the particles and the walls of the cooling section. The process is characterized by the ratio of diffusive vapor transport to/from the particles to the convective transport to/from the cooling section walls, which can be expressed in terms of the dimensionless "coupling number" (Saleh and Shihadeh, 2007):

$$Cn = 2\pi \frac{N_{tot} d_{p,in} FDd_t}{h_m} \quad (5.7)$$

Cn represents the rate at which the vapor in the gas phase is scavenged by the droplets relative to the rate at which it is absorbed by the walls of the cooling section. The larger *Cn*, the greater the potential for re-condensation on the particles.

5.3 Experimental

The experimental setup used in this study (Figure 5.1) is similar to the one described in Saleh et al. (2008). Aerosol is produced by spraying aqueous solutions using

a constant output atomizer, and is sent to a 20 liter chamber to mix with dry, particle-free air at 40 SLPM for dilution and drying. A flow of 1 SLPM is drawn through a diffusion-dryer to remove any remaining water, while the excess is sent to exhaust. The 1 SLPM aerosol flow is then sent through a TD with a heating section of 1 m length and 2.5 cm inner diameter. The residence time in the heating section of the TD is controlled by varying the extraction flowrate using a mass flow controller. The maximum average residence time, which corresponds to a zero bypass flowrate, is around 30 s. The default cooling section is a copper tube of 1 m length and 0.63 cm inner diameter. We have used other configurations for the cooling section, as described below. Reference and heated aerosol size distributions are measured using a Scanning Mobility Particle Sizer (SMPS).

To investigate equilibration time scales, we measured the change in aerosol particle concentration (ΔC) at different residence times in the TD. Equilibration was considered achieved at a certain residence time if ΔC did not increase with further increase in residence time. For each tested aerosol, ΔC values were measured at average residence times of 9, 12, 15, 20, and 30 s. The experimental matrix used to investigate equilibration in TDs is shown in Table 1. All experiments were performed at reference temperature of 25 ^{0}C and TD set temperature of 40 ^{0}C. We chose adipic acid aerosol (C_0 = 390 μg/m^3, N_{tot} = 10^{12} particles/m^3, $d_{p,cs}$ = 65 nm) as the base case. To illustrate the dependence of equilibration time scales on aerosol loading, we varied the initial particle

concentration. The effect of volatility (C_{sat} at TD temperature) was demonstrated by performing experiments with pimelic acid, which has C_{sat} value a factor of 3 larger than adipic acid at 40 ^{0}C (Saleh et al., 2008). The effect of mixture complexity was tested with a mixture of succinic, adipic, pimelic, and azelaic acids. For the dicarboxylic acids used in this study, C_{sat}(25 ^{0}C) is much smaller than C_{sat}(40 ^{0}C); C^*_g of the organic vapor in the gas phase can thus be approximated as:

$$C_g^* = \frac{C_g}{C_{sat}(40^oC)} = \frac{\Delta C + C_{sat}(25^oC)}{\Delta C_{\max} + C_{sat}(25^oC)} \approx \frac{\Delta C}{\Delta C_{\max}} \tag{5.8}$$

where ΔC_{max} is the maximum change in aerosol concentration, which corresponds to equilibrium.

We have also performed experiments to examine the effect of having a cooling section with or without an AC denuder. For these experiments, the residence time in the heating section of the TD was constant at 15 s. We measured ΔC for 4 cooling section configurations: 1) 1 m × 0.63 cm copper tubing, which corresponds to a residence time of 2 s; 2) 2 m × 0.63 cm copper tubing, which corresponds to a residence time of 4 s; 3) 1 m × 1.27 cm AC denuder, with a residence time of 8 s; 4) 1 LPM extraction flow was added downstream of the AC denuder, reducing the residence time to 4 s. Two model aerosols were used, adipic acid, and a mixture of succinic, adipic, pimelic, and azelaic acids. The

Experimental matrix is given in Table 1. The heating and the cooling section of the TD were kept at 45 ^{0}C and 25 ^{0}C respectively.

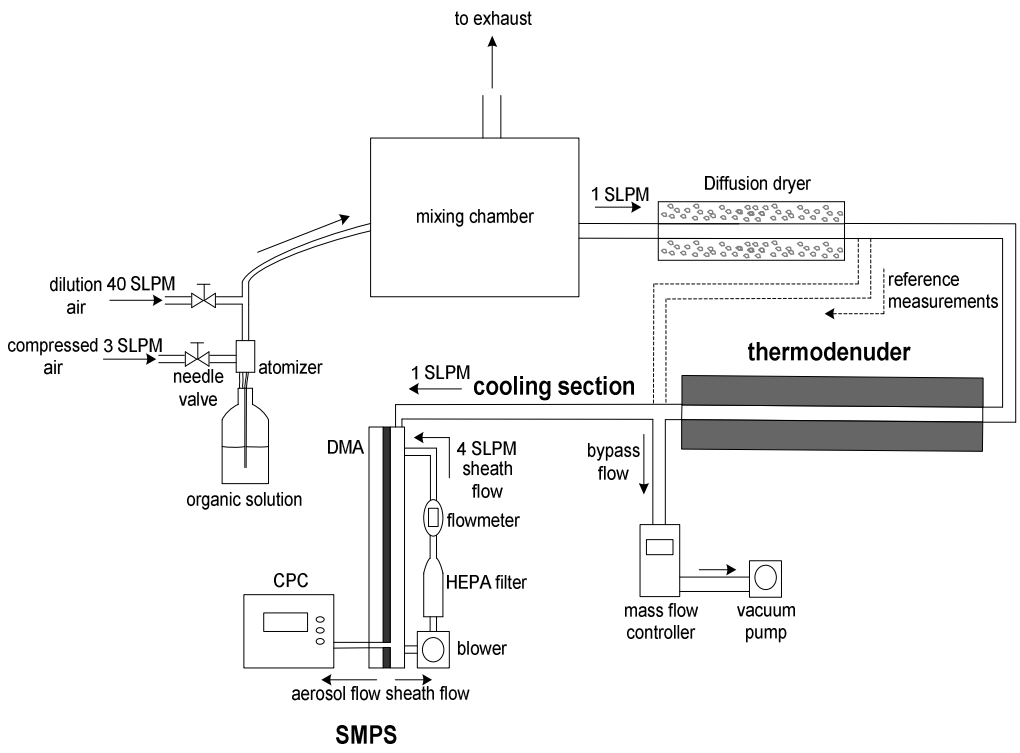

Figure 5.1: Experimental setup

Table 5.1: Experimental matrix for equilibration time scales investigation

*** the mole fractions of the acids are: 0.1-0.4-0.4-0.1**

Dicarboxylic acid	adipic	adipic	adipic	pimelic	mixture*
Initial loading (μg/m^3)	390	245	68	307	313
N_{tot} (10^{11}×particles/m^3)	10.6	6.0	2.5	7.0	9.7
$d_{p,cs}$ (nm)	65	65	60	67	61

5.4 Reuslts and discussion

5.4.1 Effect of particle size distribution

Figure 5.2 shows ΔC and C^*_g of adipic acid aerosol at different residence times in the TD for different initial particle size distributions. The results of numerical simulations using the model described in section 5.2.1 are also shown. Equilibrium corresponds to $C^*_g = 1$. It is evident that equilibration times are dependent on particle size distributions – more specifically on the total particle length – as predicted by equation (5.6). For aerosol size distributions relevant to laboratory studies, adipic acid aerosol reaches equilibrium within a residence time typical for most TDs currently employed. However, for size distributions relevant for ambient measurements, equilibration requires residence times much larger than what is available with current TD designs.

It should be noted that the asymptotic behavior exhibited by C^*_g as time progresses demonstrates that the wall losses in the thermodenuder are negligible. If the losses were significant, there would be no such asymptotic behavior, as the material will be continuously stripped by the walls, resulting in an ever increasing ΔC. The excellent agreement between the observations and the model, which assumes no wall losses in the heated section, further supports this point.

5.4.2 Effect of the evaporation coefficient

As shown in section 5.2.2, equilibration times depend on the evaporation coefficient (α) (i.e. F in equation 6)). To obtain agreement between model simulations and experimental data in Figure 2, α of approximately 0.1 is required. This is consistent with the value of α reported by Saleh et al. (2009) for adipic acid (0.08 ±0.02). To illustrate the importance of this parameter, Figure 5.3 shows model simulations for vapor build-up of adipic acid aerosol for different values of α. It is obvious that using values of α greater than 0.1 over-predicts the observed SR, while values less than 0.1 under-predict the observations.

When TD measurements are performed at non-equilibrium conditions and the volatility is calculated from evaporation kinetics model simulations, as suggested by Riipinen et al. (2010) and Cappa (2010), the results strongly depend on α, which is often unknown. Thus when α is unknown, it is critical that TDs are used in a manner such that measurements are made under equilibrium conditions. However, as described in section 5.4.1, equilibrium cannot be achieved in the TD when performing ambient measurements. The best approach pending developments in the state of the art, is to interpret ambient TD measurements using kinetic models, as done in Cappa and Jimenez (2010), while keeping in mind the substantial uncertainty due to unknown α, as pointed out by those authors.

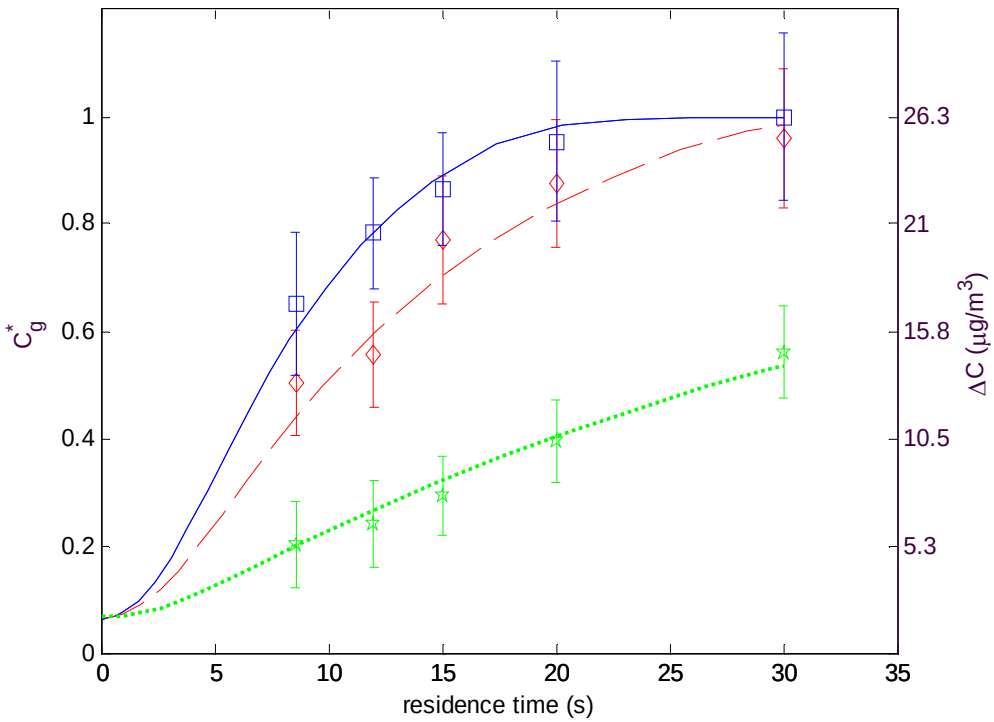

Figure 5.2: Measured and simulated particle mass change and dimensionless vapor build-up profiles for adipic acid aerosol in a TD. T_{in} = 25 ^{0}C and T_w = 40 ^{0}C. Squares & solid: C_0 = 390 μg/m^3, N_{tot} = 10^{12} particles/m^3, $d_{p,cs}$ = 65 nm; diamonds & broken: C_0 = 245 μg/m^3, N_{tot} = 6×10^{11} particles/m^3, $d_{p,cs}$ = 65 nm; stars & dotted: C_0 = 68 μg/m^3, N_{tot} = 2.5×10^{11} particles/m^3, $d_{p,cs}$ = 60 nm

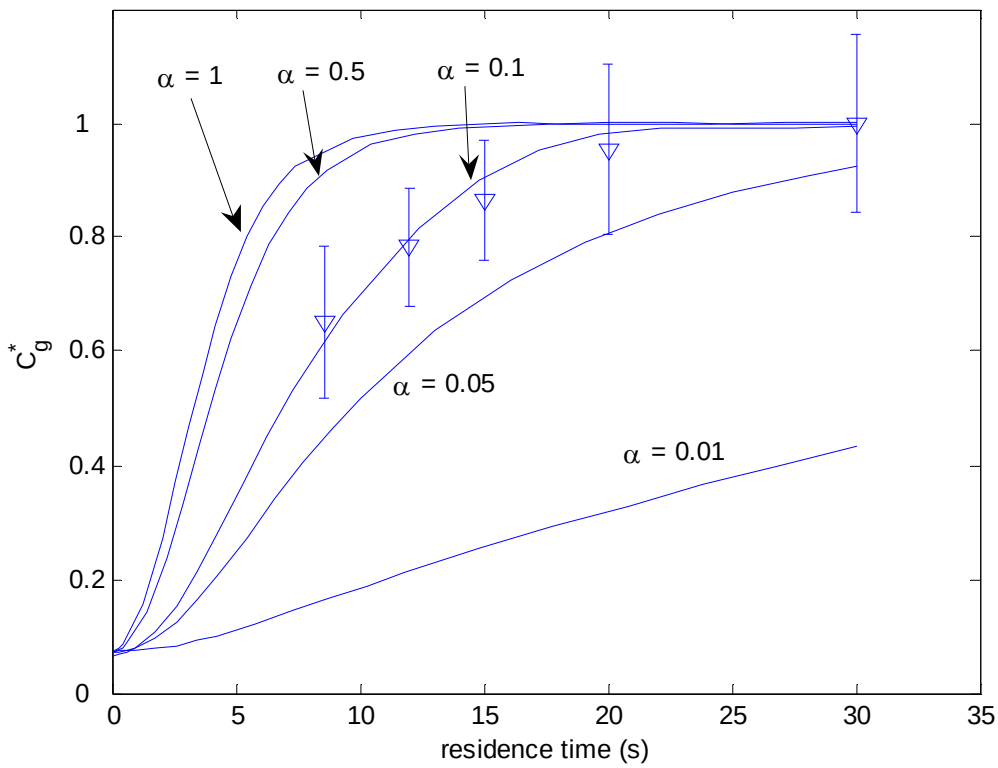

Figure 5.3: Measured and simulated vapor build-up profiles for adipic acid aerosol (C_0 = 390 μg/m³, N_{tot} = 10^{12} particles/m³, $d_{p,cs}$ = 65 nm) in a TD. The simulations were performed with α as a variable parameter as indicated in the Figure. T_{in} = 25 ⁰C and T_w = 40 ⁰C.

5.4.3 Effect of thermodynamic properties and mixture complexity

To investigate the purported effect of C_{sat}, we performed equilibration experiments with pimelic acid, which has C_{sat}(40 ⁰C) a factor of 3 greater than that of adipic acid, and with a mixture of succinic, adipic, pimelic, and azelaic acids. Experimental *SR* versus residence time for adipic acid, pimelic acid, and the dicarboxylic acids mixture is shown in Figure 5.4 along with model predictions. Particle size

distribution was held constant across the experiments to the extent possible. It is apparent that the three model aerosols exhibited similar vapor build-up profiles, which verifies the theoretical finding that equilibration time scales are neither a function of C_{sat} nor mixture complexity. For pimelic acid, α of approximately 0.25 was required for the model to match experimental data, which is in agreement with the value reported by Saleh et al. (2009) (0.24 ±0.04). For the dicarboxylic acids mixture, the effective α required in the simulation was around 0.12, which is within the range of values of the components.

It has been argued (Riipinen et al, 2010) that an aerosol with a large C_{sat} needs more time to achieve equilibrium than one with a small C_{sat} because the former must evaporate more than the latter to saturate the gas phase. However, this effect is counterbalanced by the increased evaporation rate of the larger C_{sat} aerosol (i.e. as given by the Maxwell equation). The same applies to mixture complexity. Although in a mixture the evaporation rate of each component is reduced by a factor of x_i, the mole fraction of component i in the mixture, relative to that of the pure compound, the equilibrium concentration in the gas phase of component i is reduced by the same factor according to $C_{eq,i} = x_i\, C_{sat,i}$. This analysis can be deduced directly from the non-dimensional form of the vapor concentration rate equation (equation (5.6)).

Confusion over the role of C_{sat} appears to stem from how some investigators define equilibration. For example, Riipinen at al. (2010) define equilibration as the point when the aerosol particles are within 1% or 10 nm of the equilibrium diameter d_{eq}, whichever comes first. However, thermodynamic equilibrium is determined by the gas concentration, not particle size, i.e. the problem is mass-based. The problem with the size-based criterion can be observed by performing the following thought experiment. Consider two aerosols with the same initial size (d_0 = 200 nm) and concentration (C_0 = 150 μg/m^3), but different saturation concentrations at the TD temperature ($C_{sat,1}$ = 50 μg/m^3 and $C_{sat,2}$ = 140 μg/m^3). Assuming that C_{sat} at T_0 is much smaller than C_{sat} at T(TD), the final equilibration concentrations are $C_{eq,1} = C_0 - C_{sat,1}$ = 100 μg/m^3 and $C_{eq,2} = C_0 - C_{sat,2}$ = 10 μg/m^3. For spherical particles, the equilibrium diameters can be calculated from $d_{p,eq} = \frac{6C_{eq}}{(\pi\rho N)^{1/3}}$, where ρ is the particle density and N is the number concentration. This gives $d_{p,eq,1}$ = 175 nm and $d_{p,eq,2}$ = 81 nm. Using the 1% or 10 nm equilibration criterion, we get $d_{p,1}$ = 185 nm and $d_{p,2}$ = 91 nm, giving final concentrations C_1 of 118 μg/m^3 and C_2 of 14 μg/m^3. The saturation ratios for cases 1 and 2 can be calculated from $SR_{1,2} = \frac{C_0 - C_{1,2}}{C_{sat,1,2}}$ as 64% and 97% respectively. It is obvious that case 1 would be thought to have reached equilibrium quite prematurely relative to case 2 in an evaporation kinetics simulation, which would lead to the erroneous outcome that equilibrium at state

1 is achieved faster than state 2, eventually leading to the invalid conclusion that equilibration time scales increase with increasing C_{sat}.

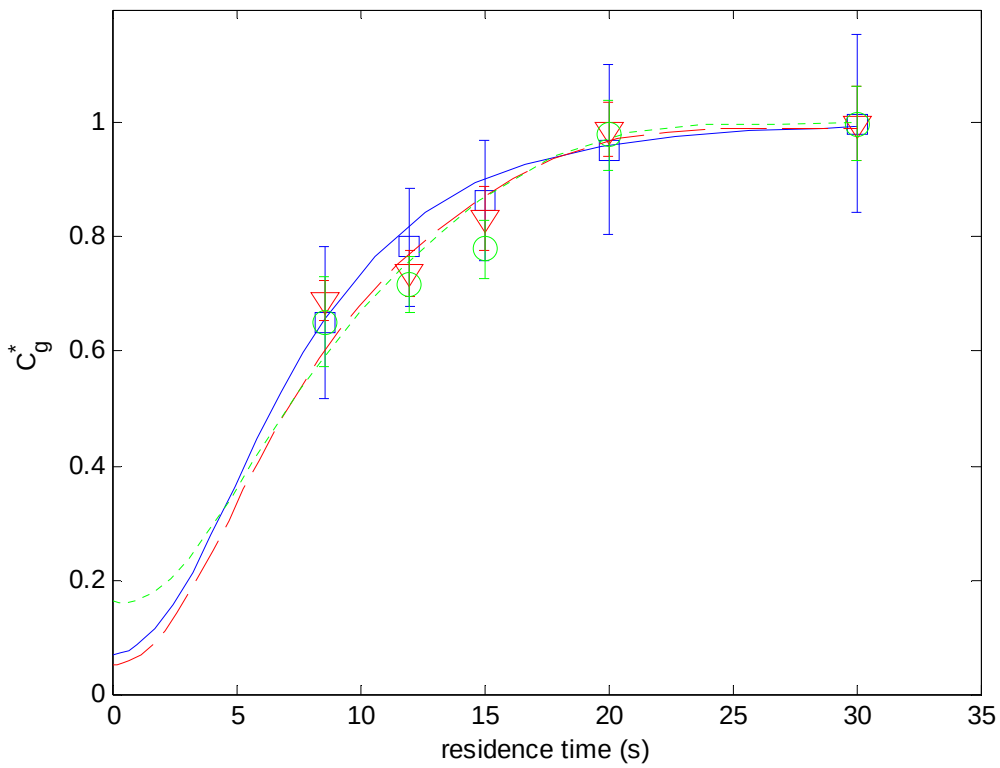

Figure 5.4: Measured and simulated vapor build-up profiles. Squares & solid: adipic acid, C_0 = 390 μg/m³ and d_{cs} = 65 nm; triangles & broken: pimelic acid, C_0 = 307 μg/m³ and d_{cs} = 67 nm; circles & dotted: succinic+adipic+pimelic+azelaic acid mixture, C_0 = 313 μg/m³ and d_{cs} = 61 nm. T_{in} = 25 ⁰C and T_w = 40 ⁰C.

5.4.4 Effect of the equilibration parameter

The equilibration parameter derived in section 5.2.2 as $t_r / \tau = 2\pi N_{tot} d_{p,in} DFt_r$ can be used semi-empirically to estimate the required residence time in a TD for a certain aerosol to equilibrate. Figure 5.5 shows C^*_g plotted as a function of t_r/τ for the

experimental data reported in Figure 5.2 and Figure 5.4. It can be seen in Figure 5.5 that when plotted this way, the experimental data coalesce, as expected from the dimensional analysis which indicated that the process is governed by t_r/τ. The model simulations shown in Figure 5.2 and Figure 5.4 also collapse to approximately the same line when plotted as a function of t_r/τ, and are presented by a single solid line in Figure 5.5. Using $C^*_g = 0.95$ as the equilibration criterion, the measured and simulated aerosols approach equilibrium for $t_r/\tau \approx 5$. Because the derivation of τ is based on the assumption that the change in particle size upon evaporation is small, the value of t_r/τ required for equilibration increases with deviation from the assumption. However, τ is still a valuable parameter to estimate equilibration times for most practical cases. Model simulations showed that for relative aerosol mass change ($\Delta C/C_0$) between 10% and 90%, t_r/τ between 5 and 9 was required for equilibration. $t_r/\tau > 9$ can thus be used to define equilibration in TDs. For an aerosol with a certain size distribution and kinetic properties, the required residence time to achieve equilibrium can thus be estimated, and the TD can be designed accordingly.

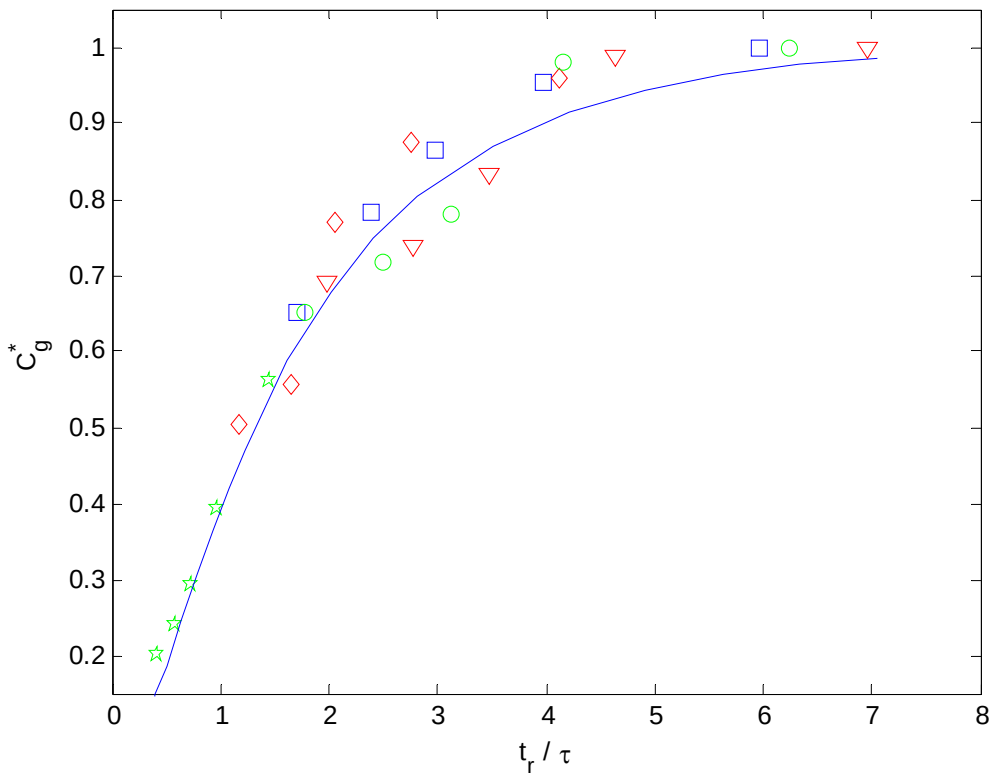

Figure 5.5: Vapor build up as a function of the equilibration parameter for the measurements in Figure 5.2 and Figure 5.4. All the simulations in Figure 5.2 and Figure 5.4 collapse on the solid line. $Cg^* = 1$ corresponds to phase equilibrium at the TD temperature

The reason why t_r/τ required for equilibrium increases as $\Delta C_{sat}/C_0$ approaches unity is that when initial particle concentration, C_0, is low, the sink diameter decreases significantly as the aerosol evaporates, causing a proportional inflation in τ, and therefore a slower overall process. This is illustrated in the bottom half of Figure 6 which shows simulations for a number of model aerosols spanning a volatility range of 3 orders of magnitude. The figure shows that the equilibration process differs *only* for the

model aerosols which are relatively lean in the particle phase (i.e. the curves corresponding to $\Delta C_{sat}/C_0$ of 0.5 and 0.8); put another way, as long as the aerosol has ample material in the particle phase relative to what is needed to saturate the vapor phase, equilibration time will be unaffected by volatility. This is more poignantly illustrated in the top half of Figure 6, where the same data is plotted versus non-dimensional time, $t_r/\tau(t)$, in which $\tau(t)$ is calculated using $d(t)$. It can be seen that all the curves, including those with large values of $\Delta C_{sat}/C_0$, collapse onto a single line, illustrating simply what is demonstrated in equation 5.5, namely that under all circumstances for which equilibration is possible τ governs the process.

When the value of α is unknown, which is often the case, τ can be calculated based on an assumed α and used to obtain a first order approximation of the required residence time. Experimental variation of TD residence time, as described in section 5.3, is then needed to verify that the aerosol has equilibrated. It should be noted that equilibration is possible to achieve only when $C_0 > C_{sat}(T_{TD}) - C_{sat}(T_0)$, otherwise the aerosol particles would evaporate completely and equilibrium will not be attained regardless of the value of tr/τ.

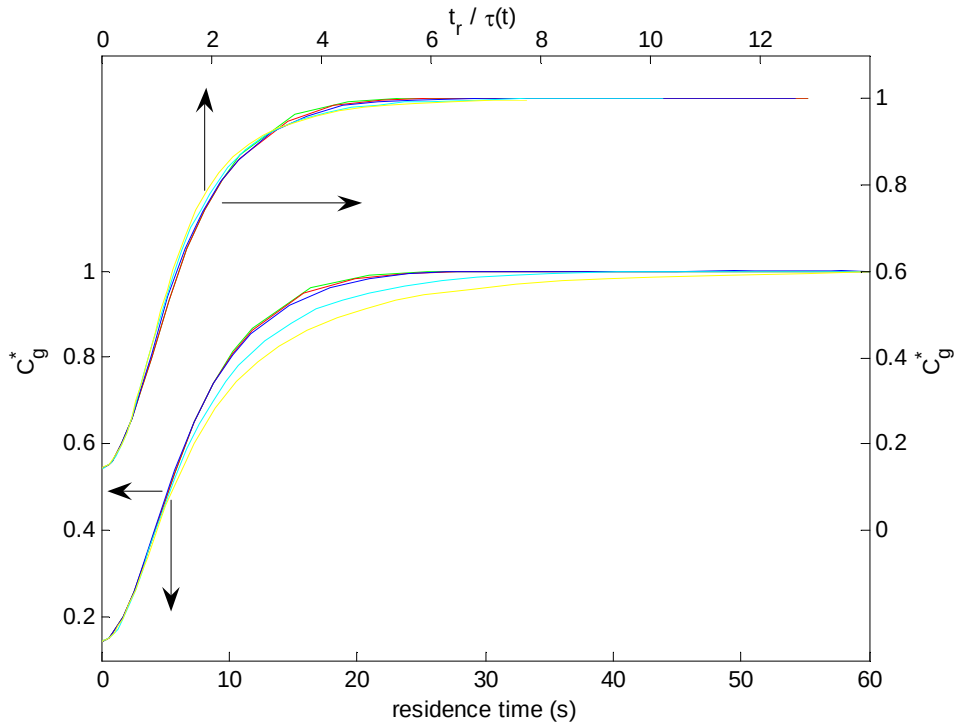

Figure 5.6: Simulated normalized vapor build-up profiles in a TD as a function of residence time (bottom x-axis and left y-axis) and time-dependent equilibration parameter (upper x-axis and right y-axis). T_0 = 25 ^{0}C; T_{TD} = 40 ^{0}C; ΔH = 100 kJ/mol; C_o = 230 μg/m^3; red: C_{sat} = 0.14 μg/m^3, $\Delta C_{sat}/C_0 = 5\times10^{-4}$; green: C_{sat} = 1.4 μg/m^3, $\Delta C_{sat}/C_0 = 5\times10^{-3}$; blue: C_{sat} = 14 μg/m^3, $\Delta C_{sat}/C_0$ = 0.05; cyan: C_{sat} = 140 μg/m^3, $\Delta C_{sat}/C_0$ = 0.5; yellow: C_{sat} = 225 μg/m^3, $\Delta C_{sat}/C_0$ = 0.8

5.4.5 Re-condensation in the cooling section

As described in section 5.2.3, the rate at which vapor re-condenses on the aerosol particles relative to the mass transfer rate to the walls is represented by the dimensionless coupling number $Cn = 2\pi \frac{N_{tot} d_{p,in} FDd_t}{h_m}$. Figure 5.7 shows maximum theoretical re-condensation fraction (RF) as a function of Cn for cooling sections with no

AC denuder. RF is defined as the ratio of the amount of vapor that re-condenses on the aerosol particles when they achieve equilibrium in the cooling section to the amount of vapor that has evaporated from the particles in the TD. RF is maximum re-condensation fraction because if the aerosol is sampled from the cooling section before it achieves equilibrium, re-condensation fraction would be less than RF. Different Cn values were generated by randomly varying aerosol size distribution and/or cooling section geometry. As expected, re-condensation becomes more important with increasing Cn. Values of $Cn < 0.7$ mark the region where re-condensation is not significant (< 10%). We should note that for ambient measurements and the vast majority of laboratory experiments, Cn is well below 0.7.

For most practical cases, incorporating an AC denuder has no significant effect. The reason is that value of C_g entering the cooling section is usually much greater than $C_{sat}(T_w)$, which renders the concentration gradient between the gas phase and the cooling section walls ($C_g - 0$) with an AC denuder very close to the case with no AC denuder ($C_g - C_{sat}(T_w)$). To illustrate, we have performed experiments with cooling sections with and without an AC denuder. The initial and final mass concentrations – downstream of the heating and cooling sections of the TD, respectively – for the cooling section configurations described in section 5.3 are given in Table 2. As shown in the table, there was no significant difference in the final mass concentration across the 4 configurations

for both model aerosols, which shows that the AC denuder had no observable effect in our experiments.

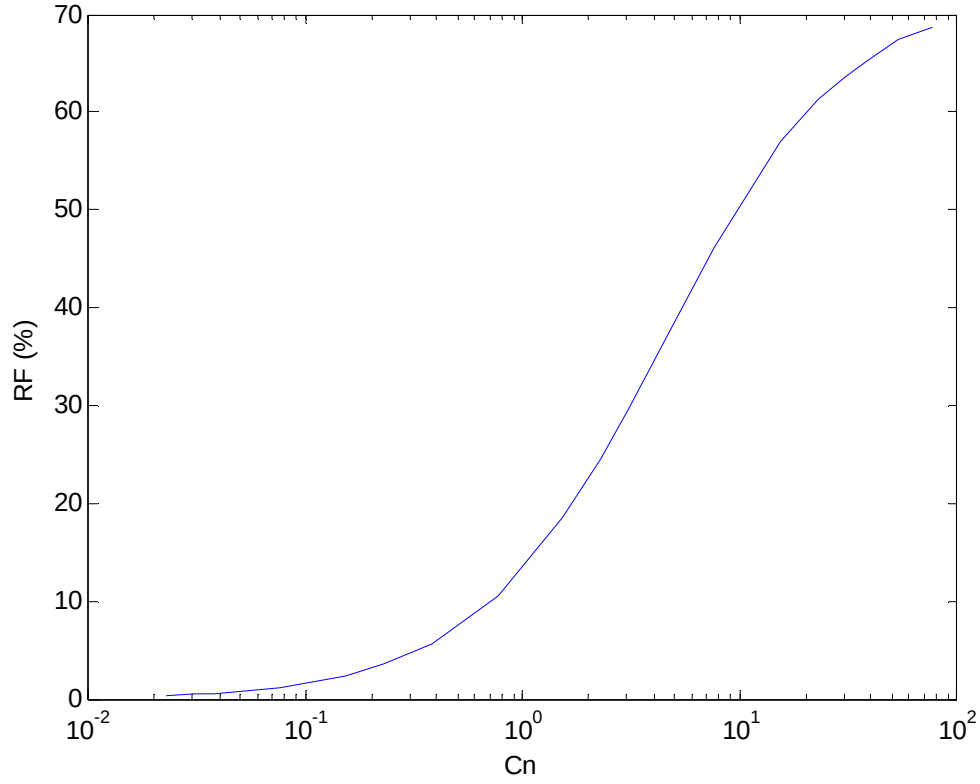

Figure 5.7: Maximum re-condensation fraction as a function of *Cn*

While harmless at short residence times, an AC denuder might become disadvantageous at long residence times, because the aerosol never achieves equilibrium. The AC denuder will continue to strip the vapor from the gas phase causing the aerosol particles to evaporate, leading to a bias in the measurement. Figure 5.8 shows theoretical RF for *Cn* of 0.5, for cases with and without an AC denuder. It is

obvious that with an AC denuder the aerosol particles will continue evaporating until they completely disappear.

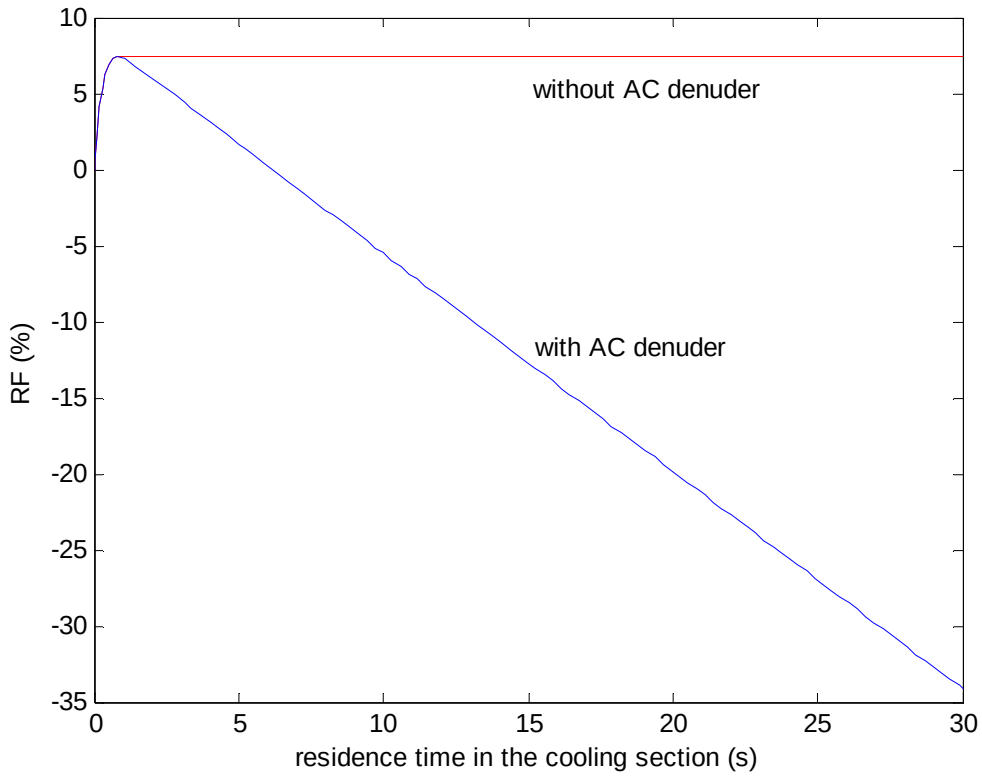

Figure 5.8: Maximum re-condensation fraction as a function of residence time in the cooling section with and without an AC denuder for *Cn* = 0.5. Negative RF indicates net evaporation of the aerosol relative to its state at the entrance of the heated TD.

Table 5.2: Initial (upstream of the heating section) and final (downstream of the cooling section) measured aerosol loadings for different cooling section configurations. * the mole fractions of the acids are: 0.1-0.4-0.4-0.1. ** A: 1 m × 0.63 cm copper tubing, 1 LPM flowrate; B: 2 m × 0.63 cm copper tubing, 1 LPM flowrate; C: 1 m × 1.27 cm AC denuder, 1 LPM flowrate; D: 1 m × 1.27 cm AC denuder, 2 LPM flowrate. * the uncertainty in the measurements is approximately ±5 μg/m3**

Dicarboxylic acid	**adipic**	**adipic**	**mixture***	**mixture***
Initial concentration (μg/m^3)**	287	151	310	196
A, B, C, D				
Final concentration (μg/m^3) ***				
A	252	138	181	98
B	249	137	181	97
C	249	137	185	105
D	250	137	180	107

5.4.6 TD design guidelines

The primary design parameters for thermodenuder studies are the tube diameter, length, and flow rate. We have shown that for the heating section, equilibration is assured when $t_r/\tau \geq 9$. Equation (5.6) can also be written in terms of the design parameters as $t_r/\tau = \frac{\pi^2}{2}\frac{N_{tot}d_{p,in}DFLd_t^2}{Q}$. This formulation shows the importance

of tube diameter; t_r/τ scales with the square of the TD diameter and linearly with TD length.

Having achieved equilibrium in the heating section, the role of the cooling section is to bring the aerosol to the temperature of the sizing instrument with as little change as possible in the particle size distribution. To the extent possible, condensation of the vapor phase should occur preferentially on the tube wall rather than on the particles flowing through it. For the problem at hand, cooling sections should be designed to minimize *Cn*. We have shown that for $Cn < 0.7$, re-condensation is not significant. It can be readily shown that for a laminar flow characterized by a constant Sherwood number, *Cn* scales with the square of the tube diameter. Thus to minimize re-condensation on the particle phase, the cooling section should have a *small* diameter, in contrast to the heating section.

5.5 Conclusions

Heat and mass transport and aerosol evaporation/growth kinetics in thermodenuders were studied both theoretically and experimentally. Numerical simulations of the evolution of aerosols in a TD using a plug flow computational model exhibited excellent agreement with experimental measurements performed with pure and mixed dicarboxylic acid aerosols.

For size distributions typical for laboratory experiments, we found that pure and mixed dicarboxylic acid aerosols approach equilibrium in TDs within residence times on the order of 10 seconds. However, for size distributions relevant to ambient aerosols, equilibration cannot be achieved within residence times available with current TD designs.

We have shown through dimensional analysis and empirical measurements that contrary to common assumption, equilibration kinetics in a TD are not affected by volatility. Rather, equilibration time is only a function of aerosol size and number concentration, evaporation coefficient, and vapor diffusivity, as described by a time constant τ. Experiments and model simulations showed that $t_r/\tau = 9$ marks the onset of equilibration, which can be used to aid TD design to ensure equilibration.

The problem of re-condensation in the cooling section can be characterized by the coupling number (*Cn*). *Cn* represents the ratio of the rate aerosol particles scavenge vapor from the gas phase to the rate vapor is transported to the walls of the cooling section. To minimize re-condensation, *Cn* should be less than 0.7, which can be achieved by minimizing the diameter of the cooling section. We showed both experimentally and by simulation that re-condensation is not important for aerosol size distributions relevant to laboratory studies and ambient measurements. We also showed that for short residence times, using an AC denuder in the cooling section has no effect. Further, an

AC denuder might be disadvantageous if it has a residence time long enough to distill the vapor from the gas phase which causes further evaporation of the aerosol particles. AC denuders should thus be avoided in cooling section of TDs.

6. Determination of evaporation coefficients of semi-volatile organic aerosols

6.1 Introduction

Gas – particle interactions leading to evaporation of aerosol particles depend on particle size (d_p), as well as several properties of the aerosol species: saturation vapor pressure (P_{sat}), diffusion coefficient (D), surface free energy (σ), and accommodation or evaporation coefficient (α) (Seinfeld and Pandis, 2006). In the transition regime, assuming a quasi-steady vapor concentration field, the kinetics of particle growth or evaporation are given by:

$$\frac{dm_p}{dt} = -\frac{2\pi d_p D C_m}{RM}\left(KP_{sat} - P_g\right) \tag{6.1}$$

where,

d_p is the particle diameter;

D is the diffusion coefficient of the species in air, and can be estimated as a function of temperature using semi-empirical expressions (Reid, 1987);

R is the universal gas constant;

M is the molar mass of the species;

P_{sat} is the saturation pressure of the species;

P_g is the partial pressure of the species in the surrounding gas phase;

K is Kelvin correction factor due to curvature, and is given by $K = \exp\left(\frac{4\sigma M}{\rho_p T d_p}\right)$,

where ρ_p is the density of the particle, T is the temperature and σ is the surface free energy;

C_m is Fuchs-Sutugin correction factor for non-continuum effects, and is given by (Fuchs and Sutugin, 1971): $C_m = \frac{1+Kn}{1+0.3773Kn+1.33Kn(1+Kn)/\alpha}$, where α is the evaporation coefficient.

The evaporation coefficient is generally defined as the ratio of the molecular flux desorbed from a particle to the maximum theoretical flux predicted by kinetic theory. At equilibrium, the inbound and outbound molecular fluxes from a particle are equal, and thus the maximum rate at which vapor molecules can be desorbed is taken as the maximum rate they can be added to the particle surface during condensation. This maximum is given by the frequency at which vapor molecules collide with the surface (i.e. assuming every collision results in a molecule "sticking"), assuming inbound molecules carry a Maxwell-Boltzmann velocity distribution and exist in the vapor phase at a concentration corresponding to saturation conditions.

In the free molecular regime, the relation between maximum theoretical evaporation flux, molecular velocity, and concentration (expressed as pressure assuming

ideal gas behavior) is given by $J = \frac{\bar{c}}{4} P_{sat}(T) \frac{M}{RT}$ where $\bar{c}$ is the mean molecular speed corresponding to a Maxwell-Boltzmann velocity distribution and is given by $\bar{c} = \sqrt{\frac{8kT}{\pi M}}$, in which k is Boltzmann's constant. A variety of surface and bulk interior effects may limit the rate at which molecules are made available for desorption at the particle interface (e.g. see Somorjai and Lester, 1967), and thus the vapor pressure at the particle interface during evaporation may be considerably depressed relative to saturation. In addition, the velocity distribution of molecules leaving the particle interface may not be Maxwellian (Li and Davis, 1996). These and other phenomena (L'vov, 2001) can render the evaporation coefficient well below unity.

When used to characterize evaporation rates of semi-volatile species such as the solids used in this study, the evaporation coefficient serves as a lumped parameter embedding finite rate solid-state kinetics as well as the intrinsic surface desorption dynamics it was meant to describe. It nonetheless remains useful for modeling aerosol evaporation in atmospheric studies. The reader is referred to Somorjai and Lester (1967) for a thorough review on the subject.

Although the concept of the condensation coefficient was introduced in the mid nineteenth century by Maxwell (1859, 1860a, b), there is no reliable theoretical basis to date to estimate its magnitude. There is generally a very large discrepancy between α

values obtained by molecular dynamics (MD) simulations and experiments (Davis, 2006). α of different compounds has been investigated using various experimental techniques. For an extensive review on the available techniques, the reader is referred to Davis (2006). α of water has received much attention because of its importance in cloud microphysics. Values in the range of 0.04 to 1 have been reported, with more recent measurements providing values closer to 1 (Li et al., 2001; Voigtlander et al., 2007; Winkler et al., 2006; Pruppacher and Klett, 1996). α values for a number of other species have also been reported. Sulfuric acid was reported to have α of approximately 0.65 (Poschl et al., 1998). Values of 0.73 and 0.79 were observed for condensation of sulfuric acid onto ammonium sulfate and sodium chloride aerosols (Jefferson et al., 1997). α close to 1 was reported for condensation of ammonia onto droplets of 15-65% sulfuric acid solution (Hanson and Kosciuch, 2007). Values around 0.11 were reported for nitric acid condensing to sulfuric acid solutions (Xue et al., 2005). Ammonium nitrate was reported to exhibit α values of 0.5-0.8 in pure form (Dassios and Pandis, 1999) and of 0.25, if coated with dioctyl phthalate (Cruz et al., 2000).

There is paucity of data on α of organic compounds relevant to organic ambient aerosols. Li and Davis (1996) found α close to unity for dibutyl phthalate droplets evaporating in an electrodynamic balance. Riipinen et al. (2006) also reported α close to unity for succinic acid in aqueous solution. Their findings were based on a comparison

between Tandem Differential Mobility Analysis (TDMA) experiments and simulations performed with an evaporation / condensation model (BCOND). On the other hand, Stanier et al. (2007) estimated that α values of less than 0.1 are required to match their evaporation simulations using a basis-set approximation with TDMA measurements for SOA generated in a smog chamber by α-pinene ozonolysis. Another smog chamber study by Bowman et al. (1997) estimated α between 0.1 and 1 for aerosol resulting from m-xylene/NOx experiments. As noted above, the evaporation coefficient may embed a number of processes other than surface desorption, and, especially in the case of complex aerosols such as SOA, these processes can be rate-limiting, resulting in low values for α. Cruz and Pandis (2000) reported α values of greater than 0.2 for condensation of dioctyl phthalate and glutaric acid on inorganic and organic particles.

6.2 The IV-TDMA method

A major difficulty associated with estimating α in the transition regime is that its effect on particle evaporation or condensation rate overlaps with that of P_{sat} and σ, as evident in equation (6.1). In this study, we demonstrate a novel method, dubbed integrated volume-tandem differential mobility analysis (IV-TDMA), to separate the effects of these variables, allowing each α and σ to be determined by a single-parameter least-squares technique. With this technique, the traditional Tandem Differential Mobility Analyzer (TDMA)-thermodenuder approach is complemented with

measurements of aerosol vapor pressure under saturated conditions using the Integrated Volume Method (IVM, Saleh et al, 2008). The IVM relates changes in total particle volume as an aerosol passes from one equilibrium state to another, to vapor pressure at a given temperature using the Clausius-Clapeyron equation. Once the vapor pressure is determined, TDMA-thermodenuder experiments are performed to characterize evaporation kinetics. The latter are first performed for particle sizes at which the curvature effects are negligible (200-500 nm), allowing for single-parameter optimization of the evaporation coefficient while constraining the surface free energy. Having obtained the evaporation coefficient, measurements are repeated for smaller particle sizes (100-200 nm) for which curvature effects are prominent, and single-parameter optimization is used to obtain the surface free energy. Thus, the main three parameters that govern aerosol evaporation in TDMA experiments, namely saturation pressure, surface free energy and evaporation coefficient are decoupled. We illustrate the IV-TDMA technique by applying it to C-4, -6, and -7 dicarboxylic acids, namely succinic acid, adipic acid, and pimelic acid, which are pertinent to ambient / atmospheric OA (Grosjean et al., 1978; Sempere and Kawamura, 1994).

6.2.1 The IVM

The IVM was described in detail in Chapter 2. Here, we just reiterate the main advantage of the IVM, which is that the aerosol is investigated at equilibrium states,

excluding kinetics from the analysis. Thus, the knowledge of α is not required to estimate P_{sat}.

6.2.2 The TDMA method

In TDMA, quasi-monodisperse aerosol is heated in a thermodenuder and the size change due to evaporation is measured. As opposed to the IVM, the aerosol in TDMA is required to be as far from equilibrium as possible, such that the concentration of the vapor of the aerosol species in the gas phase is negligible compared to the saturation concentration. The particle evaporation kinetics equation (equation (6.1)) is thus simplified to:

$$\frac{dm_p}{dt} = -\frac{2\pi d_p D C_m K P_{sat}}{RM} \tag{6.2}$$

We note that the energy equation of the aerosol particles can be dropped because the thermal inertia of the aerosol particles and the latent heat effects are negligible. This was verified by comparison with a coupled heat-mass transfer model for aerosol evaporation/condensation in tubular flow (Saleh and Shihadeh, 2007).

In the coupled IV-TDMA method, parameters in equation (6.2) are obtained as follows:

- $P_{sat,0}$ is calculated using the IVM. P_{sat} at any temperature can be calculated with the knowledge of ΔH using Clausius-Clapeyron equation (equation (2.4)).

- The diffusion coefficient, D, can be estimated as a function of temperature using semi-empirical expressions (Reid, 1987).
- By choosing large enough particle diameters, typically larger than 200 nm for the dicarboxylic acids investigated in this study, Kelvin correction (K) is small compared to Fuchs-sutugin (C_m) correction and thus σ can be constrained. Figure 6.1 depicts the relative importance of K and Cm as a function of particle size for the dicarboxylic acids investigated in this study; it is obvious that the effect of α ($C_m << 1$) is more important than the effect of σ ($K \approx 1$).
- The initial and final particle sizes, and the residence time in the thermodenuder are measured as described in section 6.3.2.

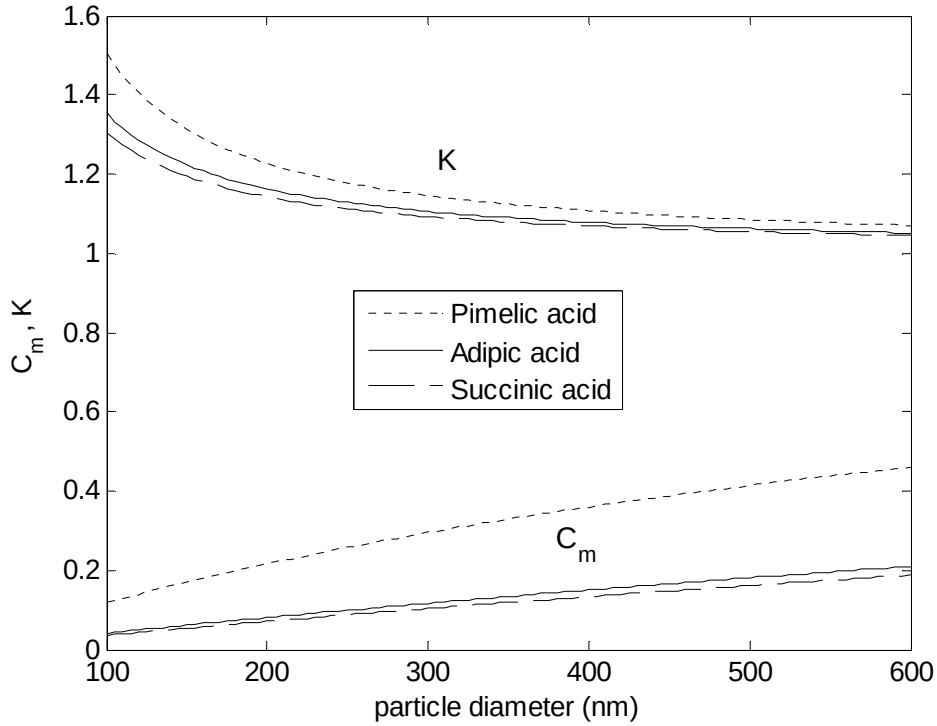

Figure 6.1: Relative importance of Fuchs-Sutugin correction ($0 < C_m < 1$) and Kelvin effect ($K > 1$) for 100 nm – 600 nm particles at 298 K

The only unknown remaining in equation (6.2) is α. Equation (6.2) is numerically integrated using MATLAB packaged ODE solver (ODE23) for a range of α values. single-parameter least squares optimization is performed to obtain the best value of α that produces a set of initial – final (evaporated) pairs of particle sizes.

Having estimated α, we apply the TDMA for particle sizes in the range 100 nm – 200 nm, where Kelvin effect is prominent, and equation (6.5) is optimized for σ.

6.3 Experimental section

6.3.1 Experimental setup and procedure

The experimental setup and procedure for IVM was described in details in Chapter 2.

A schematic of the TDMA experimental setup is given in Figure 6.2. Dry polydisperse organic aerosol is produced in a similar fashion as in the IVM experiments, and a quasi-monodisperse fraction is selected by a Differential Mobility Analyzer (DMA, TSI model 3071). The monodisperse flow is then rapidly pre-heated and diluted prior to entering the thermodenuder. This step is needed to simplify data interpretation (see section 6.2.2) and is achieved in the following way. Prior to the thermodenuder, the flow is split into a second line which passes a HEPA filter and then an inline resistance heater as illustrated in Figure 6.2. The filtered and preheated air is then returned to a point right before the split, forming a loop. The air flow in the loop is maintained at 8 SLPM using an in-line pump. The temperature of the mixed streams is monitored using an RTD, and a PID controller is used to maintain a set temperature at the outlet of the inline heater. The extraction line upstream of the HEPA filter in the pre-heating loop is 0.5 m long (not shown to scale in Figure 6.2) to allow the aerosol to cool to room temperature; otherwise, evaporation from the particles accumulated in the HEPA filter would cause

the vapor pressure in the loop to build up over time, bringing it closer to the saturation concentration at the set-temperature.

The heated and diluted aerosol is then introduced into the thermodenuder, which is a 1 m long 3.5 cm inner diameter stainless steel tube maintained at a temperature equal to that set at the preheating loop. The thermodenuder temperature is maintained by two resistance heaters wound around the tube, each with an independent PID controller. The temperature feedback for the PID controllers is provided by RTD's installed at 25 cm and 75 cm axial distance from the denuder inlet. Additional RTD's are installed at 12 cm, 50 cm, and 90 cm to verify that a uniform temperature distribution is achieved. Temperatures are maintained within 0.5 ^{0}C. To achieve a maximally uniform velocity profile within the denuder, it is fitted with static mixer inserts to generate plug-flow conditions. Particle residence time distribution in the thermodenuder is obtained by analyzing the response to a step input in aerosol concentration. The step is generated by a computer actuated three-way valve installed at the thermodenuder inlet. When the valve receives a signal, it switches from filtered to unfiltered ambient air, and logging of the CPC counts begins. The logging ends once the CPC output reaches steady state. The concentration versus time curve is differentiated to obtain the residence time distribution, which is shown in Figure 6.3. The mode of the distribution is 46.2 s and the

standard deviation is 7.8 s. When the CPC delay (1.7 s) is accounted for, the true thermodenuder residence time mode is 44.5 s.

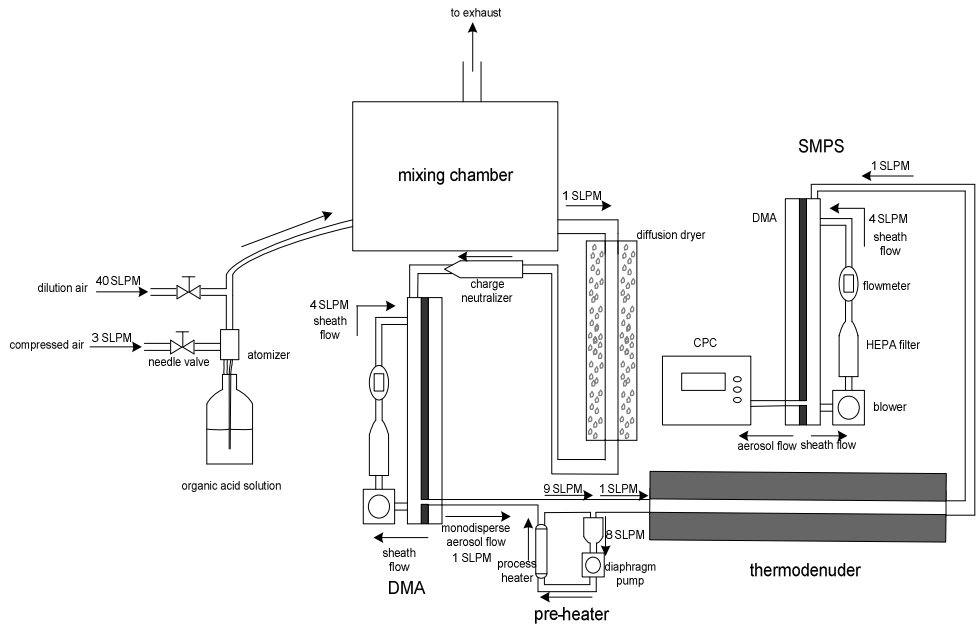

Figure 6.2: TDMA experimental setup

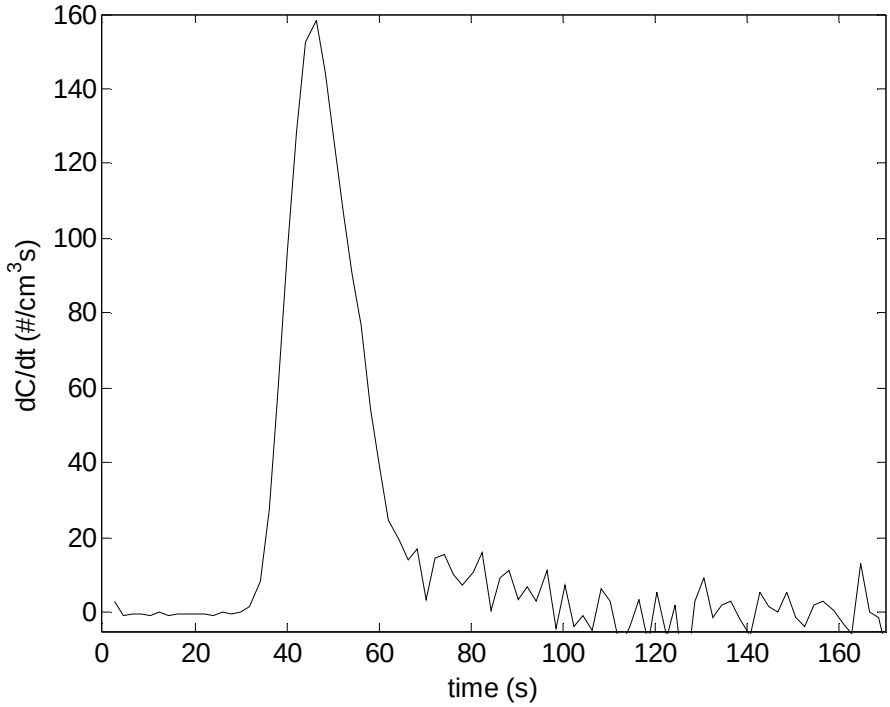

Figure 6.3: Residence time distribution in the thermodenuder

The final particle size at the exit of the thermodenuder is measured using an SMPS. To verify that we have vapor free conditions in the gas phase, as required in TDMA experiments (section 6.2.2), we measure the initial ($C_{initial}$) and the final (C_{final}) total aerosol particle mass concentrations. We compare the difference between these two concentrations (which is the vapor concentration released to the gas phase) to the species saturation concentration at the experimental temperature ($C_{sat,T}$). The ratio ($C_{initial}$ - C_{final}) / $C_{sat,T}$ was always less than 1%, which is very small compared to the 30% uncertainty in P_{sat} (see section 6.3.2).

6.3.2 Uncertainty analysis

Uncertainty of the IV-TDMA measurements is associated with the following parameters:

- P_{sat} obtained by IVM: the uncertainty is approximately 30% (Saleh et al., 2008).
- Particle size: the uncertainty in particle size measurements using a DMA is estimated to be 3% (Kinney and David, 1991).
- Residence time in the thermodenuder: the uncertainty is estimated to be the standard deviation of the residence time distribution (7.8 s).
- For surface free energy estimation, we also consider the uncertainty in the estimated evaporation coefficients.

To assess the propagation of uncertainty in our model, we use a Monte-Carlo approach with 100 simulations, each with perturbed values of the above parameters defined as:

$$X^{perturbed} = \bar{X} + \phi u_X \tag{6.3}$$

where $\bar{X}$ is the mean value of one of the parameters (saturation pressure, particle diameter, residence time, or accommodation coefficient), u_X is the corresponding uncertainty, and ϕ is a random variable drawn from a normal distribution with mean of 0 and standard deviation of 1. Results from the simulations are used to calculate mean values and uncertainties in the evaporation coefficients and surface free energies.

6.4 Results and discussion

6.4.1 Evaporation coefficients and surface free energies

Decrease in particle size due to evaporation in TDMA experiments is shown in Figure 6.4 for succinic, adipic, and pimelic acid. Data points on the right side of the plots (larger diameters) are used for α determination, and points on the left side (smaller diameters) are used for σ determination. The set-temperature at which each experiment was performed was found by trial and error to produce measurable size changes for the residence time in the thermodenuder. Set-temperatures for different experiments are given in Table 6.1. The initial and final particle sizes for each acid are listed in Table 6.2.

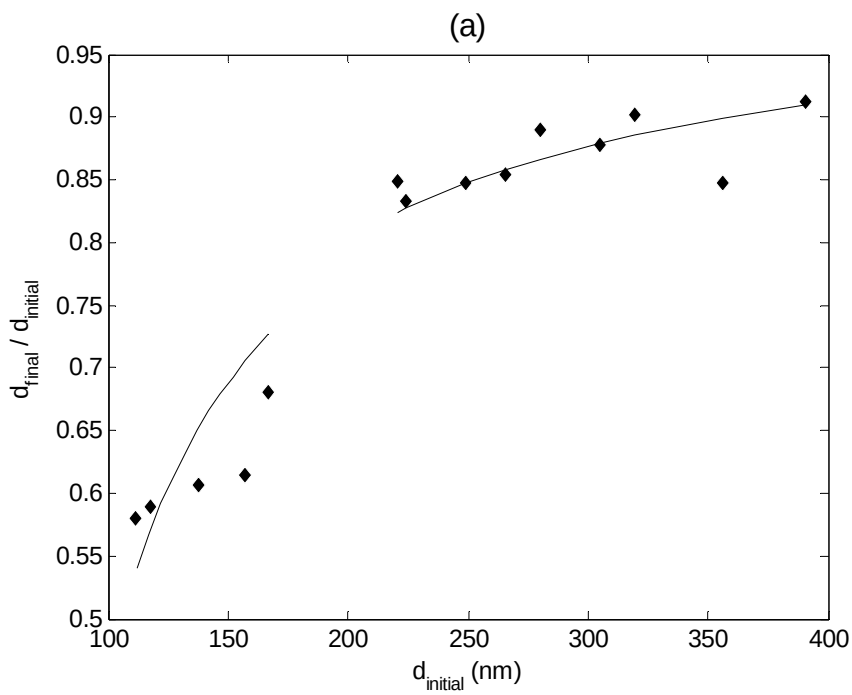

Figure 6.4

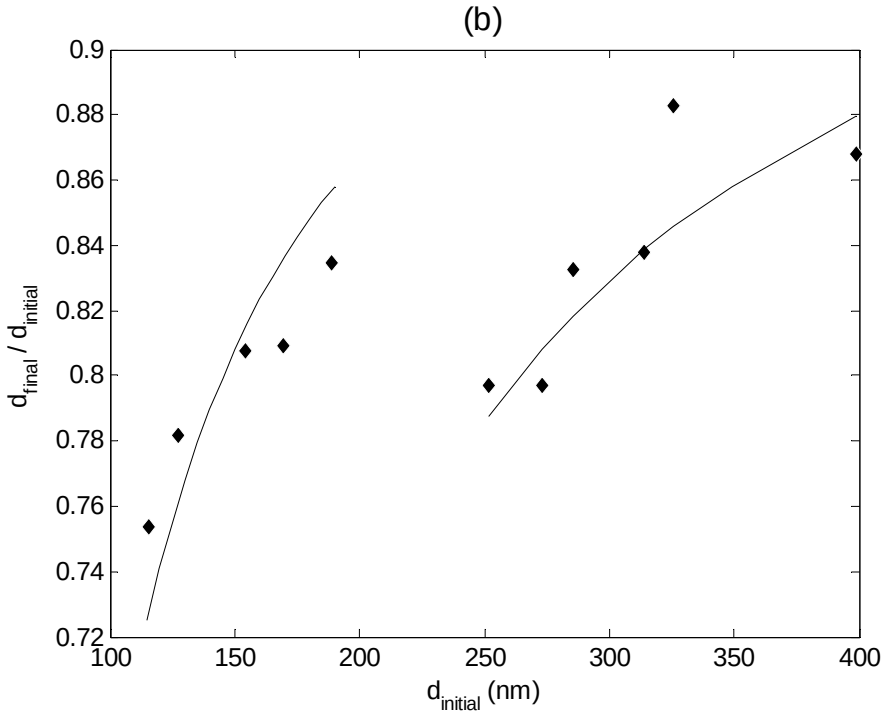

Figure 6.4 (continued)

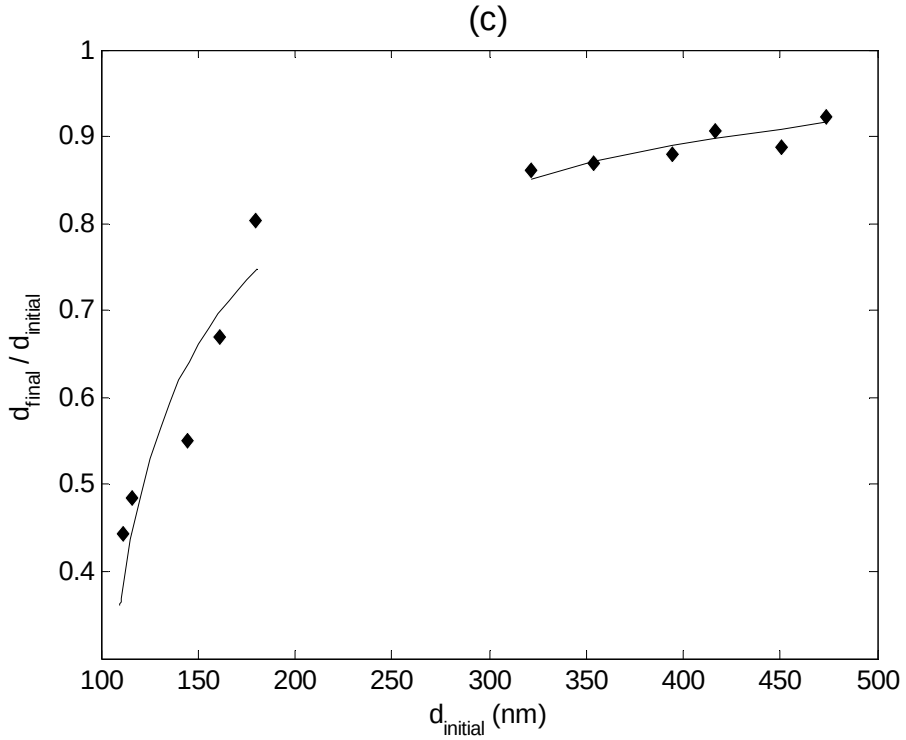

Figure 6.4 (continued): Change of particle size upon evaporation in TDMA experiments for (a) succinic acid, (b) adipic acid, and (c) pimelic acid. Solid lines are theoretical fits based on optimization of equation (6.2) to reproduce the observed size changes. Points on the right side of the plots (larger diameters) are used for α determination, and points on the left side (smaller diameters) are used for σ determination.

Values of evaporation coefficients and surface free energies are shown in Table 6.3; also given are the surface free energy values reported by Tao and McMurry (1989) and Bilde et al. (2003). Both evaporation coefficients and surface free energies exhibit an increase with increasing number of carbon atoms; however, more dicarboxylic acids need to be investigated before this trend can be generalized. Bilde et al. (2003) have not observed such a dependence of surface free energies on carbon number. Tao and

McMurry (1989) reported virtually identical surface energies for glutaric and adipic acids with the latter having slightly lower surface free energy. However, they observed a clear increase in surface free energies with increasing carbon number in C14-C18 monocarboxilic acids.

Table 6.1: Thermodenuder set-temperatures for TDMA experiments

Investigated property	Acid	Thermodenuder set-temperature
α	Succinic	40 ^{0}C
	Adipic	50 ^{0}C
	Pimelic	37 ^{0}C
σ	Succinic	40 ^{0}C
	Adipic	45 ^{0}C
	Pimelic	35 ^{0}C

Evaporation coefficients are significantly less than unity for the three dicarboxylic acids investigated in this study. While our experiments were done with pure substances, these results are in line with the findings of Stanier et al. (2007) and Bowmann et al. (1997) on evaporation coefficients associated with SOA generated in smog chamber studies, indicating evaporation coefficients smaller than one.

Table 6.2: Initial and final particle sizes (nm) for TDMA experiments

	succinic acid	adipic acid	pimelic acid

	initial size	final size	initial size	final size	intial size	final size
α determination	220	187	252	201	322	277
	224	187	272	218	354	308
	249	211	285	238	394	347
	265	227	314	263	417	378
	280	249	326	288	451	400
	395	268	399	346	473	437
	320	288				
	356	302				
	391	356				
σ determination	112	65	115	87	112	50
	118	69	127	99	116	56
	138	84	155	125	144	79
	157	97	169	137	161	108
	167	114	189	157	180	145

To investigate the validity of our assumption that the effects of α and σ are decoupled, we first perform α optimization assuming no Kelvin effect. Using the calculated α value, we optimize for σ, and then use the calculated σ value to re-calculate α. For succinic acid and adipic acid, the values obtained for α are the same in both cases (with and without Kelvin effect), thus confirming the decoupling. However, for pimelic acid, we observed some σ-dependence in calculating α, and we had to perform three iterations of α and σ optimizations for convergence. The reason for this dependence is that σ and α for pimelic acid are relatively large, and thus Kelvin and Fuchs-Sutugin corrections are relatively close, as can be inferred from Figure 6.1.

Table 6.3: Evaporation coefficients and surface free energies of the dicarboxylic acids

Property	Acid	This work	Tao and McMurry	Bilde et al. (2003)

			(1989)	
α	Succinic	0.07 (± 0.02)		
	Adipic	0.08 (± 0.02)		
	Pimelic	0.24 (± 0.04)		
σ (J/m^2)	Succinic	0.15 (± 0.07)		0.125
	Adipic	0.17 (± 0.12)	0.28	0.06
	Pimelic	0.23 (± 0.08)		0.08

6.4.2 Temperature dependence of the evaporation coefficient

The values of α reported in Table 6.3 for the dicarboxylic acids were obtained at temperatures 15 ^{0}C – 20 ^{0}C above the ambient (Table 6.1). The reason, as described in section 6.3.1, is that if the experiments were to be performed at temperatures close to the ambient, impractically long residence times would be required in the thermodenuder to achieve measurable size changes. To assure that the measured α values are representative for ambient conditions, we investigated the temperature dependence of α. It should be noted that the temperature-dependence of α is a highly debatable issue, with some studies observing no dependence (Winkler et al., 2006) and others reporting it (Davidovits et al., 2006).

TDMA experiments were performed for each compound at 4 different temperatures. The flowrate in the thermodenuder was adjusted for each set-temperature to obtain size changes which are measurable, but not too large so that the Kelvin effect is

constrained (see section 6.3.1). The set-temperatures and corresponding flowrates for each dicarboxylic acid are given in Table 6.4.

Measured α as a function of temperature is shown in Figure 6.5. Over a temperature range of 20 ^{0}C, adipic acid and succinic acid exhibit no observed temperature dependence, while pimelic acid exhibits a weak negative dependence, which is, however, within the uncertainty of the measurements. These results indicate that the difference in α between experimental and ambient temperature, if any, is small, and thus the values obtained in this study are representative for ambient conditions.

Table 6.4: Flowrates in thermodenuder for each set-temperature for α determination TDMA measurements

dicarboxylic acid	set-temperature (^{0}C)	set-flowrate (LPM)
succinic	40	1
	45	4
	50	5
	55	8
adipic	40	0.5
	50	1
	55	5
	60	7
pimelic	37	1
	45	5
	50	9
	55	11

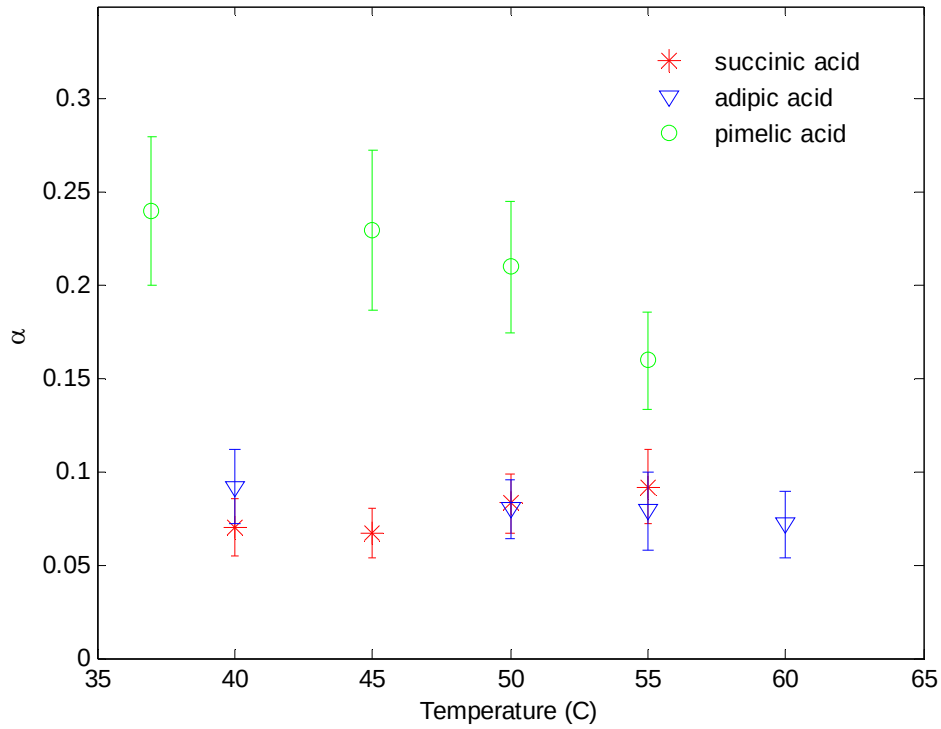

Figure 6.5: Evaporation coefficients of the dicarboxylic acids as a function of temperature

6.5 Conclusions

The IV-TDMA method is developed and used to determine evaporation coefficients of C-4, -6, and -7 dicarboxylic acids, as well as their saturation pressures, enthalpies of vaporization, and surface free energies. The novelty of IV-TDMA lies in the decoupling of the evaporation kinetics equation, such that each of the properties is obtained in a separate step – first IVM for saturation pressure and enthalpy of vaporization, then TDMA at large particle sizes for evaporation coefficient, and finally

TDMA at small sizes for surface free energy – rather than relying on multi-dimensional optimization.

The evaporation coefficients obtained in this study for the three dicarboxylic acids are significantly less than one. This highlights the importance of investigation of evaporation coefficients of ambient/atmospheric semi-volatile organic aerosols to improve the understanding of their phase change kinetics.

7. Conclusions

This dissertation presents novel experimental approaches for determination of thermodynamic and kinetic properties of semi-volatile organic aerosols. Two experimental techniques were developed: 1) the integrated volume method (IVM) for determination of thermodynamic properties and 2) the integrated volume – tandem differential mobility analysis (IV-TDMA) method for determination of kinetic properties.

Previous methods relied on interpreting aerosol evaporation rates using evaporation kinetic models to estimate thermodynamic properties, which required assumptions on the usually unknown evaporation coefficient. By the development of the IVM, we eliminated the effect of the uncertainty in evaporation kinetics on the measured thermodynamic properties. The IVM operates at thermodynamic equilibrium states and requires no information on the kinetics that lead from one state to another, and thus eliminates the need for any assumption on the evaporation coefficient. We demonstrated the use of the IVM to determine saturation pressure and enthalpy of vaporization by applying it to several dicarboxylic acids. This part of the dissertation was published in the *Journal of Aerosol Science* (Saleh et al., 2008).

The IVM was extended to measure activity coefficients of compounds in binary mixtures. We applied the method to several model systems where we addressed 1) organic polar – polar interactions where non-ideal behavior was observed; 2) organic

polar – non-polar interactions where phase separation was observed; 3) organic – inorganic interactions where phase separation was also observed; 4) organic – ambient matrix interactions, where non-ideal behavior was observed. The major finding of these experiments was that there is a strong indication that organic compounds in ambient aerosols do not form ideal solutions, and that the occurrence of phase separation is highly probable. This part of the dissertation was published in *Aerosol Science and Technology* (Saleh and Khlystov, 2009).

We have investigated three controversial issues associated with the IVM as well as other methods which utilize thermodenuders and/or aerosol generation by spray atomization and drying: 1) Equilibration time scales in thermodenuders where found to be a function of only aerosol size distribution and kinetic properties. Dimensional analysis was presented to aid researchers design their thermodenuders such that equilibrium can be achieved. 2) Re-condensation in the cooling section of thermodenuders was shown to be not important for aerosol loadings relevant to laboratory and ambient studies, which renders the use of activated carbon denuders in the cooling section unnecessary. 3) Finally, residual solvent in aerosols generated by spray atomization and drying was found to have no effect on measured thermodynamic properties. These results were published in *Atmospheric Measurement Techniques* (Saleh at al., 2010) and *Aerosol Science and Technology* (Saleh et al., 2010).

The IV-TDMA was developed to measure the evaporation coefficient of semi-volatile organic aerosols. The novelty of IV-TDMA lies in the decoupling of the evaporation kinetics equation, such that each of the properties is obtained in a separate step – first IVM for saturation pressure and enthalpy of vaporization, then TDMA at large particle sizes for evaporation coefficient, and finally TDMA at small sizes for surface free energy – rather than relying on multi-dimensional optimization. Evaporation coefficients on the order of 10^{-1} were measured for several dicarboxylic acids. These findings provide strong evidence that evaporation kinetics of organic aerosols is not ideal, and highlight the importance of investigation of evaporation coefficients of ambient/atmospheric semi-volatile organic aerosols to improve the understanding of their phase change kinetics. This part of the dissertation was published in *The Journal of Aerosol Science* (Saleh et al., 2009).

References

An, W. J., Pathak, R. K., Lee, B. H. & Pandis, S. N. (2007). Aerosol volatility measurement using an improved thermodenuder: Application to secondary organic aerosol. *Journal of Aerosol Science, 38*, 305.

Asher, W., E., Pankow, J., F., Erdakos, G., B., and Seinfeld, J. (2002). Estimating the vapor pressure of multi-functional oxygen-containing organic compounds using group contribution methods. *Atmospheric Environment, 36*, 1483.

Bardouki, H., Liakakou, H., Economou, C., Sciare, J., Smolik, J., Zdimal, V., Eleftheriadis, K., Lazaridis, M., Dye, C., and Mihalopoulos, N. (2003). Chemical composition of size-resolved atmospheric aerosols in the eastern Mediterranean during summer and winter. *Atmospheric Environment, 37*, 195-208.

Bilde, M., Svenningsson, B., Monster, J. & Rosenorn, T. (2003). Even – odd alteration of evaporation rates and vapor pressures of C3 – C9 dicarboxylic acid aerosols. *Aerosol Science and Technology, 37*, 1371-1378.

Booth, A.M., Markus, T., McFiggans, G., Percival, C.J., McGillan, M.R., and Topping, D.O. (2009). Design and construction of a simple Knudsen Effusion Mass Spectrometer (KEMS) system for vapor pressure measurements of low volatility organics . *Atmospheric Measurement Techniques, 2*, 355.

Bowman, F., M., Odum, J., R., Seinfeld, J., H., Pandis, S., N. (1997). Mathematical model for gas-particle partitioning of secondary organic aerosols. *Atmospheric Environment, 31,* 3921-3931.

Cappa, C., D., Lovejoy, E., R., and Ravishankara, A., R. (2007). Determination of evaporation rates and vapor pressures of very low volatility compounds: A study of the C4-C10 and C12 dicarboxylic acids. *Journal of Physical Chemistry A., 111,* 3099-3109.

Cappa, C., D., Lovejoy, E., R., and Ravishankara, A., R. (2007). Evaporation rates and vapor pressures of the even numbered C8-C18 monocarboxylic acids. *Journal of Physical Chemistry A., 112,* 3959.

Cappa,C.D., E. R. Lovejoy, and A. R. Ravishankara. (2008). Evidence for liquid-like and nonideal behavior of a mixture of organic aerosol compounds, *PNAS, 105,* 1868.

Cappa. C. D. and Jimenez, J. L. (2010). Quantitative estimates of the volatility of ambient organic aerosol. *Atmospheric Chemistry and Physiscs, 10*, 5409.

Chattopadhyay, S., Herbert, J. T., and Ziemann, P. J. (2001). A method for measuring vapor pressures of low volatility organic aerosol compounds using a thermal desorption particle beam mass spectrometer. Analytical Chemistry, 73, 3797.

Clegg, S.L., M. J. Kleeman, R. J. Gri_n, and J. H. Seinfeld. (2008). Effects of uncertainties in the thermodynamic properties of aerosol components in an air quality model part 2: Predictions of the vapor pressures of organic compounds. *Atmospheric Chemistry And Physics, 8*, 1087.

Choi, M. Y., Chan, C. K., (2002). The effects of organic species on the hygroscopic behaviors of inorganic aerosols. *Environmental Science & Technology, 36*, 2422.

Chow, J., C., Watson, J., G., Fujita, E., M., Lu, Z., Lawson, D., R., and Ashbaugh, L., L. (1994). Temporal and spatial variations of $PM_{2.5}$ and PM_{10} aerosol in the southern California air quality study. *Atmospheric Environment 28*, 2061-2080.

Chung, S. H., & Seinfeld, J. H. (2002). Global distribution and climate forcing of carbonaceous aerosols. *Journal of Geophysical Research, 107*, 4407.

Clegg, S. L., Seinfeld, J. H., Brimblecombe, P., (2001). Thermodynamic modelling of aqueous aerosols containing electrolytes and dissolved organic compounds. *Journal of Aerosol Science, 32*, 713.

Cruz, C., N. and Pandis, S., N., (2000). Deliquescence and hygroscopic growth of mixed inorganic-organic atmospheric aerosol. *Environmental Science & Technolog, 34*, 4313-4319.

Cruz, C., N., Dassios, K., G., and Pandis, S., N. (2000). The effect of dioctyl phthalate films on the ammonium nitrate aerosol evaporation rate. *Atmospheric Environment, 34*, 3897-3905.

Dassios, K., G. and Pandis, S., N. (1999). The mass accommodation coefficient of ammonium nitrate aerosol. *Atmospheric Environment, 33*, 2993-3003.

Davidovits, P., Kolb, C. E., Williams, L. R., Jaybe, J. T., and Worsnop, D. R. (2006). Mass accommodation and chemical reactions at gas-liquid interfaces. *Chemical Reviews, 106*, 1232-1354.

Davis, E., J. (2006). A history and state-of-the-art of accommodation coefficients. *Atmospheric Research, 82,* 561-578.

Davis, M. & Thomas, G. H. (1960). The lattice energies, infra-red spectra, and possible cyclization of some dicarboxylic acids. *Transactions of the Faraday Society*, *56*, 185-192.

Donahue, n. M., Robinson, A. L., Stanier, C.O., and Pandis, S.N. (2006). Coupled partitioning, dilution, and chemical aging of semivolatile organics. *Environmental Science & Technology, 40*, 2635.

Dzepina, K., Volkamer, R. M., Mandronich, S., Tulet, P., Ulbrich, I. M., Zhang, Q., Cappa, C. D., Ziemann, P. J., and Jimenez, J. L. (2009). Evaluation of new secondary organic aerosol models for a case study in Mexico city, *Atmospheric Chemistry and Physics Discussions, 9*, 4417.

Erdakos, G. B., Asher, W., Seinfeld, J. H., and Pankow, J. F., (2006a). Prediction of activity coefficients in liquid aerosol particles containing organic compounds, dissolved inorganic salts, and water Part 1: Organic compounds and water by consideration of short- and long-range effects using X-UNIFAC.1. *Atmospheric Environment, 40,* 6410.

Erdakos, G. B., Chang, E. I., Pankow, J. F., Seinfeld, J. H., (2006b). Prediction of activity coefficients in liquid aerosol particles containing organic compounds, dissolved inorganic salts, and water Part 3: Organic compounds, water, and ionic constituents by consideration of short-, mid-, and long range effects using X-UNIFAC.3. *Atmospheric Environment, 40,* 6437.

Fredenslund, A., Jones, R. L., & Prausnitz, J. M. (1975). Group-contribution estimation of activity coefficients in nonideal liquid mixtures. *A.I.Ch.E. Journal*, *21*, 1086.

Faulhaber, A.E, Thomas, B.M., Jimenez, J.L., Jayne, J.T., Worsnop, D.R., and Ziemann, P.J. (2009). Characterization of thermodenuder – particle beam mass spectrometer system for the study of organic aerosol volatility and composition . *Atmospheric Measurement Techniques, 2*, 15.

Fuchs, N. A. & Sutugin, A.G. (1971). High dispersed aerosols. In *Topics in Current Aerosol Research* (G. M. Hidy and J. R. Brock, eds. Pergamon Press, Oxford, Vol. 2, pp. 1-60.

Fuzzi, S., Andreae, M., O., Huebert, B., J., Kulmala, M., Bond, T., C., Boy, M., Doherty, S., J., Guenther, A., Kanakidou, M., Kawamura, K., Kerminen., V., M., Lohmann, U., Russel, L., M., and Poschl, U. (2006) Critical assessment of the current state of scientific knowledge, terminology, and research needs concerning the role of organic aerosols in the atmosphere, climate, and global change. *Atmospheric Chemistry and Physics, 6,* 2017-2038.

Grosjean, D., Cauwenberghe, K. V., Schmid, J. P., Kelly, P. E,, and Pitts, Jr., J. N. (1978) Identification of C3-C10 aliphatic dicarboxylic acids in airborne particulate matter. *Environmental Science and Technology,* 12, 313.

Hanson, D. and E. Kosciuch. (2003). The NH3 mass accommodation coefficient for uptake onto sulfuric acid solutions. *Journal of Physical Chemistry A, 107,* 2199-2208.

Heald, C., L., Jacob, D., J., Park, R., J., Russell, L., M., Huebert, B., J., Seinfeld, J., H., Liao, H., and Weber., R., J. (2005). A large organic aerosol source in the free troposphere missing from current models. *Geophysical Research Letters, 32,* 18-21.

Hinds, W. C. (1999). *Aerosol Technology*. Second Edition, John Wiley & Sons.

Hogrefe, O., Lala, G.G., Frank, B.P., Schwab, J.J. & Demerjian, K.L. (2006). Field evaluation of a TSI model 3034 Scanning Mobility Particle Sizer in New York City: Winter 2004 intensive campaign. *Aerosol Science and Technology*, *40*, 753.

Hueglen, C., Gehrig, R., Baltensperger, U., Gysel, M., Monn, C., and Vonmont H. (2005). Chemical characterization of PM2.5, PM10, and coarse particles at urban, near-city and rural sites in Switzerland. *Atmospheric Environment, 39*, 637.

Huffmann, J. A., Ziemann, P. J., Jayne, J. T., Worsnop, D. R., and Jimenez, J. L. (2008). Development of fast-stepping/scanning thermodenuder for chemically-resolved aerosol volatility measurements, *Aerosol Science and Technology, 42*,395.

Incropera, F. P. & DeWitt, D. P. (2002). *Fundamentals of heat and mass transfer.* New York: John Wiley & Sons Inc.

Jang, M., Kamens, R. M., Leach, K. B., and Strommen, M. R. (1997). A thermodynamic approach using group contribution methods to model the partitioning of semivolatile organic compounds on atmospheric particulate matter. *Environmental Science and Technology*, *31*, 2805.

Jefferson, A., Eisele, F., L., Zeimann, P., J., Weber, R., J., Marti, J., J., and McMurry, P., H. (1997). Measurements of the H2SO4 mass accommodation coefficient onto polydisperse aerosol. *Journal of Geophysical Research-Atmospheres, 102,* 19021-19028.

Kawamura, K. and Kaplan, I. R. (1987). Motor exhaust emissions as a primary source for dicarboxylic acids in Los Angeles ambient air, *Environmental Science and Technology, 21*, 105.

Khlystov, A., Stanier ,C. & Pandis, S.N. (2004). An algorithm for combining electrical mobility and aerodynamic size distributions data when measuring ambient aerosol. *Aerosol Science and Technology*, *38(S1)*, 229.

Khlystov, A., Lin, M., Bolch, M. A. & Ma, Y. (2009). Positive artifact formation during sampling semi-volatile aerosol using wet denuders. *Atmospheric Environment*,*43*, 364 .

Kinney, P., D., and Pui, D., Y., H. (1991). Use of the electrostatic classification method to size 0.1 μm SRM particles – a feasibility study. *Journal of Research of the National Institute of Standards and Technology, 96*, 147-176.

Kiss, G., Tombacz, E., Varga, B., Alsberg, T., and Persson, L. (2003). Estiamtion of the average molecular weight of humic-like substances isolated from fine atmospheric aerosol. *Atmospheric Environment, 37*, 3783.

Koren, H. & O'Neill, M. (1998). Experimental assessment of the influence of atmospheric pollutants on respiratory diseases. *Toxicology Letters, 103,* 317.

Krivacsy, Z., Gelencser, A., Kiss, G., Mezsaros, E., Molnar, A., Hoffer, A., Meszaros, T., Sarvari, Z., Temesi, D., Varga, B., Baltensperger, U., Nyeki, S., and Weingartner, E. (2001). Study on the chemical character of water-soluble organic compounds in fine atmospheric aerosol at the Jungfraujoch. *Journal of atmospheric chemistry, 39*, 235.

Lehtinen, K., J., Korhonen, H., Dal Maso, M., and Kulmala, M. (2003). On the concept of condensation sink diameter. *Boreal Environment Research, 8,* 405-411.

Lewandowski, M., Jaoui, M., Kleindienst, T., E., Offenberg, J., H., and Edney, E., O. (2007). Composition of $PM_{2.5}$ during the summer of 2003 in Research Triangle Park, North Carolina. *Atmospheric Environment, 41*, 4037.

Lewtas, J. (2007). Air pollution combustion emissions: Characterization of causative agents and mechanisms associated with cancer, reproductive, and cardiovascular effects. *Mutation Research, 636,* 95.

Li, Y., Q., Davidovits, P., Shi, Q., Jayne, J., T., Kolb, C., E., Worsnop, D., R. (2001). Mass and thermal accommodation coefficients of H2O(g) on liquid water as a function of temperature. *Journal of Physical Chemistry,105,* 10627-10634.

Li, W.G., and Davis, E., J. (1996). Aerosol evaporation in the transition regime. *Aerosol Science and Technology, 25,* 11-21.

Lide, D.R. (1987), *Handbook of Chemistry and Physics*. Florida: Taylor and Francis.

L'vov, B.V. (2001). The physical approach to the interpretation of the kinetics and mechanisms of thermal decomposition of solids: the state of the art. *Thermochimica Acta, 373*, 97-124.

Mader, B., T., Yu, J., Z., Xu, J., H., Li, Q., F., Wu, W., S., Flagan, R., C., and Seinfeld, J., H. (2004). Molecular composition of the water-solube fraction of atmospheric carbonaceous aerosols collected during ACE-Asia. *Journal of Geophysical Research, 109*, D06206.

Maria, S. F., Russel, L. M., Gilles, M. K. & Myneni, S. C. B. (2004). Organic aerosol growth mechanisms and their climate-forcing implications. *Science, 306*, 1921.

Maxwell, J., C. (1859). On the dynamic theory of gases. *British Association of Advanced Sciences, Rep. 9.*

Maxwell, J., C. (1960a). Illustration of the dynamical theory of gases: Part I. On the motions and collisions of perfectly elastic spheres. *Philosophical Magazine, 19,* 19-32.

Maxwell, J., C. (1960b). Illustration of the dynamical theory of gases: Part II. On the process of diffusion of two or more kinds of moving particles among one another. *Philosophical Magazine, 20,* 21-37.

Monster, J., Rosenorn, T., Svenningsson, B., & Bilde, M. (2004). Evaporation of methyl- and dimethyl- substituted malonic, succinic, glutaric and adipic acid particles at ambient temperatures. *Journal of Aerosol Science, 35*, 1453.

Moore, R. H. and Raymond, T. M. (2008). HTDMA analysis of multicomponent dicarboxylic acid aerosols with comparison to UNIFAC and ZSR. *Journal of Geophysical Research, 113*, D04206.

Murphy, D., M., Thomson, D., S., Mahoney, M., J. (1998). "In situ measurements of organics, meteoritic material, mercury, and other elements in aerosols at 5 to 19 kilometers." *Science, 282,* 1664.

Odum, J.R., Hoffman, T., Bowman, F., Collins, D., Flagan, R.C., and Seinfeld, J.H. (1996). Gas/particle partitioning and secondary organic aerosol yields. *Environmental Science & Technology, 30*, 2580.

Offenberg, J. H., Kleindienst, T. E., Jaoui, M., Lewandowski, M. & Edney, E. O. (2006). Thermal properties of secondary organic aerosol. *Geophysical Research Letters, 33*, L03816

Ohta, S. and Okita, T. (1990). A chemical characterization of atmospheric aerosol in Sapporo. *Atmospheric Environment, 24*, 815-822.

Pankow, J.F. and Barsanti, K.C. (2009). The carbon number – polarity grid: a means to manage the complexity of the mix of organic compounds when modeling atmospheric organic particulate matter. *Atmospheric Environment, 43*, 2829.

Peng, C., Chan, M. N., Chan, C. K., (2001). The hygroscopic properties of dicarboxylic and multifunctional acids: measurements and UNIFAC predictions. *Environmental Science & Technology, 35,* 4495.

Poschl, U., Canagaranta, M., Jayne, J., T., Molina, L., T., Worsnop, D., R., Kolb, C., E., and Molina, M., J. (1998). Mass accommodation coefficient of H2SO4 vapor on aqueous sulfuric acid surfaces and gaseous diffusion coefficient of H2SO4 in N-2/H2O. *Journal of Physical Chemistry A, 102*, 10082-10089.

Pruppacher, H., R., and Klett J., D. (1996). *Microphysics of Clouds and Precipitation*. 2nd ed. Dordrecht: Kluwer Academic Publishers.

Raatikainen, T., Laaksonen, A., (2005). Application of several activity coefficient models to water organic–electrolyte aerosols of atmospheric interest. *Atmospheric Chemistry and Physics, 5,* 2475.

Rader, D. J. & McMurry, P. H. (1986). Application of the tandem differential mobility analyzer to studies of droplet growth and evaporation. *Journal of Aerosol Science, 17*, 771-787.

Riipinen, I., Svenningsson, B., Bilde, M., Gaman, A., Lehtinen, K., Kulmala, M. (2006). A method for determining thermophysical properties of organic material in aqueous solutions: Succinic acid. *Atmospheric Research, 82*, 579-590.

Riipinen, I., Pierce, J.R., Donahue, N.M, and Pandis, S.N. (2010). Equilibration time scales of organic aerosol inside thermodenuders: Evaporation kinetics versus thermodynamics. *Atmospheric Environment*,*44*, 597 .

Robinson, A. L., Donahue, N. M., Shrivastava, M. K., Weitkamp, E. A., Sage, A. M., Grieshop, A. P., Lane, T. E., Pierce, J. R. & Pandis, S. N. (2007). Rethinking organic aerosols: Semivolatile emissions and photochemical aging. *Science, 315*, 1259.

Rogge, W. F., Mazurek, M. A., Hildemann, L. M., Cass, G. R., and Simoneit, B. R. T. (1993). Quantification of urban organic aerosols at a molecular level: Identification, abundance and seasonal variation. *Atmospheric Environment, 27*, 1309.

Sakurai, H., Park, K., McMurry, P., Zarling, D., Kittelson, D., and Ziemann, P. (2003). Size-dependent mixing characteristics of volatile and nonvolatile components in diesel exhaust aerosols. *Environmental Science and Technology, 37*, 5487-5495.

Saleh, R. & Shihadeh, A. (2007). Hygroscopic growth and evaporation of an aerosol with boundary heat and mass transfer. *Journal of Aerosol Science, 38*, 1.

Saleh, R., Walker, J., and Khlystov, A. (2008). Determination of saturation pressure and enthalpy of vaporization of semi-volatile aerosols: The integrated volume method. *Journal of aerosol science, 39*, 876.

Saleh, R., and Khlystov, A. (2009). Determination of activity coefficients of semi-volatile organic aerosols using the integrated volume method. *Aerosol Science and Technology, 43*, 838.

Saleh, R., Shihadeh, A., and Khlystov, A. (2009). Determination of evaporation coefficients of semi-volatile aerosols using and integrated volume – tandem differential mobility analysis (IV-TDMA). *Journal of aerosol science, 40*, 1019.

Saleh, R., Khlystov, A. and Shihadeh, A. (2010). Effect of aerosol generation method on measured thermodynamic properties of dicarboxylic acid aerosols. *Aerosol Science and Technology, 44*, 302.

Saleh, R., Shihadeh, A., and Khlystov, A. (2010). On transport phenomena and equilibration time scales in thermodenuders. *Atmospheric Measurement Techniques Discussions, 3*, 2931.

Saxena, P., and L. M. Hildemann (1996), Water-soluble organics in atmospheric particles: A critical review of the literature and application of thermodynamics to identify candidate compounds. *Journal of Atmospheric Chemistry, 24*, 57.

Seinfeld, J. H. & Pandis, S. N. (1998). *Atmospheric chemistry and physics: From air pollution to climate change.* New York: John Wiley & Sons Inc.

Sempere, R., and Kawamura, K. (1994). Comparative distributions of dicarboxylic acids and related polar compounds in snow, rain and aerosols from urban atmosphere. *Atmospheric Environment, 28*, 449.

Sinclair, D. and LaMer, V. (1949). Light scattering as a measure of particle size in aerosols. *Chemical Reviews, 44*, 245.

Smith, J.M. & Van Ness, H.C. (1987), *Introduction to chemical engineering thermodynamics*. Chemical Engineering Series. New York: McGraw-Hill.

Solomon, S., D. Qin, M. Manning, R.B. Alley, T. Berntsen, N.L. Bindoff, Z. Chen, A. Chidthaisong, J.M. Gregory, G.C. Hegerl, M. Heimann, B. Hewitson, B.J. Hoskins, F. Joos, J. Jouzel, V. Kattsov, U. Lohmann, T. Matsuno, M. Molina, N. Nicholls, J. Overpeck, G. Raga, V. Ramaswamy, J. Ren, M. Rusticucci, R. Somerville, T.F. Stocker, P. Whetton, R.A. Wood and D. Wratt, 2007: Technical Summary. In: *Climate Change 2007: The Physical Science Basis. Contribution of Working Group I to the Fourth Assessment Report of the Intergovernmental Panel on Climate Change* [Solomon, S., D. Qin, M. Manning, Z. Chen, M. Marquis, K.B. Averyt, M. Tignor and H.L. Miller (eds.)]. Cambridge University Press, Cambridge, United Kingdom and New York, NY, USA.

Somorjai, G.A. & Lester, J.E. (1967). Evaporation mechanism of solids, in*: H. Reiss (Ed.), Progress in Solid State Chemistry*. Pergamon Press, Oxford, 1–51.

Stanier, C. O., Pathak, R. K. & Pandis, S. N. (2007). Measurement of the volatility of aerosol from α-pinene ozonolysis. *Environmental Science and Technology, 41*, 2756-2763.

Tang, N, I. and Munkelwitz, H. R. (1990). Determination of vapor pressure from droplet evaporation kinetics. *Journal of Colloid and Interface Science, 141,* 109-118.

Tao, Y. & McMurry, P. H. (1989). Vapor pressure and surface free energies of C14 – C18 monocarboxylic acids and C5 and C6 dicarboxylic acids. *Environmental Science and Technology, 23*, 1519-1523.

Topping, D. O., McFiggans, G. B., Coe, H., (2005). A curved multicomponent aerosol hygroscopicity model framework: part 2—including organic compounds. *Atmospheric Chemistry and Physics, 5,* 1223.

Turpin, B., J., Huntzicker, J., J., Larson, S., M., Cass, G., R. (1991) Los-Angeles summer midday particulate carbon - primary and secondary aerosol. *Environmental Science and Technology, 25*, 1788-1793.

Voigtlander, J., Stratmann, F., Niedermeier, D., Wex, H., and Kiselev, A. (2007). Mass accommodation coefficient of water: A combined computational fluid dynamics and experimental data analysis. *Journal of Geophysical Research-Atmospheres, 112,* D20208.1-D20208.8.

Vutukuru, S., R.J. Griffin, and D. Dabdub (2006). Simulation and analysis of secondary organic aerosol dynamics in the South Coast Air Basin of California. *Journal of Geophysical Research-Atmospheres, 111,* D10S12.1-D10S12.13.

Wang, S.C. & Flagan, R.C. (1990). Scanning electrical mobility spectrometer. *Aerosol Science and Technology, 35*, 718.

Wehner, B., Philippin, S., and Wiedensohler, A. (2002). Design and calibration of a thermodenuder with an improved heating unit to measure the size-dependent volatile fraction of aerosol particles, *Journal of Aerosol Science, 33*, 1087.

Wexler, A. S. and Seinfeld, J. H. (1990). The distribution of ammonium salts among a size and composition dispersed aerosol. *Atmospheric Environment, 24*, 2131.

Winkler, P., M., Vrtala, A., Rudolf, R., Wagner, P., E., Riipinen, I., Vesala, T., Lehtinen, K., E., J., Visanen, Y., and Kumala, M. (2006). Condensation of water vapor:

Experimental determination of mass and thermal accommodation coefficients. *Journal of Geophysical Research-Atmospheres*, *111,* D19202.1-D19202.12.

Xue, H., W., Moyle, A., M., Magee, N., Harrington, J., Y., and Lamb, D. (2005). Experimental studies of droplet evaporation kinetics: Validation of models for binary and ternary aqueous solutions. *Journal of the Atmospheric Sciences, 62,* 4310-4326.

Biography

Born in 1980 in Abu Dhabi, UAE, Rawad Saleh later lived in the KSA, Lebanon, Turkey, and the USA. Rawad received a B.Sc. in Mechanical Engineering from Middle East Technical University (METU), Turkey in 2003, M.Sc. in Mechanical Engineering from the American University of Beirut (AUB), Lebanon in 2005, and a Ph.D. in Environmental Engineering from Duke University in 2010.

Rawad started his research work in the Aerosol Lab at AUB under the supervision of Prof. Alan Shihadeh as a research assistant (2003 – 2005) and then as a research engineer (2005 – 2007). He joined Prof. Andrey Khlystov's research group at Duke University in August 2007, where he completed his Ph.D in December 2010. Rawad has authored and co-authored ten peer reviewed publications in the areas of aerosol science and tobacco smoke sampling and instrumentation in *The Journal of Aerosol Science, Aerosol Science and Technology, Atmospheric Measurement Techniques, Food and Chemical Toxicology, and Atmospheric Environment.*

In the course of his graduate studies, Rawad has received several awards, including Abdelhadi Debs award for academic excellence (2006), Senol Utku award for best pre-PhD peer-reviewed journal paper (2009), and the AAAR student poster award in 2008 and 2009.